THE UNIVERSITY
of EDINBURGH

Role of mouse Disrupted in Schizophrenia 1 in cortical interneuron development.

By

Malgorzata Borkowska

Thesis submitted for the degree of Doctor of Philosophy at the University of Edinburgh

2014

Disclaimer

I (Malgorzata Borkowska) performed all of the experiments written in this thesis. No part of this work has been or is being submitted for any other degree or qualification.

Signed:

Date:

Acknowledgements

First of all, I would like to thank my supervisors Prof David Price and Dr Kirsty Millar for giving me a chance to pursue what I was interested in. For their advice, guidance and infinite patience I am very grateful.

I would like to thank members of DBUG for creating a great working environment – I have learnt and achieved so much during my time here and it would not have happened without you! In particular, I would like to thank Mike Molinek, Kathy Howe, Sally Till and Viv Allison for all the technical help and training. Big thanks go to my fellow PhD students: Cass Li, Danai Katsanevaki, Elena Ferrari Dora, Hannah Parkin, Nikky Huang, Calvin Chan and Mel Chiang – you guys have always made my day!

Very special thanks go to Kerstin Hasenpusch-Theil, for all the patience that was needed to explain basic molecular biology to me; and to Tomasz Nowakowski for training, encouragement and being one of the most inspiring people I know.

Last but definitely not least, I would like to thank my partner, Adrian Zagrajek, and my parents, Krystyna and Janusz, for always being there for me and believing in me, even when I did not.

Table of Contents

Abstract

Schizophrenia is a relatively poorly understood, debilitating psychiatric disorder affecting around 0.5% of the population worldwide. The main characteristics of the disease are hallucinations, delusions and cognitive impairment such as difficulty in learning. It has been recently suggested that Disrupted-in-Schizophrenia-1 (DISC1) might be one of the main genetic risk factors for this disease. Mouse Disc1 has been implicated in brain development, mainly in neurite outgrowth, integration of new-born neurons, neuronal precursor proliferation/differentiation and neuronal migration. Disc1 function in the cortical excitatory cells was studied in fair detail but there is little data on Disc1 role in cortical interneuron development. In this study I have investigated development of the cortical interneurons in 21 days old mice with ENU-induced point mutations in the mouse Disc1 sequence - L100P and Q31L; previously characterized as 'schizophrenic-like' and 'depressive-like' respectively. Bin analysis was performed on five brain regions: frontal and central primary somatosensory (fSSp and SSp respectively) cortices, ventral auditory (vAud) cortex, visual (Vis) cortex and medial prefrontal cortex (MPFC); for four major interneuronal markers: parvalbumin (PV), somatostatin (STT), calretitnin (CLR) and glutamate decarboxylase 67 (GAD67). A significant decrease in PV (protein and mRNA) expression was observed in a subclass of the cortical interneurons in the fSSp, SSp, vAud and Vis cortices of L100P homozyogous (L100P) and heterozygous (L100P +/-) mouse brains when compared to their wild-type (WT) littermates. No such difference in the PV positive cells was found in the MPFC in the L100P mouse brain. Other interneuronal markers expression was not different in the L100P and L100P +/- brain from that in the WT littermate controls. Furthermore, there was no significant difference in any of the interneuronal markers expression in the Q31L mouse brain cortex. A minor change in the relative distribution of the interneurons (GAD67 positive cells) was found in the L100P but not Q31L brain. With no difference in the number of the interneurons and the nature of PV expression regulation, the cell non-autonomous effect of L100P Disc1 on this subpopulation of intereneurons was investigated. Overexpression of the mouse Disc1-100P *in utero* in the radial glia cells born at E14.5 (future layer II/III and IV excitatory cells) resulted

in a significant decrease in the PV positive cells in all of the electroporated regions (fSSp, SSp, vAud and Vis cortices) when compared to mouse WT Disc1 overexpression. Furthermore, a decrease in the PV cells on the contralateral side was observed in the SSp and Vis cortices. This study demonstrates that mouse Disc1 is involved in the generation of parvalbumin expressing interneurons within the cortex in a cell non-autonomous way. The L100P point mutation in Disc1 led to downregulation of parvalbumin, which in turn would result in abnormal inhibitory properties of this interneuron subtype.

Abbreviations

CA3	cornu ammonis 3 (hippocampus)
CB	calbindin
CBP	calcium binding protein
CGE	caudal ganglionic eminence
CR/CLR	calretinin
Disc1	Disrupted in Schizophrenia 1
Disc1-100P	overexpressed Disc1 construct with L100P point mutation
Disc1-WT	overexpressed wild type Disc1 construct
DLFC	dorso-lateral frontal cortex
fSSp	frontal primary somatosensory cortex
GABA	gamma-aminobutyric acid
GABAR	GABA receptor
GAD	glutamate decarboxylase
IRES-GFP	overexpressed empty vector
IZ	intermediate zone
L100P/L100P or Q31L/Q31L	mice homozygous for L100P or Q31L mutation in *Disc1*
L100P/+ or Q31L/+	mice heterozygous for L100P or Q31L mutation in *Disc1*
LGE	lateral ganglionic eminence
MGE	medial ganglionic eminence
MPFC	medial prefrontal cortex
MZ	marginal zone

NPY	neuropeptide Y
POA	preoptic area
PV	parvalbumin
RGP/RGC	radial glial progenitor/radial glia cells
SOM/SST	somatostatin
SSp	primary (barrel) somatosensory cortex
SVZ	subventricular zone
TF	transcription factor
vAud	ventral auditory cortex
VIP	vasoactive intestinal peptide
Vis	primary visual cortex
VZ	ventricular zone

Chapter 1: General Introduction

1.1 Overview

Mammalian cortex development is one of the peak achievements of vertebrate brain evolution. This highly complex yet organised and precise process reaches its pinnacle in humans. Because of our well developed neocortex, in comparison to other species, we are able to acquire, process and store vast amounts of information from the surrounding world. Abilities such as thinking, emotions, language, learning and other higher cognitive functions would not be possible without it. This fascinating part of the brain consists of many neuronal cell types distributed within six layers, allowing efficient and precise functioning. However, the two most essential classes of neurons in the neocortex are excitatory projection neurons (~70-80%) and inhibitory (in most cases) interneurons (~20-30%). In this thesis, I have focused on the development of the cortical interneurons in a mouse model of psychiatric disorders. In this study, I investigated the role mouse Disrupted-in-schizophrenia 1 (Disc1) has on the migration and maturation of the cortical interneurons in five distinct cortical regions. In the first part of this introduction I will give an overview of different subtypes of the cortical interneurons as well as their generation, migration and maturation. The second part will focus on Disc1's structure and its role in the development of the neocortex.

1.2 Cortical interneurons

1.2.1 Importance of cortical interneurons

Proper and effective functioning of the cortex depends on a correct relationship between excitation and inhibition (E/I ratio). In the cerebral cortex excitatory and inhibitory cells form an interconnected and highly dynamic network of feed-forward and feed-back circuits to modulate one another's activity. Inhibitory cells are responsible for regulation of the excitatory cells activity in the cortex - an increase in excitation results in an increased recruitment of interneurons resulting in an increased inhibition. In a way, these cells are responsible for maintaining the E/I balance by regulating the excitatory input. The E/I ratio appears to be stable between individual pyramidal cells and across them, meaning that the excitation and inhibition are proportional to each other despite variation in the signal amplitudes in different pyramidal cells (Xue et al., 2014). However, this balance between excitation and inhibition is not constant - it can be affected by the intensity of the stimulus, synaptic plasticity or adaptation of the neuronal response (Heiss et al., 2008; Taub et al., 2013). Nevertheless, disruption in the E/I balance has been believed to be one of the underlying causes of a range of psychiatric disorders, from autism spectrum to schizoaffective disorders (Lewis et al., 2005; Rubenstein, 2010; Ramamoorthi and Lin, 2011; Lisman, 2012; Murray et al., 2012).

There are few potential mechanisms behind inhibitory cells regulating the excitatory signal. The simplest proposes that the input from an excitatory cell will activate both the inhibitory and excitatory cells in a manner that allows a fast yet shortened excitatory stimulus - feedforward inhibition (Trevelyan and Watkinson, 2005; Isaacson and Scanziani, 2011). Depending where the inhibitory cells form a synaptic connection with the targeted excitatory cell (the initial segment of an axon, the dendrites, the soma) as well as the ability to recruit more inhibitory cells will shape the propagating impulse.

Unlike pyramidal neurons, the cortical interneurons are not a uniform group. Different interneurons can be distinguished from one another depending on their morphology, molecular markers, activity, cortical positioning and the site of connection to pyramidal neurons or other inhibitory neurons. This large variation in a seemingly small group of neurons provides a much bigger computational power to the cortical circuit. Among the interneuron types it is possible to discriminate between basket cells, chandelier cells, Martinotti cells, bipolar cells and more. The basket cells comprise about 50% of the cortical interneurons in rodents and can be further classified into large, small and nested basket cells. These fast-spiking cells with perismomatic innervation express a calcium binding protein, parvalbumin, and have been shown to take part in both the feedforward and feedback inhibition of the neural circuit (Hu et al., 2014). Parvalbumin-expressing interneurons are firing early after stimulation and are optimized for a precise timing of action potential initiation by narrowing the time window for excitatory postsynaptic potentials summation (Pouille and Scanziani, 2001; Hu et al., 2014). Moreover, their fast signalling enables regulation of a fast and precise GABA release, hence they greatly minimize the delay of feedforward and feedback inhibition (Hu et al., 2014). Disruption in the parvalbumin interneurons function leads to reduction in the inhibition and hyperactivity of the neuronal system - some of the underlying features of psychatric disorders such as schizophrenia (Cobos et al., 2005; Lodge et al., 2009; Lewis et al., 2012).

1.2.2 Classification of the interneurons in the neocortex

1.2.2.1 Morphology

The general morphology of the cortical interneurons includes a soma, dendrites, axons and synapses. The shape and size of the soma vary greatly while the dendritic tree is not as complex as in the excitatory cells (Ascoli et al., 2008). Interneurons can exhibit different polarity of their primary dendrite(s) with some restricted to a specific cortical layer or column. Interestingly, soma shape is dependent to some extent on the number and the polarity of the primary dendrites. Other features related

to the dendrites and included in the morphological classification of the interneurons are the frequency and size of the dendritic branching, change of the diameter along the branch as well as the number of the dendritic spines, though the latter tend to be lost in most of the interneurons as they mature.

Another important feature in the classification of the interneuron according to their morphology is their axonal morphologies and connectivity. A study from Gord Fishell's group suggested that the axonal morphology of the cortical interneurons as well as their synaptic properties is strongly related to the time and place of their birth (Butt et al., 2005). The axon starts either from the cell soma or from the primary dendrite but their connections vary largely. Though they reside predominantly in the layer where the soma is, they can extend horizontally within the layer, ascend and/or descend into superficial or deeper layers of the cortical column respectively, or even extend to multiple layers and regions, though there is little evidence for the existence of such interneurons in the cortex (Ascoli et al., 2008; Tomioka et al., 2005). Axonal branching, diameter, myelination, axonal arbour density as well as the bouton size, number and type of synapses should also be taken into consideration. The location of the synapse formed on the targeted cell also varies between different subtypes - it can be cell soma, axon and/or particular part of the dendritic arbour. The positioning within the cortex, morphological characteristics and site of connection of different interneurons are presented in Fig 1.01 and Fig 1.02 A.

1.2.2.2 Molecular markers

Although classification of the interneurons based on their morphology seems fairly straightforward, in order to clearly distinguish between the interneuronal sub-types, it is necessary to use a combination of markers expressed by a particular cell type. All inhibitory cells in the cortex express either/both of two isoforms of glutamate decarboxylase (GAD): GAD65 and GAD67. GAD is the enzyme that catalyzes convertion of glutamate to gamma-aminobutyric acid (GABA). In cortical interneurons, GAD65 is activated by phosphorylation and is predominant in the axonal endings while GAD67 is inhibited by phosphorylation as is found mainly in

the cell soma (Esclapez et al., 1994; Wei et al., 2004). One of the main ways to distinguish different subtypes of the cortical interneurons is using three specific calcium binding proteins (CBPs). The CBPs are a family of proteins that take part in the calcium cell signalling pathway and thus in a variety of functions within the cell. Of importance to neurons, cellular calcium is required in vesicle fusion and as a secondary messenger in signal transduction. The CBPs that are markers for interneuron subpopulations are parvalbumin (PV), calbindin (CB) and calretinin (CR). These in turn correspond to three broad discharge response classes. The fast-spiking interneurons and the irregular spiking interneurons express PV and CR respectively. The third class consist of bursting interneurons which have the ability to fire repetitively with a frequency adaptation. This class of interneurons overlaps with CB expression (Markram et al., 2004). It is also worth noting that about 40-50% of GABAergic interneurons in the cortex are parvalbumin positive while 15% are calretinin positive. Other groups of markers used to identify interneuronal subclasses are neuropeptides, namely somatostatin (SOM), neuropeptide Y (NPY), cholecystokinin (CCK) and vasoactive intestinal peptide (VIP). However, just as in the case of CBPs, one has to remember that virtually no single neuropeptide correlates with a single morphological or electrophysiological feature of the specific interneuron type (Markram et al., 2004). Still, a combination of markers might indicate a particular subtype. An example of a subdivision of interneurons based on the three most expressed markers in mice is shown in Fig 1.02 B.

Fig 1.01 Spectrum of cortical interneuron types depending on morphology and layer positioning. (A) Positioning, axon arborization and innervation patterns of several classes of the interneurons in the neocortex. Cell axons are shown in black while dendrites are shown in red. BPC: bipolar cell; ChC: chandelier cell; DBC: double bouquet cell; LBC: large basket cell; MC: Martinotti cell; NBC: nested basket cell; NGC: neurogliaform cell; SBC: small basket cell (adapted from Kubota, 2014).

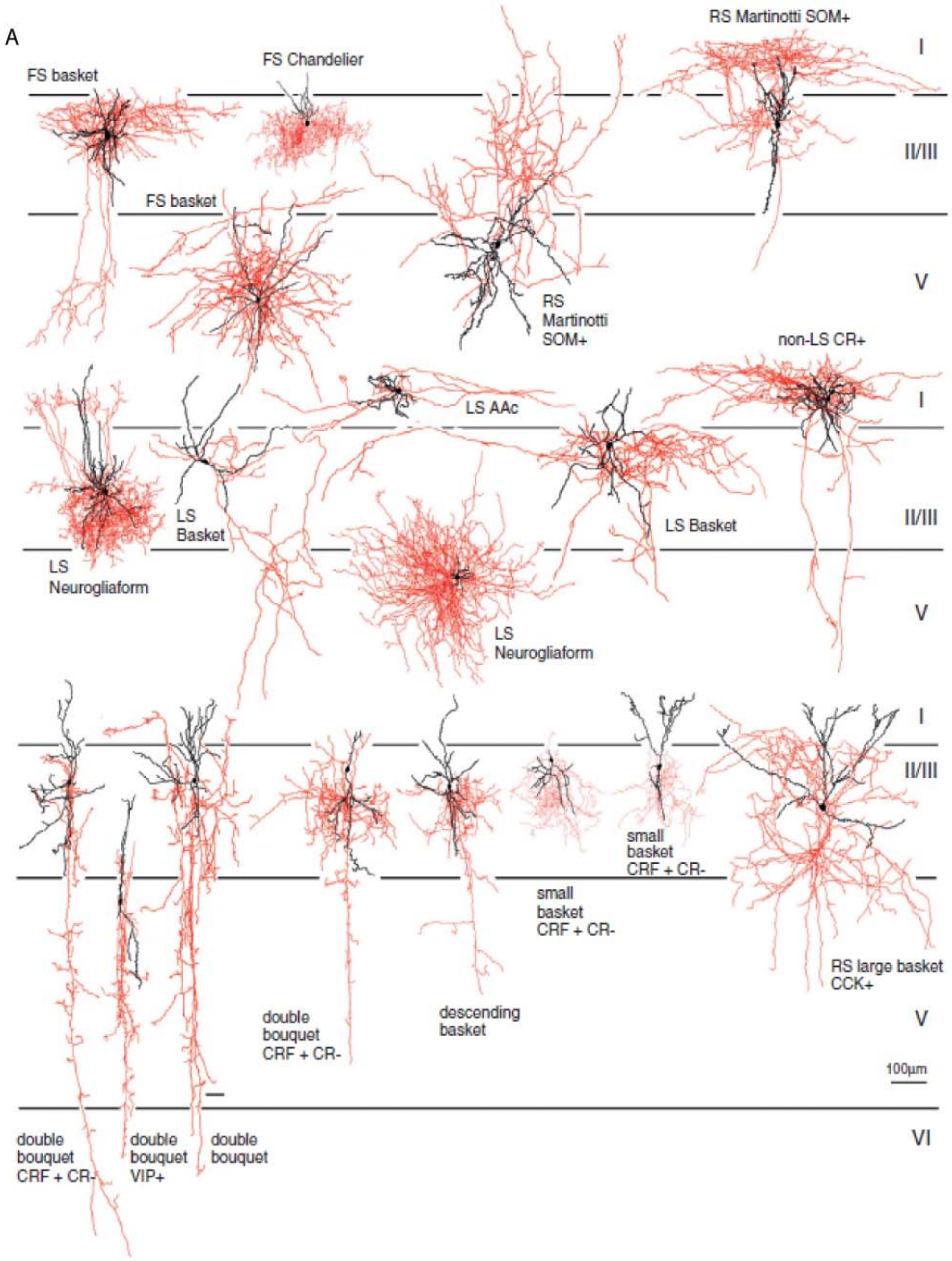
A
RS Martinotti SOM+
FS basket
FS Chandelier
I
II/III
FS basket
V
RS
Martinotti
SOM+
non-LS CR+
LS AAc
I
LS
Basket
LS Basket
II/III
LS
Neurogliaform
V
LS
Neurogliaform
I
II/III
small
basket
CRF + CR-
small
basket
CRF + CR-
RS large basket
CCK+
double
bouquet
CRF + CR-
descending
basket
V
100µm
double
bouquet
CRF + CR-
double
bouquet
VIP+
double
bouquet
VI

Fig 1.02 Cortical interneurons division according the site of contact with the excitatory neurons and biochemical markers expressed. (A) A model grouping the neocortical interneurons depending on the site of connection they make. Axons are shown in blue and dendrites in red, while axonal buttons are shown as blue dots and soma is of different colour for every cell type. The cells are positioned with pia on the top and white matter downwards (adapted from Markram et al., 2004). **(B)** Three largest cortical interneuron subgroups based on neurochemical markers, morphology, axonal targeting site on pyramidal neurons and electrophysiology. * Refers to some of the characteristic axon targets; ǂ refers to firing patterns induced by intracellular injections of depolarising currents; RSNP: regular-spiking non-pyramidal BSNP: burst-spiking non-pyramidal; FS: fast spiking. (adapted from Wonders and Anderson 2006).

A

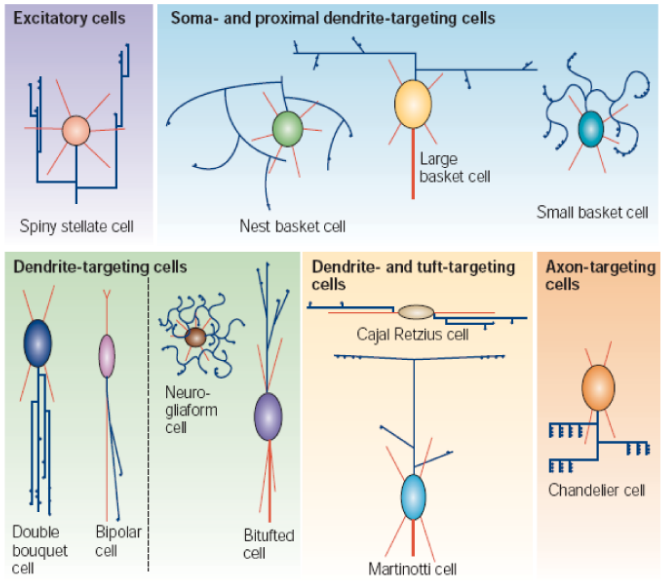

B

Neurochemical marker	Relative % of GABA+ cells	Characteristic morphology	Axonal targeting on projection neurons*	Intrinsic physiology‡
Somatostatin	~30%	Small basket	Proximal dendrites/soma	RSNP
		Martinotti	Distal dendrites	BSNP
Parvalbumin	~50%	Large basket	Proximal dendrites/soma	FS
		Nest basket	Soma	FS/RSNP
		Chandelier	Axon initial segment	FS
Calretinin	~15%	Small bipolar	Proximal dendrites; also, other GABA+ cells	RSNP/BSNP

In this study, I have used three markers of the cortical interneuron subpopulations: parvalbumin, calretinin and somatostatin. Parvalbumin is a calcium binding protein expressed in approximately half of the cortical interneurons. It is mainly a marker of the two large subpopulations of the cortical inhibitory cells: large basket cells and chandelier cells. Unlike other calcium binding proteins, parvalbumin has a strong affinity to both calcium and magnesium ions, being bound to the latter during the resting state (Haiech et al., 1979). With the influx of calcium, magnesium dissociates slowly from the parvalbumin making it the slow-onset calcium buffer and allowing biexponential decay of calcium transient, with an accelerated initial rate of this transient (Lee et al., 2000). This in turn has an effect on the paired-pulse ratio - a ratio of amplitude of the second response to first; which in turn is a measurement of the synaptic plasticity (Caillard et al., 2000). Study of parvalbumin deficient mice showed that this CBP acts as a potent inhibitor of paired-pulse facilitation (Caillard et al., 2000). Furthermore, these fast spiking cells have been suggested to be involved in gamma oscillations – a pattern of neuronal activity that exhibits a frequency between 30-80Hz - which in turn are hypothesised to be implicated in higher functions, for example perception and information processing in the brain (Grey and Singer, 1989; Sohal et al., 2009). Parvalbumin is not expressed in the rodent brain until late in the second postnatal week when it starts to be expressed in the visual cortex around the time of eye opening (Alcantara et al., 1993; Patz et al., 2004). It has been suggested that the expression of parvalbumin in the interneurons might be regulated by the formation of functional synapses with the excitatory cell (Sugiyama et al., 2008, Donato et al., 2013).

Another CBP used in this study, calretinin, is expressed in approximately 15% of cortical interneurons in rodents. It belongs to the family of calbindins, together with calbindin and secretagogin; and just like its other two family members it contains six EF-hand calcium binding subunits. However, in the case of calretinin only domains 1-4 are fully functional with the domain 5 having low affinity for calcium while domain 6 remains inactive (Stevens and Rogers, 1997; Faas et al., 2007). Calretinin regulates intracellular calcium ions in a non-linear manner - at calcium influx at low basal calcium levels it act like a slow buffer allowing the calcium signalling to

diffuse within the cell. However, if the basal levels are high, it acts like a fast buffer immediately binding the free calcium ions (Dargan et al., 2004). Little is known when it comes to the transcriptional regulation of calretinin but it seems to undergo cell-specific regulation (Billing-Marczak et al., 2004). It is worth noting that large subgroups of interneurons that is believed to contain calretinin are the multipolar interneurons expressing vasointestinal peptide (VIP) (Rudy et al., 2011). In this study I have not investigated this particular subpopulation of interneurons; these cells suppress the activity of the somatostatin expressing cells and a proportion of interneurons containing parvalbumin, and subsequently leading to the disinhibition of the circuit (Pi et al., 2013).

Unlike parvalbumin and calretinin, somatostatin is a neuropeptide and is expressed in approximately 30% of cortical interneurons. It is mostly known for its role in regulating the release of the growth hormone from the anterior pituitary gland by acting as an inhibitory neurotransmitter on the pituitary somatotroph cells. It also plays a role as a neuromodulator and as a regulator of cell proliferation in some tumours (Volante et al., 2008). In cortical interneurons it seems to be predominantly used as a marker of particular subtypes of inhibitory cells - Martinotti and X94 cells - but can also be expressed together with other interneuronal markers (Ma et al., 2006). Although the proportion of somatostatin expressing interneurons in the cortex is lower than that of parvalbumin expressing interneurons, their morphological and electrophysiological variety is large (Wang et al., 2004; Ma et al., 2006). From the literature, I could not find what the exact role of somatostatin is in the cortical interneurons but assuming its inhibitory role as a neurotransmitter as well as neuromodulator it is possible that it acts in tandem with GABA to provide a variety of inhibitory functions associated with the somatostatin expressing cells.

1.2.2.3 Electrophysiological features

Together with the morphological and biochemical classification of the interneurons it is worth mentioning the electrophysiological features that distinguish the cortical inhibitory cells. This feature is to some extent connected with the two other

interneuronal classifications, but there are also cases where there is no correlation between the features mentioned above. Still, some properties like firing frequency (pattern), threshold for triggering the action potential or its membrane potential could contribute to subclassification of the cortical interneurons (Ascoli et al., 2008). Most probably the most used electrophysiological feature of the inhibitory cells is the firing pattern which would be used to classify the interneurons into the cells that are fast-spiking, non-fast spiking, adapting, irregular and so on (Fig 1.03).

Taken together, regardless of the subclassification used it is clear that, although being a much smaller subgroup of cortical neurons than excitatory neurons, interneurons are a complex and much varied group of cells, both morphologically and physiologically (Fig 1.04). Nonetheless it has to be appreciated that it is this variation that enables the inhibitory cells to perform their circuit function with extreme precision.

Fig 1.03 Firing patterns of the cortical inhibitory cells. Wide variety of the firing properties of the cortical interneurons allows for a more flexible tuning of their targeted cells (adapted from Ascoli et al., 2008).

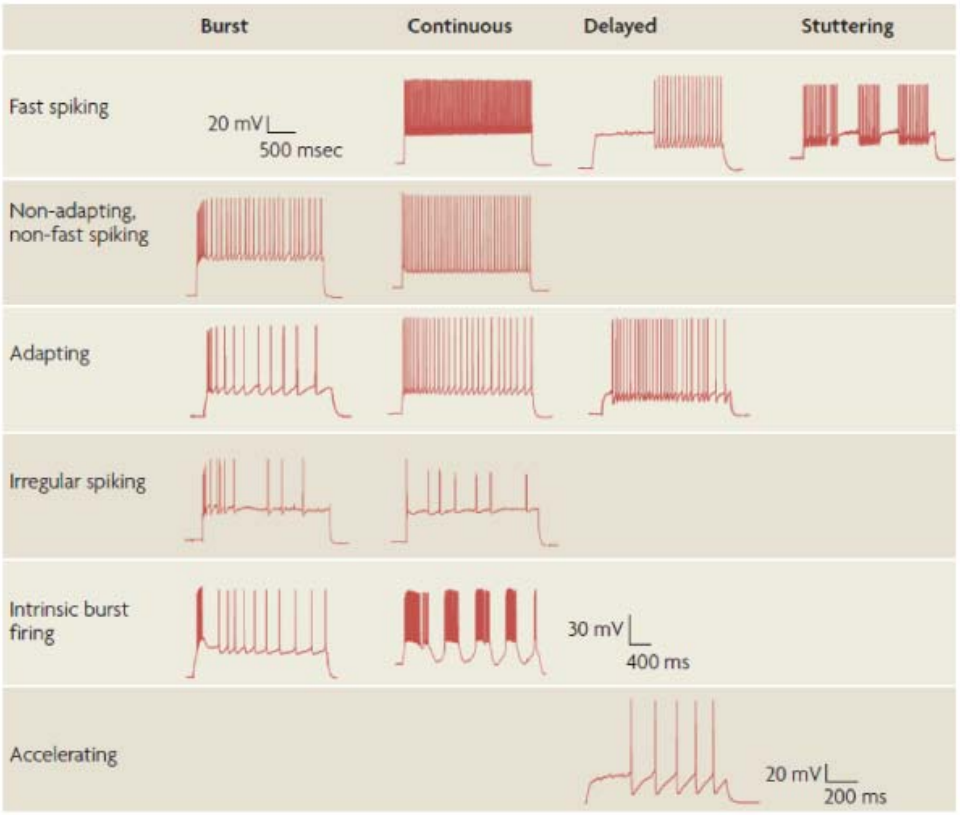

Fig 1.04 Summary of cortical interneuron classification: integration of morphological features, connectivity, biochemical markers expressed and intrinsic properties. A wide range of cortical interneurons is categorised using a combination of different neuronal characteristics. Highlighted in black are the properties characterising a basket cell (adapted from Kepecs and Fishell 2014).

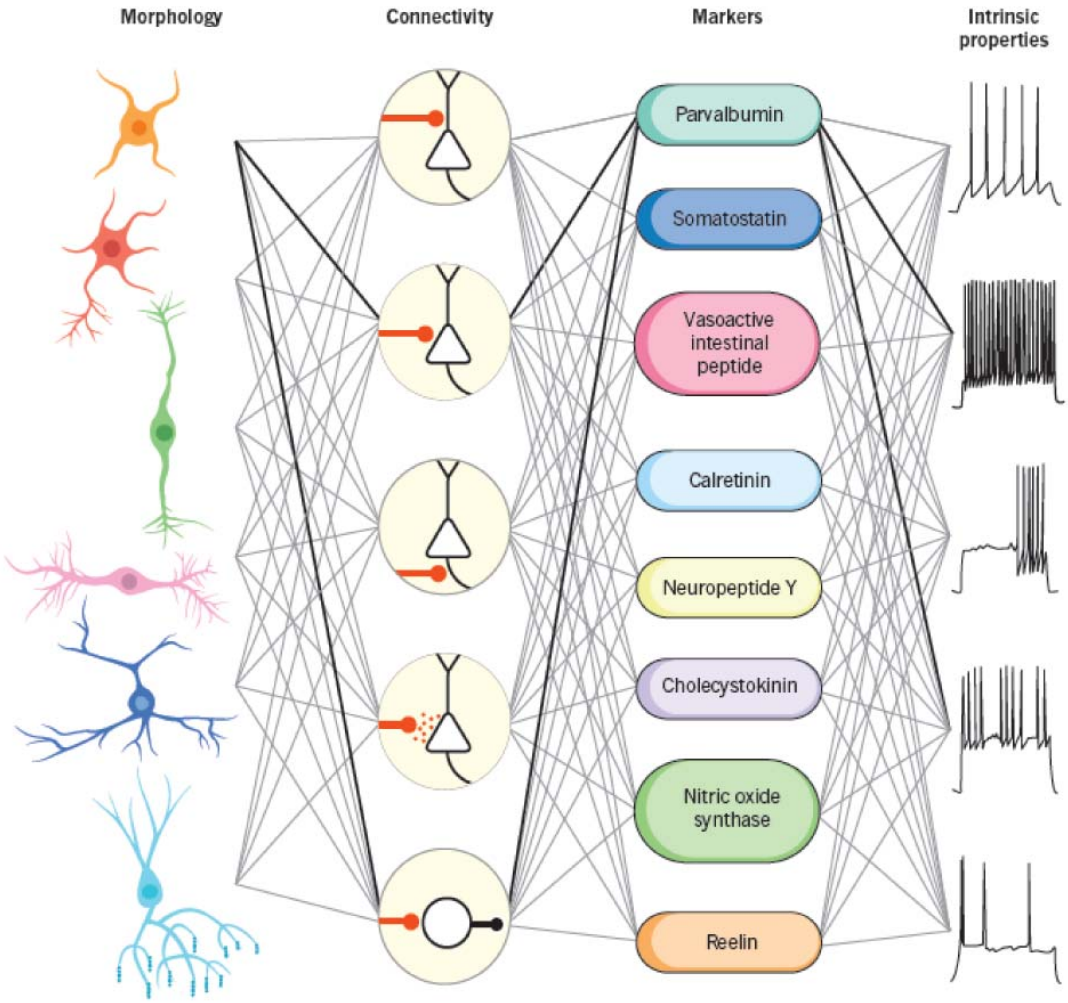

1.2.3 Birthplace and fate acquisition of different types of cortical interneuron

Unlike projection neurons, interneurons are primarily born in the ganglionic eminence (GE), a structure at the base of the telencephalon (subpallium) in rodents. The GE is a transient structure during development which in adult brain gives rise to the basal ganglia. It can be divided into three distinct parts: medial GE (MGE), caudal (CGE) and lateral (LGE) (Fig 1.05 A). The interneurons born in the LGE are mainly destined to migrate rostrally to populate the olfactory bulb in rodents, but also have a minor contribution to the cortical interneuron population (reviewed in Metin et al., 2006). However, none of the interneuron subpopulations investigated in this study originated from the LGE; hence the contribution to the neocortex of interneurons from the LGE will not be mentioned further. A large portion of the CGE-born interneurons will populate the neocortex, though most of them will travel to the caudal parts of the telencephalon. The majority of the cortical interneurons originate in the MGE, from where they migrate laterally and, when reaching the cortex, spread uniformly according to their birthdate. It is worth noting that there is no evidence for cortical contribution to the interneuron pool in rodents. However, in human neocortex, there are two distinct lineages of cortical interneurons (reviewed in Letinic et al., 2002). The first lineage, contributing 65% of the cortical interneurons, is created in neocortical ventricular zone (VZ) and subventricular zone (SVZ) from progenitors expressing mammalian achaete-schute homolog 1 (Mash1). The other one is negative for Mash1 and originates from the GE, contributing about 35% of cortical interneurons. The reason for such discrepancy between mouse and human brain is most probably due to the immense increase in the brain size and complexity between the two species. This might also imply that due to enlargement of the neocortex in humans, an extra source of locally born interneurons evolved that would migrate in a quicker manner than their tangentially migrating counterparts.

In the rodent brain, the majority (~70%) of the cortical interneurons originate from MGE with the remaining 30% being born in CGE (Miyoshi and Fishell, 2010). Recent studies showed that a small proportion of cortical interneurons expressing both parvalbumin and somatostatin arise from the preoptic area (POA) and MGE

(Brown et al., 2011; Ciceri et al., 2013). The MGE and CGE born subpopulations of interneurons are generated in two distinct neurogenic waves. Production of the interneurons in the MGE starts as early as embryonic day 9.5 (E9.5) with a peak around E13.5. Generation of the CGE-derived interneurons shows a similar pattern but shifted by 3 days (starts around E12.5 with a peak at E16.5) (Miyoshi and Fishell, 2010, original papers Miyoshi et al. 2007 and 2010 respectively). Similarly to the cortical projection neurons, the birthdates of the interneurons within particular parts of the GE are correlated to their position within the neocortex **(**Fig 1.05 B**)**. The MGE-derived interneurons follow a similar 'inside-out' pattern to that of the migrating pyramidal cells as well as matching their birthdates. However, the CGE-born cells contribute about 75% of their total number to more superficial layers and approximately 25% to the deeper layers of the cortex (Miyoshi et al., 2010). This phenomenon occurs regardless of the birth time of the CGE-derived interneurons.

Unlike production of the excitatory cells in the proliferative zones of the dorsal telencephalon in the rodent brain, very little was known about interneuron formation in the ganglionic eminences. A recent study into the topic revealed the presence of radial glial progenitors (RGP) at the ventricular zone (VZ) of the MGE and POA that undergo asymmetric division giving rise to another radial glial cell and a daughter cell with a short process (Brown et al., 2011). The daughter cell then uses the glial process to migrate to the subventricular zone (SVZ) and either undergoes multiple symmetric divisions or detaches and starts migrating tangentially towards the cortex (Fig 1.06; Brown et al., 2011).

The birth place of the cortical interneurons also correlates with their neurochemical subgroups. The largest subtype of interneurons in the cortex, the parvalbumin expressing cells, is exclusively born within the MGE. Other types of MGE-derived cortical GABAergic interneurons are those containing somatostatin (mainly generated in MGE, with a minor contribution from CGE) and NPY (about half of them generated in the MGE, other half is produced in the CGE). There is also a minor input from MGE to the population of calretinin positive cells, which are mainly generated in the dorsal part of the CGE (for summary see Fig 1.05 C). What

might affect, and probably shape, the neurochemical fate of the cells within the proliferative zones of the ganglionic eminences is a cocktail of specific transcription factors (TFs) expressed in the GE progenitors. The main TF affecting generation of various types of cortical interneurons in the MGE is Nkx2.1. This TF contains a homeodomain (a structural domain in a protein that has an ability to bind DNA or RNA) and is expressed in the proliferative zone within the MGE but not in other parts of the ganglionic eminences. Nkx 2.1 knockout results in virtually no parvalbumin, somatostatin and NPY expressing cells without affecting calretinin expression in cortical dissociated culture (Xu et al., 2004). Together with other TFs Nkx 2.1 is expressed in progenitors and the cells that exited the cell cycle, but is downregulated when the cell is about to migrate into the cortex. This change in the Nkx2.1 expression might be directly due to change in this TF's translation as an effect of triggered migration. Another possible explanation for the Nkx2.1 downregulation in the migrating interneurons is moving away from the area of high concentrations of the signalling molecules controlling the NKx2.1 expression, namely fibroblast growth factor 8 (FGF8) and sonic hedgehog (SHH). Most probably it is the latter explanation since reduction in the hedgehog signalling in the progenitor pool of the MGE resulted in decrease of the Nkx2.1 levels and eventually reduction in the normally cycling progenitors' ability to produce interneurons expressing parvalbumin and somatostatin (Xu et al, 2005, reviewed in Wonders and Anderson, 2006). Another TF expressed by progenitors in the MGE is Lhx6, a member of the LIM homeodomain (cysteine-rich zinc-binding domain) gene family. It is suspected to take part in triggering the migration of interneurons into the cortex, which was implied by Lhx6 knockdown which showed reduction in migrating interneurons with no effect on GABA levels in the cortex (reviewed in Wonders and Anderson, 2006). Unlike Nkx2.1, it is expressed throughout the interneuronal journey to the neocortex. It is downregulated at the stage of differentiation of the MGE derived cells into interneurons that are positive for more than a single interneuron marker. The last major TFs playing a role in the interneuron fate acquisition and later in differentiation and maturation are the family of distal-less homeobox (Dlx) transcription factors, mainly Dlx1/2. When Dlx1 and 2 are both knocked out there is a reduction in NPY and SST expressing cortical interneurons, while bipolar

calretinin-containing interneurons are practically missing from the cortical culture (Xu et al., 2004). Knockout of Dlx1 results in the calretinin and somatostatin expressing interneurons without affecting the parvalbumin expressing subgroup (Cobos et al., 2005). Additionally, Dlx 1 and 2 appears to be indispensable for proper tangential migration of the interneurons from the ventral telencephalon to the cortex (Anderson et al., 2001). The transcription factors expressed in the interneurons both during proliferation in VZ/SVZ and throughout their migration to the cortex and maturation within it are presented in Fig 1.07.

Fig 1.05 Birthdates and birthplaces of the main subgroups of the murine cortical interneurons. (A) Positioning of the ganglionic eminences within the brain and the main classes of the interneurons migrating to the cortex. Note: PV: parvalbumin-expressing cells; CR: calretinin expressing cells; SS: somatostatin-expresing cells (adapted from Metin et al., 2006). **(B)** Birthdate and final positioning of the GABAergic interneurons in the neocortex. The cortical position of the majority of CGE derived interneurons is not dependent on their birthdate (adapted from Miyoshi and Fishell, 2010). (**C**) Birthplaces of specific neurochemical types of the cortical interneurons (adapted from Wonders and Anderson, 2006).

A

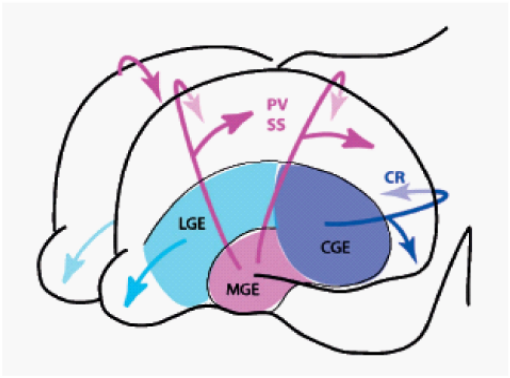

B

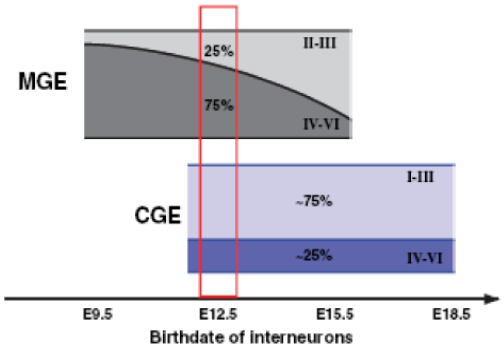

C

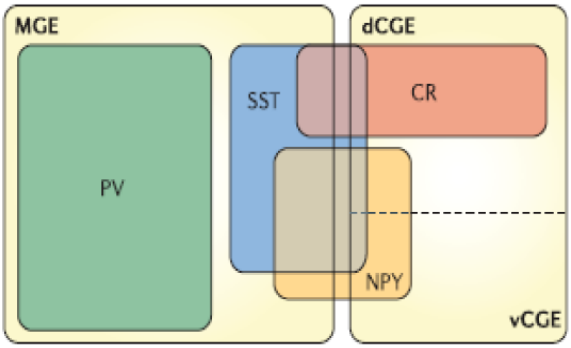

Fig 1.06 Model of generation of the layer-specific cortical interneurons in the rodent medial ganglionic eminence (MGE). Cortical interneurons sharing clonal origin (early neurogenesis – red; late neurogenesis – blue) exhibit different positioning within the cortex. Cells born earlier form vertical or horizontal clusters (red parentheses) while later born cells generate fewer cells that are restricted to a particular layer. Final cortical distribution of different types of interneurons is further shaped by cell death (empty cells) (figure adapted from Sultan et al., 2014).

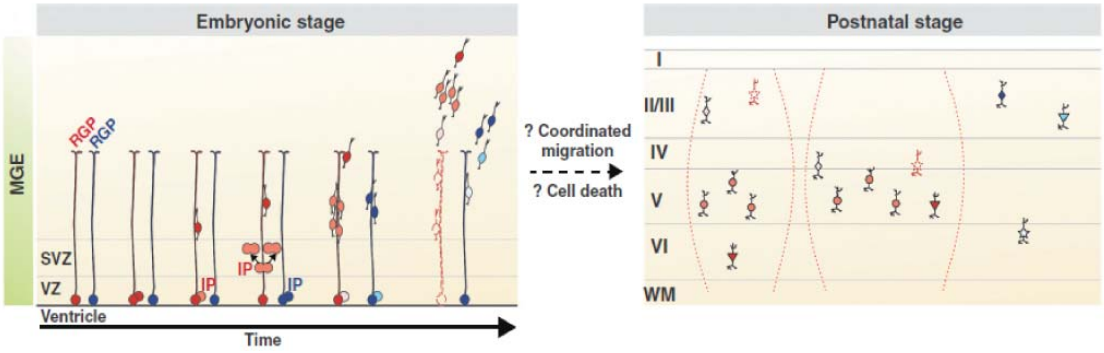

Fig 1.07 Transcriptional regulation of cortical interneuron specification and differentiation in the rodent ganglionic eminences (GEs), preoptic area (POA) and cortex. (A) A specific cocktail of transcription factors is responsible for a particular step in the cortical interneurons development from proliferation in the subventricular/ventricular zones (SVZ/VZ) of GEs and POA to differentiation and survival in the neocortex. dCGE: dorsal caudal ganglionic eminence; dMGE – dorsal medial ganglionic eminence; RLN – reelin; SST – somatostatin; VIP – vasoactive intestinal peptide; CR – calretinin; PV – parvalbumin; NPY – neuropeptide Y (adapted from Kessaris et al., 2014). (B) Ganglionic eminences and preoptic area in the developing cortex: lateral ganglionic eminence (LGE - blue), dorsal medial ganglionic eminence (dMGE – orange), medial ganglionic eminence (MGE – orange/red), preoptic area (POA – green), dorsal caudal ganglionic eminence (dCGE – purple). R – rostral, C- caudal.

A

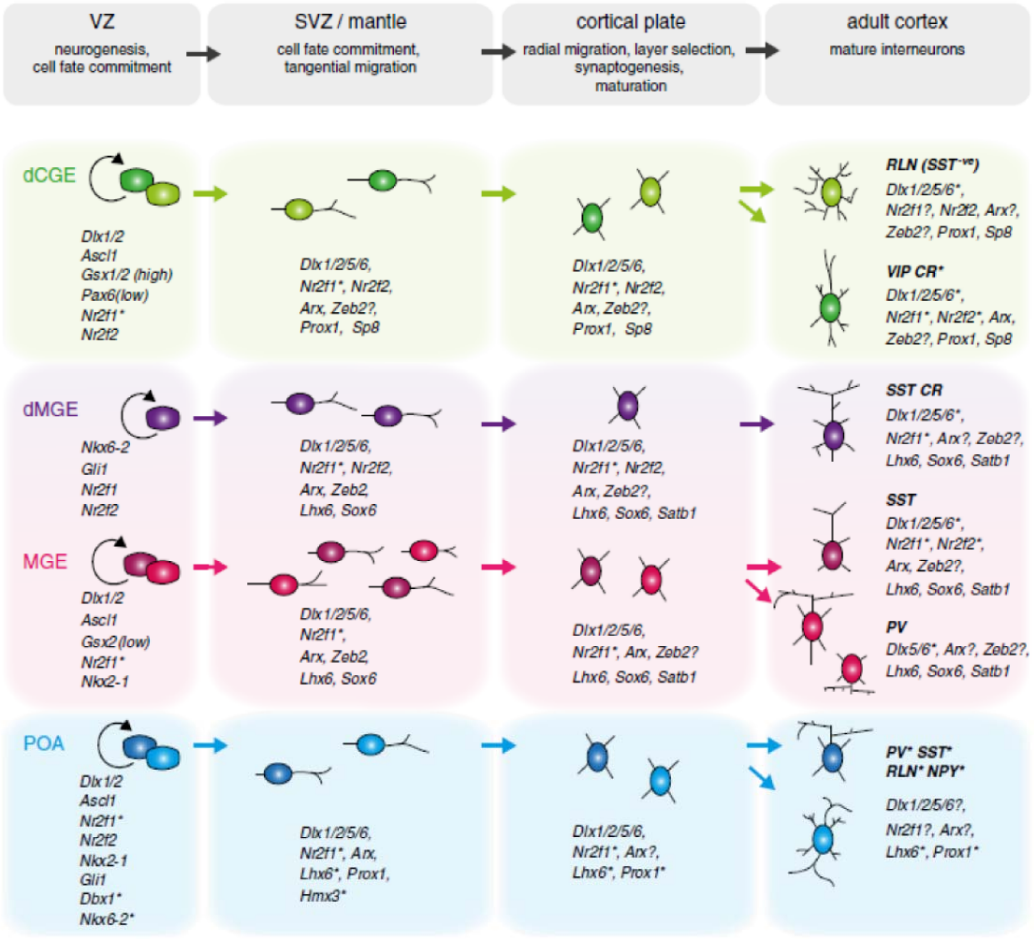
VZ
neurogenesis, cell fate commitment
SVZ / mantle
cell fate commitment, tangential migration
cortical plate
radial migration, layer selection, synaptogenesis, maturation
adult cortex
mature interneurons
dCGE
Dlx1/2
Ascl1
Gsx1/2 (high)
Pax6(low)
Nr2f1*
Nr2f2
Dlx1/2/5/6,
Nr2f1*, Nr2f2,
Arx, Zeb2?,
Prox1, Sp8
Dlx1/2/5/6,
Nr2f1*, Nr2f2,
Arx, Zeb2?,
Prox1, Sp8
RLN (SST-ve)
Dlx1/2/5/6*,
Nr2f1?, Nr2f2, Arx?,
Zeb2?, Prox1, Sp8
VIP CR*
Dlx1/2/5/6*,
Nr2f1*, Nr2f2*, Arx,
Zeb2?, Prox1, Sp8
dMGE
Nkx6-2
Gli1
Nr2f1
Nr2f2
Dlx1/2/5/6,
Nr2f1*, Nr2f2,
Arx, Zeb2,
Lhx6, Sox6
Dlx1/2/5/6,
Nr2f1*, Nr2f2,
Arx, Zeb2?,
Lhx6, Sox6, Satb1
SST CR
Dlx1/2/5/6*,
Nr2f1*, Arx?, Zeb2?,
Lhx6, Sox6, Satb1
MGE
Dlx1/2
Ascl1
Gsx2(low)
Nr2f1*
Nkx2-1
Dlx1/2/5/6,
Nr2f1*,
Arx, Zeb2,
Lhx6, Sox6
Dlx1/2/5/6,
Nr2f1*, Arx, Zeb2?
Lhx6, Sox6, Satb1
SST
Dlx1/2/5/6*,
Nr2f1*, Nr2f2*,
Arx, Zeb2?,
Lhx6, Sox6, Satb1
PV
Dlx5/6*, Arx?, Zeb2?,
Lhx6, Sox6, Satb1
POA
Dlx1/2
Ascl1
Nr2f1*
Nr2f2
Nkx2-1
Gli1
Dbx1*
Nkx6-2*
Dlx1/2/5/6,
Nr2f1*, Arx,
Lhx6*, Prox1,
Hmx3*
Dlx1/2/5/6,
Nr2f1*, Arx?,
Lhx6*, Prox1*
PV* SST*
RLN* NPY*
Dlx1/2/5/6?,
Nr2f1?, Arx?,
Lhx6*, Prox1*

B

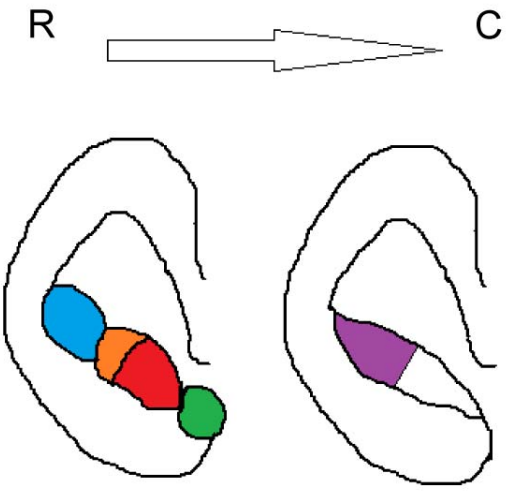
R
C

1.2.4 Tangential migration of cortical interneurons

Unlike the pyramidal neurons in the cortex, the interneurons have a long and winding road to travel from the ganglionic eminences to their destined position in the cortex. The processes involved in triggering the migration from the GE, the guidance factors directing the migrating cells and the precise mechanisms of detecting such cues are the main keys to successful interneuron migration.

To begin with, the immature interneuron has to be stimulated to leave the proliferative zone of the GE and start its initially non-directional motion. Recent study has shown that the daughter cell migrating along the process of the radial glial cell nested in the VZ of the MGE attains a typical shape of tangentially migrating cells - a bipolar shape - when it is the furthest from its mother cell (Brown et al., 2011). How exactly it detaches and begins its migration remains unclear. The motogenic (movement stimulating) factors shown to have an impact on interneuron cell migration are hepatocyte growth factor/scatter factor (HGF/SF) and neurotrophins like brain-derived neurotrophic factor (BDNF) or neurotrophin-4. The former have been shown to stimulate the cell to migrate from the subpallial telencephalon in slice culture. Moreover, using antibodies against HGF/SF inhibits such movement, implying the need for this factor in stimulating the cell to migrate (Powell et al., 2001; reviewed in Marin and Rubenstein 2001). As for the neurotrophins as motogenic factors, BDNF and neurotrophin-4 have been shown to increase the rate of migration of the MGE interneurons via the TrkB signalling pathway (Polleux et al., 2002).

So how exactly does an interneuron react to the molecular cues stimulating its migration? The mechanism behind the response to the motogenic cues is not clear but the movement of the cell triggered by the motogenic cues was believed not to have an apparent direction. However, it has recently been shown that this randomness of tangential migration seems not to be true and the clones of the same radial glial progenitors tend to cluster and migrate together (Brown et al., 2011, Ciceri et al., 2013). Generally, the direction of cell motion is based on the polarity of

the cell i.e. the highly polarised part of the cell is a marker of the direction of cell movement. From there a leading process is generated, which generally works similarly to that of the growth cones of axons, i.e. they are a form of probe that reacts to external cues and adjust its behaviour accordingly. The movement of the neuronal cell as a reaction to the information from the leading process is known as locomotion. There are three distinct steps of locomotion. The first is the extension of the leading process to probe the surroundings. Next, there is a translocation of the nucleus in the direction of the leading process, a process known as nucleokinesis (Fig 1.08 A; see Metin et al., 2006 for more details regarding proteins and dynamics involved in this process). Lastly, the remaining 'trailing' process is eliminated and the whole cycle begins again. These three phases of cell locomotion are used in interneuron migration with one difference being that the cell uses two branches of the leading process to search for the migration permissive area (Fig 1.08 B; for more details see a review by Marin et al., 2010). This greatly increases the area scanned and most probably speeds up interneuron migration so that they can arrive at their final destination in the cortex and mature in time to form connections with other cortical neurons.

The navigation mechanism of the migrating interneurons reacts to chemoattractants and chemorepellents of the ventral telencephalon. One of the best studied chemoattractants for the MGE-born cells is Neuregulin-1 (Nrg1), an epithelial growth factor (EGF) receptor family member. Most probably, Nrg1 acts via a member of the receptor tyrosine-protein kinase ErbB4 and PI3K cascade, stimulating locomotion. In the developing telencephalon, there are two Neuregulin1 isoforms: type III Nrg1, which is expressed by a permissive migratory route through the LGE to the cortex; and type I/II Nrg1 which is expressed exclusively in the pallium and stimulates the movement of the migrating interneurons from MGE towards the forming cortex (Marin et al., 2010). It is worth noting here that there are two major routes for the tangenentially migrating MGE-derived interneurons: one through LGE towards the intermediate zone (IZ) of the neocortex, while the other heads more ventrally first, bypassing the repulsive striatum and entering the neocortex via the marginal zone (MZ) (Fig 1.09). The main chemorepellents preventing the migrating

Fig 1.08 Mechanism of the interneuron locomotion. (A) Proteins involved in the dynamics of nucleokinesis. Note the pulling force of the microtubule system on the nucleus (N) and the pushing motion of the myosin II behind it (adapted from Marin et al., 2010). **(B)** Changes in the morphology of the leading process in the MGE-derived interneuron migration. Note the nuclear translocation step (T), extension and branching of the leading process and the retraction of the one that was not used for leading the migration (adapted from Metin et al., 2006).

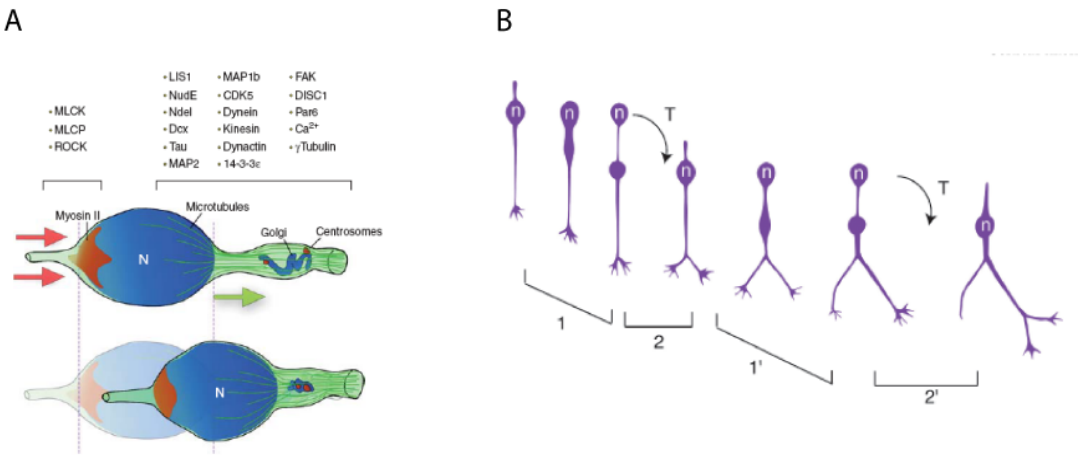

interneurons passing through the striatum are the class III semaphorins (Sema3A/F) expressed there, acting via Neuropilin1 and 2 (Nrp1 and Nrp2), co-receptors to the tyrosine kinase receptor (Fig 1.09 B; for a review see Marin et al., (2010)). Additionally, Slits, ligands for the roundabout (Robo) receptors that repel the migrating cells from the midline, are speculated to have an effect on the migrating GABAergic interneurons by being expressed in the striatum, though it has been shown that the knockout of Slit 1 and 2 causes no change in the avoidance of this part of the brain by the migrating interneurons (reviewed in Nakajima (2007)). What is more, the neurons are repelled from crossing the midline most probably also by Slits (Rajagopalan et al., 2000). Lastly, it has been shown that Cxcl12, a chemokine present in the meninges and the intermediate progenitors (IP) in the SVZ, is involved in the regulation of the tangential migration via SVZ and MZ routes, by binding to its receptor (CXCR4) present on the migrating cells (Li et al., 2008; Lopez-Bendito et al., 2008; Tanaka et al., 2010).

The interneurons use the extracellular GABA levels in their vicinity to navigate when migrating tangentially through the forming cortex (Bortone and Polleux, 2009; Cuzon et al, 2006; Lopez-Bendito et al., 2003). During development, low concentrations of GABA can be detected in the marginal zone (MZ)/cortical layer I, the cortical plate and the subventricular zone, with a concentration gradient with highest expression in the MZ and lowest in the ventricular zone (Behar et al., 1996; Behar et al., 2000). Since these are the areas targeted by the migrating neurons, it has been suggested that this neurotransmitter has a chemoattractant role during cortical development. A study by Cuzon et al. (2006) also showed presence of GABA in the MGE around E14.5-E15.5. What is more, tangentially migrating cells express GABA receptors (namely $GABA_AR$, $GABA_BR$ and $GABA_CR$) on their surface (Behar et al., 1996; Behar et al., 1998; Behar et al., 2000; Cuzon et al., 2006). It has been shown that the activation of metabotropic $GABA_BR$ promotes migration of the radial glia cells while ionotropic $GABA_AR$ stops migration when the cells reach their targeted position (Behar et al., 1998). Both receptors have been shown to be present on the migrating interneurons (Lopez-Bendito et al., 2003; Cuzon et al., 2006). $GABA_BR$ has been shown to play a role in the choice of the route to the cortex – selectively

blocking this receptor in the migrating interneurons resulted in an increase in the number of cells taking the VZ/SVZ route instead of MZ and IZ routes (Lopez-Bendito et al., 2003). Conversely, it was a tonic activation of $GABA_AR$ on the tangentially migrating neurons that stimulated their motility (Cuzon et al., 2006). What is more, this study showed that tangentially migrating interneurons became more sensitive towards GABA on their route to the cortex and suggested it could be due to different subunit composition of the $GABA_AR$ at different stages of development (Cuzon et al., 2006). Taken together, GABA signalling is believed to take part in promoting and directing the tangential migration of the cortical interneurons.

Lastly, it is worth mentioning that another means of help for the migrating interneurons on their way up to the cortex might be other neurons. It has been suggested that they might use the previously formed cortico-thalamic tracts, a network of precocious neurons and corticofugal axons in the IZ and MZ of the cortex (Metin and Godement, 1996, Bystron et al., 2005). However, it is most likely that until the interneurons arrive in the IZ and MZ of the cortex they tend to use external guidance cues instead of potential scaffolds (for a review see Nakajima, 2007).

Fig 1.09 Tangential migration of the cortical interneurons. (A) The migratory routes from the MGE to the cortex. Migrating intenreurons tend to avoid the septum and the straitum most probably due to repulsive action of Slits and Semaphorins respectively. **(B)** A diagram presenting the chemoattractive and chemorepulsive guidance cues acting on the migratory MGE-derived interneurons. Note: CP: cortical plate; LV: lateral ventricle; Ncx: neocortex; Sp: septum; St: straitum; SDF1 – stromal cell-derived factor 1 (also known as CXCL12); NRG1 – neuregulin 1 (adapted from Hernandez-Miranda et al., 2010).

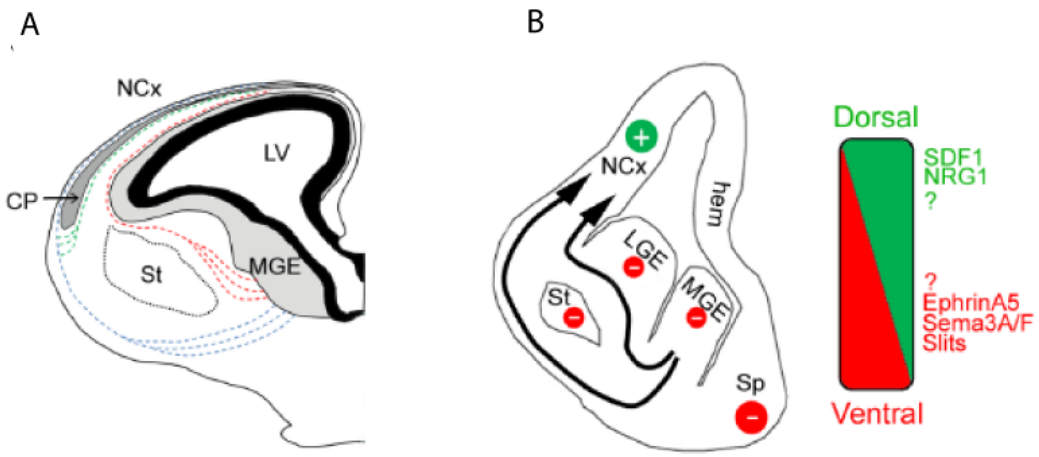

1.2.5 Radial migration of the interneurons in the neocortex

Upon arrival into the marginal zone and intermediate zone, the interneurons cease their tangential orientation of migration. Once they are 6 -8 days old they switch to radial relocation into their destined cortical layers which allows earlier born interneurons to invade the cortical plate earlier than those born later (Lopez-Bendito et al., 2008). The switch from tangential to radial migration occurs postnatally in mouse neocortex and is in parallel with the final stages of the projection neurons migration into the cortex. However, before the interneurons invade the cortical plate, they reside in the MZ for 1-2 days before migrating into the cortical plate (Lopez-Bendito et al., 2008). During that time, they exhibit multidirectional tangential migration within the MZ allowing them to spread throughout the cortical area, presumably via $GABA_A$ receptor activation in response to GABA concentration in this cortical region (Inada et al., 2011) and/or via Cxcl12/CxcR4 signalling (Lopez-Bendito et al., 2008). Since both $GABA_AR$ and Cxcl12/CxcR4 signalling have been involved in the start, direction and termination of the tangential migration in the MZ it would be interesting to investigate their relationship in regulation of these processes.

Once they reach cortex, the immature interneurons that migrated to the cortex via marginal zone will start a downward motion in the direction of the ventricle, while the interneurons migrating via the intermediate zone will migrate towards the pia in a manner similar to that used by the pyramidal neurons (Fig 1.10 A). The switch between dispersion of the interneurons and their radial migration into the cortex was suggested to be dependent on the Cxcl12/CXCR4 signalling as knockout of the CxcR4 resulted in a premature entry of these cells into cortical plate (Lopez-Bendito et al., 2008). The radial migration of the majority of the interneurons seems not to be directly dependent on reelin signalling, unlike the migration of the glutamatergic neurons (see a review by Nakajima, 2007; Pla et al., 2006). A transplantation study showed that interneurons lacking Dab1, an intracellular adaptor protein necessary for reelin signalling, exhibited correct laminar distribution in the wild type cerebral cortex, but wild type interneurons could not migrate properly in the Dab1 knockout

neocortex (Pla et al., 2006). On the other hand, the interneurons lose their correct laminar distribution in *reeler* mice (reelin null strain) strongly suggesting influence from the mispositioned pyramidal neurons (Hevner et al., 2004). What the interneurons most probably use to find their destined location in the cortex is the interaction between them and the simultaneously born projection neurons that have already settled within their destined layers (Hevner et al., 2004). It has been shown than the cortical interneurons use the extracellular GABA levels in their vicinity to navigate radially through the forming cortex (Bortone and Polleux, 2009; Cuzon et al, 2006; Lopez-Bendito et al., 2003). Once they reach their correct laminar position in the cortex they up-regulate the potassium/chloride cotransporter KCC2 which in turn changes the responsiveness of the cell to GABA via $GABA_AR$, resulting in a reduction in their motility (Bortone and Polleux, 2009; Inamura et al., 2012). It has been suggested that the KCC2 regulation could be cell-intrinsic but external cues are also believed to be playing a role in the slowing down of the tangentially migrating interneurons (Inamura et al., 2012). It is possible that these cues could be the excitatory cells, as embryonic neurons growing on postnatal neurons in culture had a markedly reduced motility (Inamura et al., 2012).

1.2.6 Integration of the cortical interneurons

The interneurons' location within the six layers of the newly formed cortex depends on the birthplace and birthtime of the cell. For instance, the cells born at E12.5 in the MGE will populate mainly layers IV-VI with a small number in layers II/III while CGE-born interneurons born at the same time are mainly found in layers I and II/III, with a minority populating layer IV-VI (Fig 1.10 B). This is in accordance with the time shift of the CGE-born interneurons with respect to those born earlier in the MGE which was already mentioned above. What is more, it seems that a proportion of cells sharing the same lineage tend not only to tangentially migrate together but also to cluster together both within the layer and cortical column (Fig 1.06; Brown et al., 2011, Ciceri et al., 2013). There seems to be two distinct lineages of interneurons born in the MGE – those responsible for production of interneurons that are to

populate deeper layers and those destined for the superficial layers (Ciceri et al., 2013).

As discussed before, birthdate and place of origin of cortical interneurons is not the sole factor that contributes to their layer-specific positioning. To correctly integrate into the cortical circuit, interneurons receive cues from the excitatory cells. Pyramidal cells in the neocortex could be classified based on the connections they make, which in turn correlates with the laminar position they occupy. Deeper layers are populated by subcortical projection neurons that target thalamus (layer VI) and other telencephalic and subcerebral structures (layer V) (as reviewed in Bartolini et al., 2013). Furthermore, a proportion of neurons in the deeper layers are callosal projection neurons that send their projections to the contralateral side of the cortex. Layer IV is occupied by associative neurons that connect to pyramidal cells in layers II/III, which in turn send projections callosally as well as to the deeper layers. Different sub-populations of interneurons are integrated into different parts of this cortical circuit (as seen in Fig 1.01). Parvalbumin expressing cells populate all layers except layer I, with chandelier cells being present in layers II and V and basket cells fairly evenly distributed across the cortex (Taniguchi et al., 2013; Rudy et al., 2010). Somatostatin expressing Martinotti cells were found throughout the somatosensory cortex layers, with a majority of cells in layers II-V and fewer cells present in layer VI (Wang et al., 2004). Taken together, the proper layer distribution of the cortical interneurons relies on a combination of both intrinsic information and extrinsic cues.

It is worth noting that with the onset of formation of functional connections, a few important processes occur. Firstly, once the cortical layers are formed and the interneurons stop migrating and begin forming synapses (around P7), a large proportion of them (~40%) undergo apoptosis (Southwell et al., 2012). Furthermore, it has been suggested that a large variety of cortical interneuron subgroups arises from a few initial classes generated in the ventral telencephalon through activity-regulated gene expression (Kepecs and Fishell, 2014).

Fig 1.10 Postnatal radial migration of the interneurons born in MGE and CGE. **(A)** Once tangentially migrating neurons reach the proper cortical column, they switch to radial migration. Depending on the route taken and both intrinsic signalling and external cues they either migrate down towards the ventricle (marginal zone route), migrate in the direction of the pia (subplate and intermediate zone routes) or turn towards the ventricle and then migrate towards the pia (SVZ route) (adapted from Faux et al., 2012). **(B)** Birthplace and origin of the cortical interneurons influence their cortical positioning. The diagram shows a case of layer-specific integration of E12.5-born interneurons after entering the cortical plate from both IZ and MZ. Note the majority of the later born interneurons from CGE populating more superficial layers while earlier born MGE-derived neurons occupy deeper parts of the newly formed cortex (adapted from Miyoshi and Fishell, 2011).

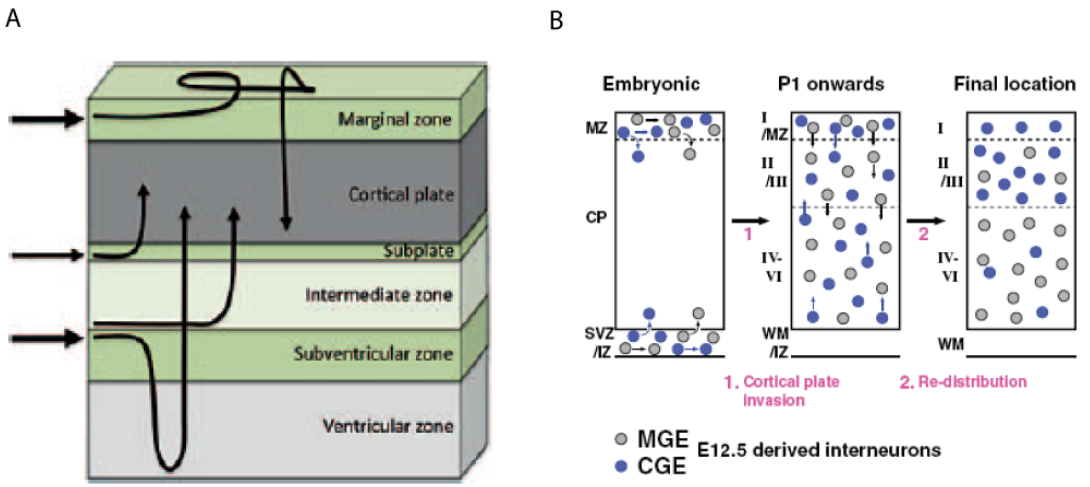

1.3 Disc1 in developing cerebral cortex

1.3.1 Disc1 and schizophrenia

Major psychiatric disorders like schizophrenia or bipolar affective disorder are complex and devastating brain diseases. Around 1 in 50 individuals will be affected by one or other at some point in their lives (Porteous and Millar, 2006). Apart from the relatively high incidence in the population (about 1% for both schizophrenia and bipolar disorder) these two disorders also share some clinical symptoms and therapeutic approaches, though this aspect still remains controversial (Millar et al., 2007). What is more, both disorders are believed to be an effect of both environmental and genetic factors (Roberts, 2007; Kas et al., 2009).

Environmental factors such as urban birth, season of birth, parental age, infection during pregnancy and pregnancy and birth complications have been shown to be associated with schizophrenia (Tsuang, 2000). As for the genetic factors behind this disease, support came from multiple family studies (including twin studies) and genome wide association studies (GWAS). Results from five twin studies of schizophrenia conducted in Europe and Japan showed higher concordance (presence of the same trait) in monozygotic (30-65%) than dizygotic twins (0-28%) (Cardno and Gottesman, 2000; Kringlen, 2000), though there were studies that showed even higher concordance in monozygotic twins for instance, 83% concordance in a Finish twin study (Cannon et al., 1998). Interestingly, children of both affected parents had a risk of developing schizophrenia similar to that of the identical twin with affected sibling (~46%) while the risk of offspring of a single affected parent to develop the disease was ~17% (reviewed in Tsuang, 2000). These results suggest that schizophrenia has a clear genetic component but it can be overcome by environment..

A search for genes behind schizophrenia has been facilitated by pedigree analysis of large families with high incidence of schizophrenia and population-wide GWAS studies. An example the former approach is a study of a large Scottish family with a

balanced translocation between chromosomes 1 and 11 (q42.1; q14.3) (Jacobs et al., 1970). Initially no phenotype was reported but follow-up data reported by clinicians showed a higher incidence of referrals to psychiatrist and mental institutions due to an array of psychiatric disorders ranging from schizophrenia to major depression (St Clair et al., 1990; Blackwood et al., 2001). Members unaffected by the translocation did not show any of those disorders (Blackwood et al., 2001). Interestingly, not all members with the translocation were affected - out of 29 affected, 8 were not diagnosed with any of those disorders; suggesting incomplete penetrance of this mutation and possible environmental factors affecting the development of the disease (Blackwood et al., 2001). It was established that *Disrupted-In-Schizophrenia-1* (*DISC1*), a large multi-exon gene with multiple isoforms, was present at the breakpoint on chromosome 1 (Millar et al., 2000b). As a result of the translocation, DISC1 expression was reduced at both transcriptional and protein levels, which in turn is the most likely cause of the frequent occurrence of psychiatric disorders in this family (Millar et al., 2005b). Variants in this gene were further linked to the increased incidence of psychiatric disorders using linkage studies conducted in Finnish, Taiwanese, North American, Icelandic and British populations (Porteous and Millar, 2006). However, there is mixed data regarding *DISC1* association to psychiatric disorders coming from GWAS studies. Some studies show that common variants in *DISC1* do not associate with schizophrenia (Mathieson et al., 2012) nor does *DISC1* locus appear in the large GWAS studies of genes associated with psychiatric disorders (Schizophrenia Psychiatric GWAS Consortium, 2011; Cross-Disorder Group of the Psychiatric Genomics Consortium, 2013). On the other hand, *DISC1* and some of its interactome genes have been found to associate with psychiatric disorders in studies conducted on smaller populations (Jia et al., 2012; Tomppo et al., 2012; Costas et al., 2013). These could be most likely due to failure of the GWAS studies to detect rare risk variants.

1.3.2 Disc1 structure and localisation in the mouse brain

DISC1 has multiple protein isoforms of which the predicted full-length Disc1 has 854 amino acids and is believed to consist of two regions: an N-terminus head region (~1-325) and an alpha-helix coil-coil-containing C-terminus domain (~326-854) (Chubb et al., 2008; Soares et al., 2011). The most conserved regions of the head domain have nuclear localisation signal and a short serine/phenylalanine rich motif, while the more conserved C-terminal tail domain consists of regions of potential coil-coils (Fig 1.11 A). The structure of both terminals suggests that Disc1 protein plays a role in protein-protein interaction and it has been shown to bind to PDE4B, NDE/NDEL, Lis1, dynein, dynactin and GSK3β to name a few (Fig 1.11 B; for a review see Chubb et al., 2008). Furthermore, several of the Disc1 interactors have also been linked to psychiatric disorders (Thompson et al., 2013; Chubb et al., 2008).

In the mouse brain, Disc1 is expressed broadly throughout the brain during development and adulthood (Schurov et al., 2004). In the embryonic mouse brain, the start of Disc1 expression is correlated with the time of neuronal cell birth and migration (around embryonic day 13.5) and is most prominent in the proliferative zones of the developing cortex, in hippocampus and olfactory bulb (Schurov et al., 2004, Mao et al., 2009). Furthermore, apart from the brain, Disc1 has been shown to be highly expressed in organs such as heart and placenta (Millar et al 2000b). Other organs that have been reported to express Disc1 are kidneys, liver and testes (as reviewed in Chubb et al., 2008).

1.3.3 Role of Disc1 in neurogenesis/proliferation

Disc1 is highly expressed in the proliferative zones of both developing and adult rodent brain which makes it a possible regulator of cell proliferation. To further elucidate this role in the neurogenic process, different animal models of Disc1 disruptions were studied. In one such model, generated to mimic the 1:11 translocation found in the Scottish family, truncation of the mouse Disc1 resulted in a reduction in neuronal proliferation at mid-gestation measured by the incorporation

of the S-phase marker, 5-bromo-2-deoxyuridine (BrdU) at E15.5 (Shen et al., 2008). Interestingly, the mice carrying the truncated Disc1 showed reduced cortical thickness with an enlargement of the ventricles resembling the anatomical characteristics found in the post-mortem brain tissue of schizophrenia patients. Similar observations were made in an extensive study of two mouse strains carrying ENU induced point mutation in the *Disc1* gene: L100P and Q31L (Clapcote et al., 2007). A further investigation of those two mutants revealed a relative reduction in the number of neurons in the cortex of a weaning animal as well as a decrease in BrdU incorporation at various embryonic ages (Lee et al., 2011). These two examples of different disruptions in the *Disc1* gene resulting in similar deficits in neuronal proliferation suggest its role in generation of the neurons in the brain but with no indication as to the potential mechanism behind this process. This was investigated by the Tsai group in an elegant study of Disc1 knockdown *in vitro* and *in utero* and its potential involvement in the regulation of proliferation via the canonical Wnt signalling pathway (Mao et al., 2009). Briefly, Disc1 knockdown resulted in a reduction in proliferation and the number of cycling cells at the proliferative zones due to increased cell cycle exit and earlier neuronal differentiation. Since expression of β-catenin, a vital downstream effector of the Wnt signalling pathway, is required for a stable progenitor pool (Zechner et al., 2003), the possibility that Disc1 regulates this particular signalling pathway was suggested. Moreover, Mao et al. (2009) has also shown Disc1 inhibition of GSK3β, a main regulator of β-catenin, through direct interaction. This in turn offered a possible mechanism for Disc1 role in regulating proliferation. Further evidence for this hypothesis came a year later from the same group in a study of Disc1 interaction with DIX domain containing-1 (Dixdc1), a homolog of *Dishevelled* and *Axin* genes that are part of the Wnt signalling pathway. Dixdc1 interacts with Disc1 mid- and C-term regions and the result of its knockdown resembles effects seen in the Disc1 knockdown phenotype: reduced proliferation due to the early cell cycle exit and an increase in neuronal differentiation (Singh et al., 2010). The interaction between these two molecules seems to co-regulate the Wnt signalling pathway as inhibition of the binding of Disc1 and Dixdc1 resulted in reduction of the TCF/LEF-reporter

Fig 1.11 Disc1 protein structure and interactors. (A) Structure of Disc1 full length protein predicted by the transcript data. The protein can be divided into two regions: the N-terminal head domain with the nuclear localisation signal (NLS) and serine/phenylalanine (SF) rich motif; and C-termianal domain with multiple coil-coil domains. This structure suggests Disc1 functions as a scaffold for other proteins. **(B)** Some of the known Disc1 interactors and their approximate binding position in relation to the exonic structure of DISC1. Panel above the exonic structure shows some of the studied human DISC1 variants that were associated with these regions (both figures were adapted from Chubb et al., 2008, superscripts on the bottom panel refer to the source papers).

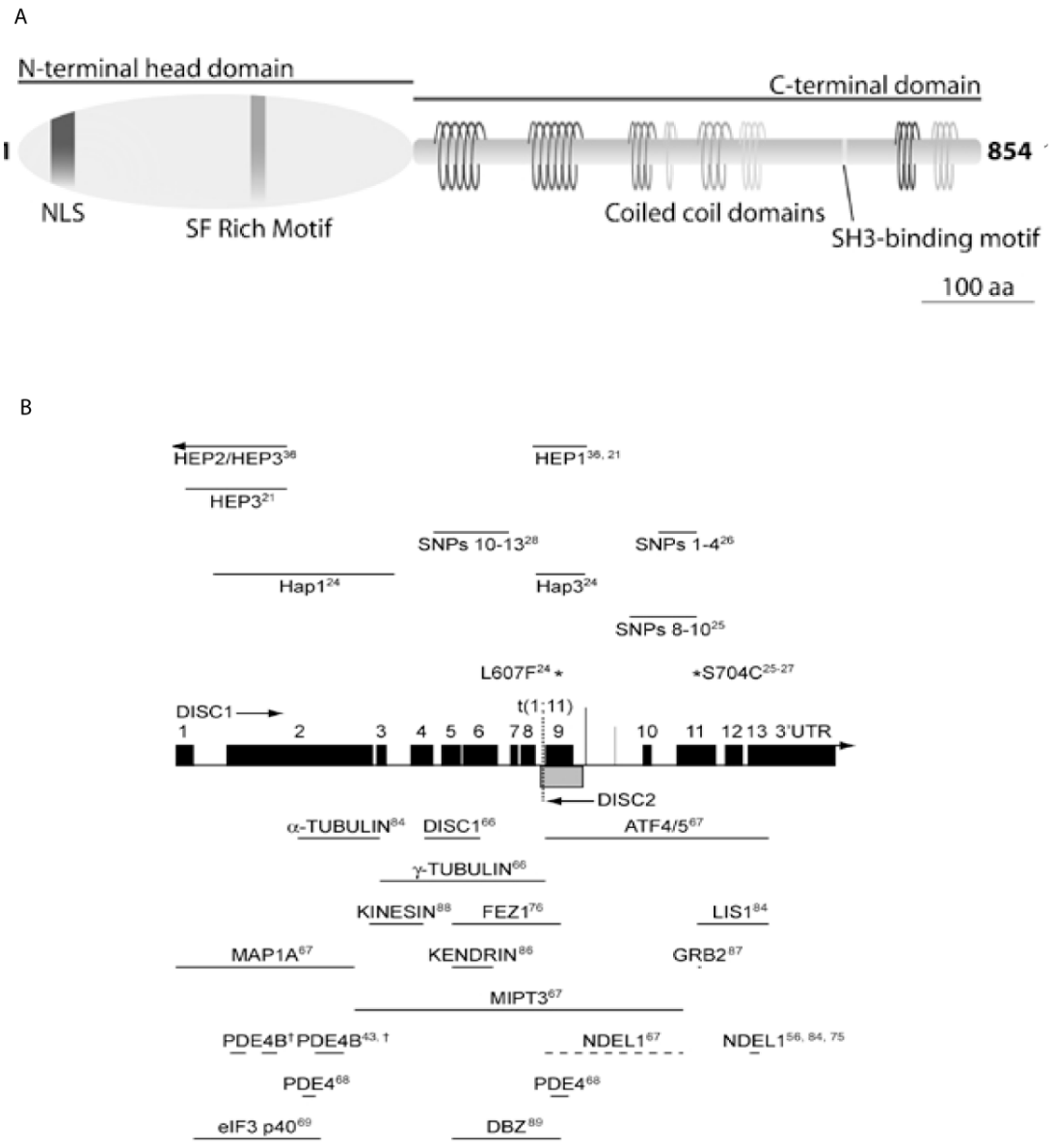

activity which in this experiment was a downstream target of the canonical Wnt signalling pathway. Moreover, the decrease in the proliferation rate due to knockdown of one of the genes can be rescued by overexpression of the other suggesting that they have an interchangeable role in regulation of the GSK3β/β-catenin pathway. In this line of investigation, rare and common human DISC1 variants have been examined in their ability to regulate GSK3β and thus cellproliferation (Singh et al., 2011). The rare A83V and more common R264Q and L607F DISC1 variants failed to activate canonical Wnt-pathway and reduced proliferation of the neural progenitors both *in vitro* and *in vivo*. Another possible Disc1 involvement in proliferation is through its interaction with Lis1 and Nde1/Ndel1. These proteins interact with dynamin, forming a complex that in turn regulates many cytoskeletal functions, for example proliferation and cell migration (Lam et al., 2010). It has been shown that in the absence of Lis1 the cortex is much smaller most probably as a result of wrongly oriented mitotic spindles in the proliferating NPCs in the cortical VZ (Yingling et al., 2008). What is more, Nde1 mutants show similar defects in cortical size and in the cortical progenitors to that of Lis1 mutants (Feng and Walsh, 2004). Interestingly, although Ndel1 rescues the proliferative defect in the Lis1 mutant it seems not to be involved in the cortical interneuron proliferation (Yingling et al., 2008; Feng and Walsh, 2004). Since Ndel1's protein sequence is quite similar to that of Nde1 (Bradshaw et al., 2013), lack of Nde1's involvement in interneuron proliferation is probably due to complementary expression of Ndel1 to that of Nde1. Nde1 is highly expressed in the VZ of the cerebral cortex while Ndel1, although abundantly expressed in the brain, is scarce in that region (Feng and Walsh, 2004).

1.3.4 Disc1 and adult neurogenesis

Disc1 expression in the adult brain is still fairly ubiquitous yet much lower when compared to the developing one. Interestingly, it is relatively highly expressed in the hippocampus and the olfactory bulbs of adult brain which are also the sites of the adult neurogenesis (Austin et al., 2004). A few groups have investigated Disc1 involvement in adult neurogenesis in the subgranular zone of the dentate gyrus (DG).

Lentivirus-mediated Disc1 knockdown in the adult mouse DG resulted in the reduced BrdU incorporation and mitotic index suggesting a reduction in proliferation, most possibly via GSK3β pathway (Mao et al., 2009). Conversely, overexpression of human DISC1 (hDISC1) in the adult DG resulted in an increase in the proliferation (Mao et al., 2009) strongly suggesting Disc1 being key to regulating normal proliferation in the adult hippocampus. Moreover, Disc1 knockdown seems to be causing premature integration of the newly born neurons, with increased dendritic growth and synapse formation (Duan et al., 2007). This might suggest earlier exit from the cell cycle and hastened maturation of the cells. A study of truncated Disc1 where a stop codon is introduced in exon 6 due to a naturally occurring 26 base pair deletion in exon 6 (Koike et al., 2006) has also been shown to decrease the proliferation in the DG (Kvajo et al., 2008). However, unlike Duan et al. (2007), Kvajo et al. (2008) showed a decrease in immature neurons as well as a disorganisation in the dendritic growth and a lower dendritic spine number, suggesting that these newly born cells might in fact be unable to mature and incorporate into the functioning DG circuit. Further investigation into the mechanism of adult neurogenesis revealed another possible mechanism through which Disc1 might regulate adult neurogenesis. Kim et al. (2009) showed that Disc1 knockdown in the hippocampus resulted in an increased activity of the AKT, a kinase which itself is a susceptibility gene for schizophrenia (Emamian et al., 2004). This resulted in changes in the morphogenesis of the neurons as well as defects in dendritic arborizations in the newly born neurons similar to those observed by Kvajo et al. (2008). By binding to AKT binding partner KIAA1212, Disc1 would inhibit the AKT activity and thus regulate the downstream signalling of the mTOR pathway which in turn would result in correct maturation of the cell. The DISC1 regulation of adult neurogenesis via the AKT/mTOR pathway is further supported by the fact that an mTOR inhibitor rescues the dendritic and morphological phenotype of the new born cells in the Disc1 knockdown model (Kim et al., 2009). Curiously, this morphological rescue was not seen when GSK3β was inhibited, suggesting that GSK3β has a role in the proliferation but not maturation of the adult born neurons.
Since AKT, just like Disc1, is a repressor of GSK3β (Cross et al., 1995), the latter might be involved in a more complex mechanism of regulating adult neurogenesis.

1.3.5 DISC1 and neuronal migration

Disc1 has been implicated in nucleokinesis by interacting with the Lis1 and Nude/NudeL, proteins required for the proper dynein complex (Shu et al., 2004). Furthermore, Disc1 has been found to associate with Fez1 and kendrin, which are centrosome proteins (Miyoshi et al., 2004). This places Disc1 at the centre of the migratory mechanism. The hypothesis that Disc1 is a part of the cortical migration process has been tested in various models of DISCopathies. The first evidence supporting that hypothesis came from knockdown studies. RNAi against Disc1 was introduced *in utero* into the SVZ of the mouse brains of different strains at various developmental ages and the deficit in the radial migration was noted at various postnatal ages (Kamiya et al., 2005, Duan et al., 2007, Kubo et al., 2010, Young-Pearse et al., 2010). Similar disruption of radial migration was found in the neocortex of the L100P and the Q31L Disc1 mutant mice (Lee et al., 2011). Further evidence came from a study of the common human DISC1 polymorphisms. The S704C variant incorporated *in utero* into the rodent brain resulted in a similar inhibition of migration, but not proliferation (Singh et al., 2011). Interestingly, the variants that disrupted cell proliferation in the SVZ did not cause any disturbance in migration. This implies a possible Disc1 involvement in migration but not through the Wnt signalling pathway. This was investigated in the Disc1 and Dixdc1 knockdowns, where increasing levels of β-catenin would not rescue the migration deficit caused by disruption of either one of these genes (Singh et al., 2011).

Disc1's role in radial migration in the neocortex has been firmly established, but its function in tangential migration of interneurons from the ventral telencephalon to the cortex or that of the cells from the SVZ through the rostral migratory stream (RMS) to the olfactory bulb has not been studied in much detail. A recent paper from the Bolz group investigated the effect of a local Disc1 knockdown in the developing medial ganglionic eminence on the migrating interneurons originating there (Steinecke et al., 2012). These cells do express Disc1 and its knockdown depletes the number of them reaching the cortex. Interestingly, Disc1 seems not to be involved in neuroblast migration via the RMS (Wang et al., 2011), suggesting a different

mechanism of neuronal migration. Lastly, Disc1 has been implicated in the movement of the nucleus during tangential migration by formation of a complex with CAMDI (coiled-coil protein associated with myosin II and Disc1) and myosin II, the latter being indispensable in the nucleokinesis (Fukuda et al., 2010).

Disc1 has also been implicated in the migration of granule cells from the dentate notch to the dentate gyrus in the developing hippocampus (Meyer and Morris, 2004). Intriguingly, there is mixed evidence when it comes to the effect Disc1 knockdown has on the migration of the CA1 pyramidal neurons (Meyer and Morris, 2004, Tomita et al., 2011), which might be due to a difference in the knockdown construct and the antibodies detecting Disc1. There is also some evidence of Disc1 being involved in the adult migration of newborn granule cells in dentate gyrus via N-methyl-D-aspartate receptor (NMDAR) activity (Namba et al., 2011). This study showed that blocking the NMDAR on the migrating granule cells resulted in downregulation of Disc1 and mispositioning of these cells, which has been rescued by expressing Disc1.

Since knocking down Disc1 in the mouse brain resulted in both impaired proliferation and disturbances in neuronal migration it has been suggested that Disc1 might act as a switch between these two events. Some evidence for this hypothesis came from the Ishizuka et al. study showing that Disc1, when unphosphorylated, regulates canonical Wnt signalling through its interaction with GSKβ/ β-catenin (Ishizuka et al., 2011). However, when phosphorylated at serine 710, Disc1 is employed to recruit the Bardet-Biedl syndrome proteins to the centrosome, which in turn activates migration. This dual role of Disc1 might give some clues regarding the impairments observed in the Disc1 knockdown models.

As mentioned previously, Disc1 protein acts as a scaffold for the Lis1/Nde1(Ndel1) complex that in turn interacts with the dynein/dynactin motor complex. On their own, disruption of either of these proteins resulted in a disrupted migration of the radial glia cells (Youn et al., 2009; Sasaki et al., 2005; Hippenmeyer et al., 2010). Interestingly, Lis1 is required for efficient neural migration in a dose-dependent

manner while Nde1/Ndel1 are more involved in the entering of the migrating neuron into the correct cortical layer (Hippenmeyer et al., 2010). What is more, Lis1 heterozygous mice were shown to have abnormal tangential migration of the interneurons (McMannus et al., 2004). Since this complex is essential for the proper migration of both radial glial cells and interneurons, it is possible that some of the migratory defects observed in the DISC1 knockdown and mutant mouse models are due to improper formation of the Disc1/Lis1/Nde1(Ndel1) complex.

1.3.6 DISC1 and neuronal integration

RNA interference and Disc1 mouse mutant studies in hippocampus and prefrontal cortex suggested Disc1's role in neuronal migration and maturation. Silencing Disc1 with short hairpin RNA in dentate gyrus (DG) of the hippocampus resulted in abnormal cell size of the newborn granule cells with the presence of ectopic dendrites and increase in dendritic length, branching and the speed with which they formed functional synapses (Duan et al., 2007). What is more, Disc1 knockdown in DG granule cells showed mispositioning of the mossy fibres connections (axons from the granule cells) and disrupted synaptic development (Faulkner et al., 2008). Furthermore, the 129 mouse strain that has a 25 base pair deletion in exon 6 of mouse Disc1 (mDisc1) resulting in a frameshift, a 'stop' codon at exon 7 and no full length Disc1 protein, showed mispositioned neurons with abnormal morphology and growth of the dendrites in the DG (Koike et al., 2006; Kvajo et al., 2008). The affected granule cells also have aberrant axonal projections that missed their targets in the CA3 region of the hippocampus (Kvajo et al., 2011). This has been suggested to be due to lack of the Disc1 control over phosphodiesterase 4 (PDE4), which in turn controls cAMP –a secondary messenger known to be necessary for netrin-1 signalling in the growth cones of the axons (Wu et al., 2006). With the lowered PDE4 activity in the hippocampus there is an increase of cAMP levels in the granular zone of the DG, which in turn results in higher activity of the cAMP-dependent transcription factor CREB, affecting the expression of factors necessary for proper axon pathfinding and dendritic growth (Kvajo et al., 2011). Such abnormal connectivity affected the electrophysiology of the CA3 region and the short-term

plasticity of the mossy fibres targeting the CA3 hippocampal region (Kvajo et al., 2011). Lastly, the mice with the Disc1 L100P and Q31L missense mutations also showed abnormal dendritic spine density and length, but not branching, in the projection neurons of the prefrontal cortex (Lee et al., 2011). In the hippocampus, these mice showed lower spine density but normal spine length and branching. Some of the effects of the Disc1 knockdown on the granule cell can be replicated by the overexpression of girdin, the AKT kinase activator that is inactive when bound to Disc1; or by increasing AKT signalling (Kim et al., 2009; Enomoto et al., 2009). Furthermore, the effects of either Disc1 knockdown or Girdin overexpression can be reversed by rapamycin, an inhibitor of the mTOR pathway (Kim et al., 2009). This strongly suggests a potential mechanism behind integration of the granule cells projection where Disc1 regulates Girdin/AKT through the mTOR pathway (Kim et al., 2009).

Disc1 seems to be playing a role in neuronal maturation, albeit most of the data on that matter come from the hippocampus, not cortex. Two possible mechanisms involving Disc1 in the hippocampal neurons have been investigated and proposed - the AKT/mTOR and cAMP signalling pathway (Kim et al., 2012; Kvajo et al., 2011). Neuronal integration in the adult brain hippocampus is dependent on intrinsic factors like for example GABA (Ge et al., 2008). Knockdown of the sodium/potassium/chloride ionic co-transporter (NKCC1) involved in GABA responses, as well as knockdown of ɤ2 subunit of the $GABA_A$ receptor reverses the dendritic growth defects observed in the Disc1 knockdown (Kim et al., 2012). Since the mechanism through which Disc1 regulated the dendritic growth was narrowed down to the AKT/mTOR pathway, it has been suggested that the maturation and integration of the adult hippocampal neurons is regulated by the synergistic action of Disc1 and GABA signalling on the AKT/mTOR pathway. Interestingly, early postnatal hippocampal neurons in mice were not much affected by the Disc1 knockdown unless an environmental stress was applied to the pregnant females, highlighting the importance of the combination of the genetic predisposition and environmental factors in the phenotype (Kim et al., 2012). Taken together, Disc1 appears to play a role in the integration of neurons into the neural network.

1.4 Disc1 L100P and Q31L mouse models of psychiatric disorders

Many animal models have been developed to study possible mechanisms behind the Disc1's role in the aetiology of psychiatric disorders. In this study I have used two Disc1 mutant mouse lines carrying ENU induced point mutations in the *Disc1* gene: L100P and Q31L. Both point mutations occur in exon 2 of the mouse *Disc1* sequence (Clapcote et al., 2007), but are not found in human. In the L100P line, transition of thymine to cytosine in position 334 results in the encoded Disc1 protein having a proline instead of leucine at a 100 residue. Likewise, a transversion of adenine in position 127 to thymine in the *Disc1* sequence in the Q31L line is predicted to result in the change from glutamine to leucine at a residue 31. Neither of the mutations results in an abnormal expression of the major Disc1 isoforms (Clapcote et al., 2007) but it is highly likely that they affect protein structure and as a result its function. One of affected functions is binding of the Disc1 to phosphodiesterase 4B (PDE4B), a cyclic AMP regulatory protein (Millar et al., 2005). One of the PDE4B binding sites on Disc1 is at the N-terminus and is affected by both L100P and Q31L mutations. As a result, PDE4B has been shown to have a reduced binding to L100P and Q31L Disc1 *in vitro* (Clapcote et al., 2007). Interestingly, PDE4B activity was decreased only in the Q31L/Q31L mouse brains suggesting different nature of the two mutations.

Interestingly, difference between the Q31L and L100P Disc1 mutations can be observed in the behaviour of the mice carrying the mutations. Study by Clapcote et al., (2007) showed two distinct phenotypes using a wide array of behavioural tests and drug treatments. For example, Q31L homozygous and heterozygous mice showed lower sociability and sucrose consumption than both WT and L100P mice but performed better in the test for the working memory than L100P animals. On the other hand, L100P mice showed lower acoustic startle response, startle reactivity and higher vertical activity than WT and Q31L mice. Moreover, the prepulse inhibition (PPI), a measurement of filtering information; was higher in the L100P homozygous and heterozygous mice than in the Q31L and the WT animals. Both lines showed decrease in the latent inhibition, a measurement of learnt inattention; and reduced

brain volume when compared to WT controls. However, the most interesting observation was different response to antipsychotics (clozapine and haloperidol) and anti-depressants (rolipram and bupropion). The PPI improved in the L100P homozygous mice upon delivery of both antipsychotic and rolipram, while Q31L homozygous mice showed increase in PPI in response to bupropion. Together with the behavioural phenotypes observed, L100P and Q31L mice were distinguished as showing schizophrenic-like and depressive-like behaviours respectively. Other studies on these mice showed exacerbation of the behavioural deficits in L100P upon maternal immune activation (Lipina et al., 2013b), enhanced dopamine function in L100P that support dopamine hypothesis of schizophrenia (Lipina et al., 2010; Su et al., 2014; Howes and Kapur, 2009) and social defeat and social anhedonia in Q31L mice (Haque et a.l., 2012; Lipina et al., 2013). Data obtained from such behavioural studies not only validate and improve the animal model of psychiatric disorders but also allow for more thorough approach in studying such disorders when conducted in combination with the molecular and cellular approach.

1.5 Aims

Generation of cortical interneurons can be divided into four main phases: fate acquisition in the ganglionic eminences, tangential migration into the margins of the cortex (marginal and intermediate zones), radial migration to reach their final positioning within the six cortical layers and integration into the neural circuit. Each of the steps is tightly controlled by internal and external signals and cues such as transcription factors, motogenic factors, chemical repellent and attractants and signalling from other neurons. Any disruption to this highly organised process might result in a spectrum of brain disorders. The growing knowledge of the processes involved in interneuron development might eventually lead to better understanding of diseases such as neuropsychiatric disorders (interneuronal defects have been implied in schizophrenia, autism and anxiety disorders) or seizure disorders.

One of genes linked to the major psychiatric disorders is Disc1. Coding for a scaffold protein that has multiple interactors, some of which are also associated with psychiatric disorders and being shown to be involved in the proliferation, migration and integration of cortical and hippocampal neurons, Disc1 seems to be an interesting candidate when it comes to the biology of cortical interneuron development. In this work I investigated the role of Disc1 in cortical interneuron development in L100P and Q31L mice. I investigated the overall density and distribution of the interneurons in four cortical regions: frontal primary somatosensory, primary somatosensory (barrel), ventral auditory and visual cortices of the 3-week old (P21) brains. Furthermore, I performed density and distribution analysis of major subclasses of the cortical interneurons: parvalbumin, somatostatin and calretinin expressing interneurons in those four regions. Additionally, I investigated parvalbumin expression in the medial prefrontal cortex.

For the second part of my work, I addressed the question of whether Disc1 is involved in the regulation of the parvalbumin expression in a non-cell autonomous way. To achieve that, I overexpressed wild-type and L100P variant of the mouse Disc1 in a proportion of the projection cells *in utero* at E14.5, targeting future

frontal/primary somatosensory, ventral auditory and visual cortices. Next, I investigated the density and distribution of the parvalbumin expressing cells in the four targeted regions in the P21 brain.

Chapter 2: Materials and Methods

2.1 Animals

All animals used in this study were maintained in agreement with the Home Office and the University of Edinburgh animal welfare guidelines. The strains used in this study were the following wild type strains: C57Bl6/J and F1 (C57Bl6/J x CBA) for *in utero* electroporation; as well as Disc1 N-ethyl_n-nitrosurea (ENU) mutant mice L100P and Q31L kept on the C57Bl6/J background (previously described in Clapcote et al., 2007). Briefly, muse males of known wild type background (in this case C57Bl6/JJcl) were injected with ENU and mated with unaffected DBA/2JJcl females. ENU is a potent mutagen that by transferring its ethyl group to nitrogen or oxygen radicals in the DNA causes random point mutations, predominantly by affecting adenine-thymine pairing (Russell et al., 1979; Justice et al., 1999). The progeny was screened for mutation by observing their phenotype and having their exon 2 of *Disc1* sequenced for any point mutations. The backcrossed progeny of the heterozygous male founders L100P and Q31L and C57Bl6/J females were further backcrossed to keep the genetic background of the C57Bl6/J line.

The numbers of males to females used for the L100P and Q31L analysis is shown in Table 2.1. No sex effects were previously reported (Clapcote et al., 2007) nor have they been observed during the analysis, though low sample size for each sex (especially in the L100P homozygous and heterozygous female groups) prevents a definite conclusion. Thus due to low number of animals homozygous for the L100P mutation, the data obtained from each sex were pooled.

L100P	males	females	males (MPFC analysis)	females (MPFC analysis)
WT	6	2	3	0
L100P/+	3	1	3	1
L100P/L100P	3	1	2	2
Q31L				
WT	2	5	n/a	n/a
Q31L/+	1	2	n/a	n/a
Q31L/Q31L	4	5	n/a	n/a

Table 2.1 Numbers of males and females used for the analysis of cortical interneurons in different cortical regions in the L100P and Q31L lines.

Embryonic days were counted from the day when the vaginal plug was found (E0.5) while postnatal days were counted from birth. The animals used to study the interneuron distribution in the neocortex were P21 L100P and Q31L homozygotes with their WT and heterozygote littermates as controls. C57Bl6/J and F1 females used for the *in utero* experiments were timed mated, electroporated at E14.5 and sacrificed at different stages post electroporation - minimum 2 days after electroporation up to P21. For post-natal stages, only F1s were used as the C57Bl6/J pups were either eaten or abandoned by the mother once born.

All pregnant females and those that underwent surgery were sacrificed by cervical dislocation. All embryos and pups up to postnatal day 4 (P4) were sacrificed by decapitation. All pups older than P4 were sacrificed by overdose of anaesthetic (0.2ml of 200mg sodium pentobarbital).

2.1.1 Post-operative care

For the in utero electroporation, the C57Bl6/J and F1 mice were time bred and housed together according to the plug check (up to 4 females per cage). Post surgery, they were given a jelly containing buprenorphine and checked upon every day for 3-5 days. On occasion of multiple surgeries on the same day, the females were housed

together and then kept together after surgery for up to 2 days, as it was observed that they recover better and quicker in the company of one another.

2.2 Genotyping

Initially, the ear notches collected from P14 mice after earmarking for identification were sent to Transnetyx for genotyping. When the L100P colony was re-established, the following protocol was followed.

2.2.1 Genomic DNA extraction

Genomic DNA was extracted two ways from either ear notches (collected at P14) or tail tips (collected at P21). Tissue was incubated with 100 µg Proteinase K in Direct PCR solution (Viagen) at 50°C with shaking for 2 hours and then incubation at 80°C with shaking for 30 mins. The samples were spun down and the supernatant was used for further genotyping.

2.2.2 Polymerase Chain Reaction (PCR)

The extracted genomic DNA was used for setting up a polymerase chain reaction (PCR) with the following primers: forward 5′-AGA CCA GGC TAC ATG AGA AGC-3′ and reverse 5′-AAG CTG GAA GTG AAG GTG TCT-3′ (Clapcote et al., 2007). A mix of 5 µl of 5x Colorless GoTaq® Reaction Buffer (Promega), 1.25 µl of 10 pM of forward and reverse primers mix (MWG Eurofins), 0.5 µl of 2.5 mM dNTP (Promega) and 0.3 µl GoTaq® DNA polymerase (Promega) was prepared and added to 1 µl (0.5-1 µg) of genomic DNA for a final volume of 25 µl per reaction. The PCR reactions were run on an MJ Thermocycler (MJ Research) with pre-heated lid option. The cycle conditions were: 94°C 3 min; 94°C 30 s, 55°C 1 min, 72°C 40 s for 25 cycles; 72°C for 10 min. To check for the product, the samples were run on a gel made of 2% agarose in Tris/Borate/EDTA buffer (TBE) with SYBR® Safe (Invitrogen).

2.2.3 ExoSap-IT PCR product clean-up

2 µl of the PCR product was cleaned up using 1 µl ExoSap-IT (GE Healthcare Life Sciences) in a final volume of 5 µl. The samples were run on the MJ Thermocycler (MJ Research) at 37°C 1 h, 80°C 20 min and kept in 4°C if not used straight away.

2.2.4 Sequencing reaction

A mix consisting of 0.5 µl BigDye® Terminator (BD) v3.1 (Invitrogen), 1.75 µl sequencing buffer, 10pmol primer (either forward or reverse) in a total volume of 6 µl was prepared. This was added to the cleaned up sample and run under following cycle conditions: 96°C 1 min; 96°C 10 s, 50°C 4 s, 60°C 4 min repeated 30 times. If necessary, the samples were stored at -20°C for ethanol/EDTA precipitation.

2.2.5 Ethanol/EDTA precipitation

Samples were spun down and 1.25 µl of 0.5 mM EDTA together with 65 µl 100% ethanol was added to each of them. Samples were mixed by inversion and incubated at room temperature (RT) for 10 min. Following the incubation, samples were spun down at 13000 rpm for 20 min to precipitate the DNA. The pellet was washed with 300 µl 70% ethanol and spun for 10 min at 13000 rpm. The step was repeated and after last spin down, the remaining ethanol was removed and the pellet was allowed to dry until there was no smell of ethanol coming from the tube (around 15 min). The samples were sent to the Medical Research Council (MRC) sequencing services at the University of Edinburgh.

2.3 Tissue preparation

2.3.1 Dissection

To collect the brain tissue from embryos, pregnant females were sacrificed by cervical dislocation. The uterine horns were exposed and the embryos were dissected out of the uterus. The embryos were sacrificed by decapitation and the brains were dissected out in ice cold phosphate buffer saline (PBS) and put in 4% paraformaldehyde (PFA). If the animals were electroporated *in utero*, the brains were always kept in PBS, regardless of age; until checked for the green fluorescent protein (GFP) expression under the Leica microscope (model MZFLIII). Adult mice were perfused with cold PBS (5-10 ml depending on age) and 4% PFA (5 ml). The brains were fixed in 4% PFA overnight at 4ºC.

2.3.2 Processing the tissue: cryostat

To cryoptrotect, the brains they were washed 3 times in PBS to remove PFA before soaking them in 30% sucrose. When the tissue had sunk in the sucrose solution, the brains were moulded in 15% sucrose/freezing medium (Lamb's OCT, ThermoScientific) before being cut on a Leica cryostat into 14 μm (embryonic brains) or 20 μm (postnatal brains) coronal sections. The moulds were kept in -20°C for up to a week – if not cut in that time then they were moved to -70°C. The sections were mounted onto Superfrost Plus (ThermoScientific) glass slides, allowed to dry and kept at -20°C. Before any immunostaining procedure was applied, the slides were allowed to equilibrate to RT (1-3 h minimum, usually overnight).

2.4 Cell Culture

2.4.1 Cells

COS7 and HEK-293 cells were maintained in Dulbecco's Modified Eagle's Medium with 4.5 g/l Glucose and L-Glutamine (D-MEM, Invitrogen) with 10% Foetal Bovine Serum (FBS, Invitrogen) at 37ºC with 5% CO_2 atmosphere in a humidified incubator. To passage the cells, the flasks were washed with pre-warmed to 37ºC PBS (Invitrogen) and trypsinised with pre-warmed TrypleExpress (Invitrogen) for 5min either at RT (most cells) or at 37ºC. The flasks were gently tapped before adding pre-warmed 10% FBS D-MEM. Cells were split in a 1:15 manner every 2-4 days, depending on type and confluency. For transfection with Lipofectamine 2000® (Invitrogen), an appropriate number of cells, depending on the dish used, was plated in 10% FBS D-MEM so that they would be ~90% confluent on the day of transfection.

2.4.2 Dissociated mouse neuron cultures

For primary neuron cultures, brains from E18.5 electroporated C57Bl6/J embryos were dissected on ice in ice cold Hank's Balanced Salt Solution (HBSS, Invitrogen) with 0.7% 1M HEPES pH 7.3 (Sigma) and 1% 200 mM L-Glutamine (Invitrogen). Brains were transferred to 30 ml of dissecting medium in a standard tube and kept on ice. After removal of the meninges, cortices and/or hippocampuses were dissected out and kept in ice cold dissection medium either in a 15 ml Falcon tube or in a 6 wells plate. Cortices were mashed with either a razor or a pipette tip prior to trypisn treatment. A solution of trypsin in HBSS (3:2 ratio) was pre-warmed to 37ºC, added to the tissue and incubated for 45 min at 37ºC in a water bath. The samples were gently pipetted up and down and centrifuged at 1500 rpm. The supernatant was then removed and the pellet was re-suspended in 5 ml (hippocampal samples) or 10 ml (cortical samples) of pre-warmed 10% FBS D-MEM with penicillin/streptomycin (Invitrogen). The spin down and resuspension steps were repeated 2-3 times, depending on the size of the pellet. After final resuspension, cells were filtrated using

a cell strainer (BD Biosciences), counted and split appropriately. Primary neuronal cultures were maintained in Neurobasal medium with 2% B27 supplement and 2 mM Glutamax (all from Invitrogen).

2.5 Plasmids

2.5.1 Mouse Disc1-100P

Plasmids initially used for in utero electroporation were made by Elise Malavasi from Kirsty Millar's group. Briefly, mouse L100P and WT Disc1 long variant coding DNA sequence (CDS) without exon 1, but with an N-terminus FLAG-tag, was cloned into a multiple cloning site (MCS) of the pcDNA4-TO® (Invitrogen) with use of EcoRI and NotI restriction enzymes. However, the Flag-tag Disc1 fusion protein were found to be impossible to detect after in utero electroporation hence the mouse Disc1 constructs were cloned into a pCAGG-IRES-(NLS) GFP vector (kindly provided by Dr Thomas Theil).

2.5.2 Subcloning of mouse Disc1 constructs into CAGG-IRES-GFP vector

2.5.2.1 Restriction enzyme digest

Disc1-Flag CDS were excised from the pcDNA4-TO plasmid using either PmeI (New England Biolabs NEB) single digest or a double digest with PmeI and XhoI (NEB) for blunt end and single sticky end cloning respectively. The CAGG-IRES-GFP vector was linearised by cutting with either SmaI (NEB) or double digest with NruI (NEB) and XhoI for blunt end and single sticky end cloning respectively. Thermosensitive alkaline phosphatase (TSAP, Promega) was used to remove phosphate groups from the 5' end of the linearised vector to prevent its re-circularisation. For restriction enzyme digest set up see Table 2.02 below:

Reagent	Single Digest PmeI	Single Digest SmaI	Double Digest (PmeI/XhoI, NruI/XhoI)	Undigested DNA
DNA plasmid	1 µg	1 µg	1 µg	1 µg
Buffer x10	5 µl	5 µl	5 µl	5 µl
Enzyme(s)	up to 40 U	up to 80 U	up to 20 U each	-
BSA	0.5 µl	-	0.5 µl	0.5 µl
TSAP	-	1 µl	1 µl (vector cut only)	1 µl
ddH_2O	to 50 µl	to 50 µl	to 50 µl	to 50 µl

Table 2.02 Restriction enzyme digests for Disc1 subcloning into CAGG-IRES-GFP vector.

For the PmeI and SmaI single digest, DNA plasmids were incubated in Buffer 4 (NEB) for up to 3 h at 37°C and 25°C respectively. For PmeI/XhoI and NruI/XhoI double digests, incubation was performed in Buffer 4 and 3 (NEB) respectively at 37°C for 3 h. All digests were heat inactivated at 65°C for 20min prior to running on a 1% agarose/TBE/SYBR®Safe gel for 30-40 min at 70 V.

2.5.2.2 DNA extraction from agarose gel

Plasmid DNA fragments resulting from a restriction enzyme digest were visualised under ultraviolet (UV) trans-illuminator. Fragments corresponding to a correct size were cut out with a scalpel and placed in eppendorf tubes. DNA was extracted using QIAquick Gel Extraction Kit (Qiagen) according to the manufacturer's protocol. DNA was eluted in water and the yield was checked using NanoDrop®.

2.5.2.3. Ligation

The ligation was set up on ice with the insert to vector ratios 3:1, 5:1 or 8:1 as well as no T4 DNA ligase and linearised vector only ligation controls. 100 ng linearised plasmid was always used. 1-2 µl of T4 DNA ligase (Promega or NEB) was added to nuclease free water (Qiagen) with appropriate buffer. Samples were incubated for 18

h in 15°C (T4 ligase from Promega) or 3 h at room temperature (NEB) followed by overnight incubation at 4°C if needed. Ligation reaction product was chilled on ice and used to transform competent cells (JM109, Promega) according to the manufacturer's protocol.

2.5.2.4 Screening bacterial colonies: Plasmid DNA extraction

10-20 colonies (depending on the ligation and transformation efficiency) were picked with sterile pipette tips and grown overnight in 5 ml LB medium with ampicillin. 3 ml of the overnight culture was spun down at 13000 rpm for 15 min to harvest the pellet. The pellet was resuspended in 150 µl P1 buffer (Qiagen), followed by cell lysis in 200 µl P2 buffer (Qiagen) and 5 min incubation at RT. DNA was then precipitated in 175 µl either N3 or P3 buffer (Qiagen) for 10 min at 4°C. Samples were spun down at 13000 rpm for 20 min and the plasmid containing supernatant was carefully removed to a new tube. If some of the white precipitate was taken up, the samples were spun again and transferred to fresh eppendorf. 2 volumes of RT isopropanol were added to the solution, mixed by hand and spun down for 30 min at 13000 rpm. The DNA pellet was washed twice in 70% ethanol, allowed to dry for up to 15 min, then re-suspended in 50 µl of double-distilled water and checked for DNA yield using NanoDrop®.

2.5.2.5. Screening bacterial colonies: Restriction enzymes digest

1 µg of plasmid DNA was cut with HindIII (NEB) restriction enzyme in the solution of Buffer 2 in water (final volume of 50 µl) for 3 h at 37°C and heat inactivated for 20 min at 65°C. Digested product was run on 1% agarose/TBE/SYBRSafe® gel for 2 h at 30 V. Samples that had band sizes that showed presence of the insert were sent for sequencing.

2.5.2.6 Sequencing

Initially samples were sent for sequencing to MWG, Germany, then to the sequencing services at the MRC in Eidnburgh. 100 ng of plasmid DNA were set up in 20 µl solution of 1 µl Big Dye (BD) v3.1, 2 µl 10x BD buffer and 10 pmol T7 primer. The cycling conditions were as stated in the genotyping section. The samples were then subjected to the EDTA/ethanol precipitation and sent for sequencing.

2.5.3 Transformation

Before transformation, selective agar plates were prepared using sterile LB agar (Sigma) with appropriate antibiotic (100 µg/ml ampicillin, Sigma). Unused selective agar plates were kept at 4°C for up to month and dried before use. Competent cells used to grow plasmids for transfection or *in utero* electroporation were JM109 or OneShot® Stbl3 (both from Invitrogen). The procedure was performed according to the manufacturer's protocol. Usually 50 µl and 100 µl of cells were spread on the pre-warmed selective agar plates for overnight incubation at 37°C.

2.5.4 Plasmid preparation: Maxi and Mini Preps

Plasmids used for transfection or nucleofection were prepared using MaxiPrep or MiniPrep kits (both Qiagen). A single colony was picked with a sterile pipette tip from the selective plates that were incubated overnight at 37°C, and placed in a 5ml Lysogeny Broth (LB) medium (Sigma) with appropriate antibiotic (100 µg/ml ampicillin, Sigma). This starter culture was grown either overnight for mini prep or up to 8 h at 37°C with shaking (225 rpm) for maxi prep. The maxi prep starter culture was then diluted appropriately and grown for 12-16 h at 37°C with shaking. To extract the DNA, the manufacturer's protocol was followed. The DNA concentration was measured using NanoDrop® (ThermoScientific).

2.6 Introduction of plasmid DNA into mammalian cells

2.6.1 In vitro transfection

Cultured cells were transfected using Lipofectamine 2000® (Invitrogen). Plasmid transfection was conducted according to the manufacturer's protocol.

2.6.2 *In utero* electroporation

In utero electroporation was performed with accordance with Home Office regulations. Surgery was performed on F1 (C57Bl6/J x CBA cross) timed mated pregnant females 13 and 14 days after the plug was found. Pregnant dams were anaesthetised with 3% Isofluorane (Merial) mixed with medical oxygen (BOC). Depth of anaesthesia was controlled by checking involuntary reflexes (toe or tail pinch reflex) and the depth of anaesthesia was monitored throughout the surgery. To prevent heat loss, the anaesthetised animal was placed on a heating pad under the light microscope (Leica). Prior to the procedure, all animals were given subcutaneous injection of 0.05 mg/kg Buprenorphine (Vetergesic, Reckitt Benckiser Healthcare) dissolved in water for injections (Norbrook). The fur on the abdomen was shaved off with an electric trimmer and sterilised with a solution of MediScrub (MediChem) in water. A 1-1.5 cm incision was made through skin with sterile scissors (WPI). The abdominal muscles were cut through along the midline and uterine horns were exposed. The embryos were taken out in threes at a time and kept moist with the pre-warmed solution of sterile PBS. 2-3 μg (~2 μg/μl) of DNA with Fastgreen dye (Sigma) mix were injected into the embryo's lateral ventricle through 4 in. (100 mm) 1/0.75 OD/ID filament thin wall Glass Capillaries (WPI) pulled with a flaming/brown micropipette puller (Sutter instruments, P87) and with the use of pneumatic picopump (PV820, WPI). The forceps-type electrodes (Nepagene, CUY650P5) were placed around the target region (at a 30° angle) with the positive electrode at the targeted area (Fig 2.01). Five 50 ms pulses of 35-40 V (depending on the age) were passed through the electrodes with the use of the edit-type CUY21 electroporator (Nepagene, Pon=50ms, Poff=950s). The embryos were placed back in

the abdomen, hydrated and the abdomen was closed with grade 5 vicryl surgical sutures (Ethicon). The skin was clipped with 7mm Reflex Clips (WPI, 500344) using Reflex Clip Applier (WPI, 500343) and the pregnant female was was placed in a clean cage on a heating mat to recover. After surgery, buprenorphine was administered orally at 0.5mg/kg. If more than one female was operated on, tools were sterilised in a glass bead steriliser.

Fig 2.01 Targeting of the frontal primary somatosensory (fSSp) cortex during the *in utero* electroporation of the E14.5 mouse embryo by proper orientation of the electrodes. Size of the electrode forceps (7mm) allowed for expression of the constructs not only in the fSSp, but also primary somatosensory (SSp), ventral auditory (vAud) and visual (Vis) cortices.

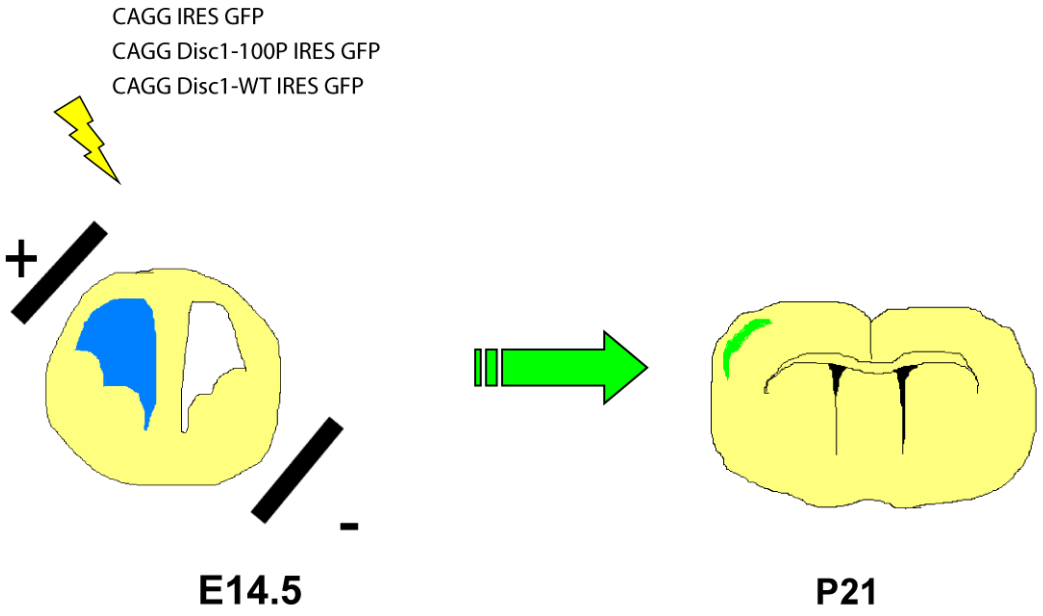

2.7 Immunodetection and hybridisation *in situ*

2.7.1 Antibodies

Various antibodies were used and optimised for both immunocytochemistry and immunohistochemistry.

To detect GFP in transfected cells, polyclonal goat anti-GFP (1:500, Sigma) was used. To detect Flag signal, monoclonal mouse anti-Flag (1:500-1:50, Sigma) was used. For immunohistochemistry, the following antibodies were used: mouse monoclonal anti-parvalbumin (PV) (1:1000, Sigma), rat polyclonal anti-somatostatin (1:200, Milipore), rabbit monoclonal anti-calretinin (1:1000, Swant) and rabbit polyclonal anti-GAD67 (Millipore) for interneuronal marker analysis; polyclonal rabbit anti-Flag (1:500-1:50 dilution for both, Sigma) and goat polyclonal anti-GFP (1:500, Abcam) to detect DISC1 constructs after *in utero* electroporation.

The following secondary antibodies were used either in 1:1000 (ICC) or 1:200 (IHC): donkey anti-goat 546, donkey anti-mouse 594 and 568, donkey anti-mouse 488, donkey anti-rabbit 488, donkey anti-rat 488, goat anti-rabbit 546, goat anti-mouse 488, goat anti-rat 488 and 546 (all Alexa Fluor Conjugates, Molecular Probes); biotynilated goat anit-rabbit (1:200, Sigma) and conjugated streptavidin 488 and 568 (Molecular Probes). DAPI (1:50000, Invitrogen) was used as a nuclear marker.

2.7.2 Immunocytochemistry

Immunocytochemistry was conducted when the neurons had been grown for up to 18 days in culture. For cells, the fixation occurred up to 2 days after transfection. Cells were fixed in either cold methanol or 4% PFA with permeabilisation in 0.5% Triton X-100. Blocking for non specific binding sites was performed with the use of either 3% PBS/BSA (neurons) or goat/donkey serum in 0.01% PBS-Triton X-100 (COS7 and HEK293 cells). Primary antibodies were incubated for 2 h followed by washes in

0.02% BSA/PBS and 1 h incubation with secondary antibodies in PBS at room temperature. Following further washing in 0.02% BSA/PBS, coverslips were mounted using VectaShield Hard Set with DAPI (VectorLabs) and stored at 4ºC in the dark.

2.7.3 Imunohistochemistry

Cryosections were allowed to dry (usually overnight at RT). Sections were washed in PBS and subjected to the antigen retrieval step of washing and boiling in 10mM sodium citrate buffer, pH6; for 10min and 20min respectively. The sections were incubated in a solution of 0.1% Triton X 100, 0.2% cold-fish gelatin and 10% goat, donkey or equine serum for 2h at RT or in 5-10% skimmed milk (for GAD67 staining). Primary antibodies were appropriately diluted in a solution of 0.1% Triton X 100, 0.2% gelatin and 5% appropriate serum solution. The sections were incubated with primary antibodies at 4°C overnight. The sections were washed, incubated with secondary antibody at RT, then incubated with DAPI solution (1:10000 DAPI in PBS) for 5min and mounted with the use of Vectashield HardSet (VectorLabs). If 3,3'-Diaminobenzidine (DAB) staining was performed, after incubation with the primary antibody endogenous peroxidases were blocked with 3% H_2O_2/10% methanol in PBS for no longer than 30mins at RT. After secondary antibody incubation sections were incubated in the avidin-biotin solution (ABC, Vector Laboratories) for 1h at RT. After washing it off, staining with 0.05% DAB in Tris buffer saline (Vector Laboratories) was performed at RT and once desired staining developed the slides were mounted with Aquatex mounting medium (Merck). The images were taken using a Leica fluorescent microscope (model DM5500B) with DFC360FX camera and analysed using Adobe Photoshop® and ImageJ (Rasband, W.S., ImageJ, U. S. National Institutes of Health, Bethesda, Maryland, USA, http://imagej.nih.gov/ij/, 1997-2011). For GAD67 staining, images were drawn by hand under camera lucida.

2.7.4 *In situ* hybridisation: probe generation

P14 cDNA from a WT mouse somatosensory cortex (courtesy of Viktoria Seidel) was used as a template for the PCR with PV5 (GGGCCTGAAGAAAAAGAACC) and PV6 (AGTACCAAGCAGGCAGGAGA) (Tanahira et al., 2009) primers. The cycling programme was as follows: 94°C 3 min; 94°C 1 min, 57°C 1 min, 72°C 1 min for 25 cycles; 72°C for 10 min. The PCR product was cleaned up using either QIAquickGel Extraction Kit or PCR Clean Up Kit (both Qiagen) according to the manufacturer's protocol. The cleaned product was then ligated into pGEM®-T Easy vector (Promega) in insert to vector ratio 3:1, 5:1 and 8:1, according to the manufacturer's protocol. After overnight ligation at 4°C the ligation reaction was used to transform JM109 competent cells (Promega) which then were spread on ampicilin selective plates with IPTG/X-gal for blue/white colonies screening. White colonies were picked up for colony PCR. Briefly, a single colony was picked up and swirled into the PCR mastermix with the PV5 and PV6 primers and run on the same cycling conditions as before. Colonies positive for the insert were grown, the plasmid was purified using Qiagen MiniPrep Kit and the DNA was sent for sequencing (with the use of SP6 and T7 RNA polymerase promoter sites) to MWG Operon. Depending on the orientation of the insert, either SP6 or T7 RNA polymerases (both from Roche) was used for *in vitro* transcription with the DIG-labelling mix (Roche). The plasmid was linearised with either PstI or SalI (both NEB) and the *in vitro* transcription reaction was set up as presented in Table 2.03:

Reagent	**Volume**
Linearised DNA plasmid	3-4 μg
10x transcription buffer	2μl
DIG labelling mix	2 μl
T7 or SP6 RNA polymerase	2 μl
ddH_2O	to 20 μl

Table 2.03 In vitro transcription of the linearised pGEM®-T-Easy vector with 563bp parvalbumin insert.

After 2h incubation at 37°C, 2 µl of DNase (Roche) were added and the sample was incubated at 37°C for 15 min. 2 µl of 0.2 M EDTA pH 8, 2.5 µl 4M lithium chloride (LiCl) and 75 µl of chilled 100% ethanol were added and the sample was incubated overnight at -20°C. Next, the sample was spun down at maximum speed for 15 min, the supernatant was removed and the pellet was washed twice with 70% ethanol. After drying the pellet till it was clear, it was resuspended in 100 µl of RNase free water and the amount of DNA was measured using NanoDrop®.

2.7.5 *In situ* hybridisation

PV probe and a control Ngn2 probe were diluted in a pre-warmed hybridisation buffer (50% formamide, 10% dextran sulphate, 1 mg/ml yeast RNA (Roche), 1x Denhart's (Invitrogen), 200 mM NaCl, 10mM Tris-HCl (pH 7.5), 1 mM Tris base, 5 mM $NaH_2PO_4 \cdot H_2O$, 5 mM EDTA (pH 8)). A dilution series was performed for PV probe (final dilution was 1:1000) while Ngn2 was used 1:1000. Diluted probes were denatured for 10 min at 85°C, distributed on the pre-warmed (overnight) cryostat sections and covered with a 22 x 64 mm glass coverslip (VWR 631-0142). Slides were incubated overnight in a pre-warmed container humidified with 30% formamide, 150 mM NaCl and 15 mM tri-sodium citrate (pH 6.5) placed in a 65°C incubator. After hybridisations, coverslips were removed and the slides were washed in 50% formamide, 150 mM NaCl, 15 mM tri-sodium citrate (pH 6.5), 0.1% Tween-20 buffer at 70°C. Next, slides were washed in maleic acid buffer (100mM Maleic acid, 150mM NaCL, 0.1% Tween-20) at RT. Sections were blocked in a maleic acid buffer containing 20% sheep serum and 2% blocking reagent (Roche) for 1h at RT in a humidified chamber. After blocking, sections were incubated overnight at 4°C with an alkaline phosphatase (AP)-tagged anti-DIG antibody (1:500, Roche) diluted in blocking solution. This was followed by washes in maleic acid buffer at RT on a rocker. Colorimetric detection of AP was performed with NBT/BCIP (Roche) diluted according to manufacturer's protocol in the AP staining solution containing 100mM NaCl, $MgCl_2$, 100mM Tris HCL pH 9-9.5, 10% polyvinyl alcohol (Sigma) and 0.1% Tween-20. When the staining was satisfactory (overnight for the PV probe, 1-2 h for

Ngn2 probe), sections were washed in PBS and mounted with Aquatex mounting medium (Merck).

2.8 Cortical interneurons analysis

In brief, a 500 μm wide box was pasted onto the images of four cortical areas: primary sensory cortex (frontal **fSSp** and barrel **SSp**), ventral auditory cortex (**vAud**) and visual cortex (**Vis**) (Fig 2.02 A-B). In the medial prefrontal cortex (**MPFC**), brain areas were distinguished using anatomical features and the Allen Brain Atlas (Allen Institute for Brain Science) (Fig 2.02 D). While the top of the box was anchored to the pia of the cortex, the bottom was stretched to the end of layer VI/beginning of the white matter. For each brain, data from two hemispheres were collected and averaged for further analysis. During analysis I was blind to the genotype. Data were normalised to the cell density within the region of interest or to the area (an example of normalisation to the area is shown in Fig 2.03). The number of animals used for each interneuronal marker was between 3 and 8. In the electroporation experiment, the number of animals used was 3-10. Two-way ANOVA was used for analysing differences in the total cell number within the chosen area of the cortex between the WT, heterozygote and mutant genotype. Analysis of the cell distribution throughout cortical layers was first checked for normal distribution and then an appropriate test was applied (two-way ANOVA with Bonferroni post hoc test or Kolmogorov-Smirnoff test). A similar approach was used for the *in utero* electroporation experiment. The statistical program used was GraphPad Prism® version 6.0 (GraphPad Software, San Diego California USA). Tables with data regarding number of animals used for specific analysis, mean and standard deviation of the mean that correspond to graphical representation in the results chapters can be found in the appendix.

Fig 2.02 Regions of interest in the P21 cerebral cortex of Disc1 L100P and Q31L mutants. Following regions of interest (ROI; red boxes) were investigated in both Disc1 mutant mice: primary frontal somatosensory cortex (A), primary somatosensory cortex and ventral auditory cortex (B), visual cortex (C) and medial prefrontal cortex (MPFC). Adapted from Allen Brain Atlas (Allen Institute for Brain Science)

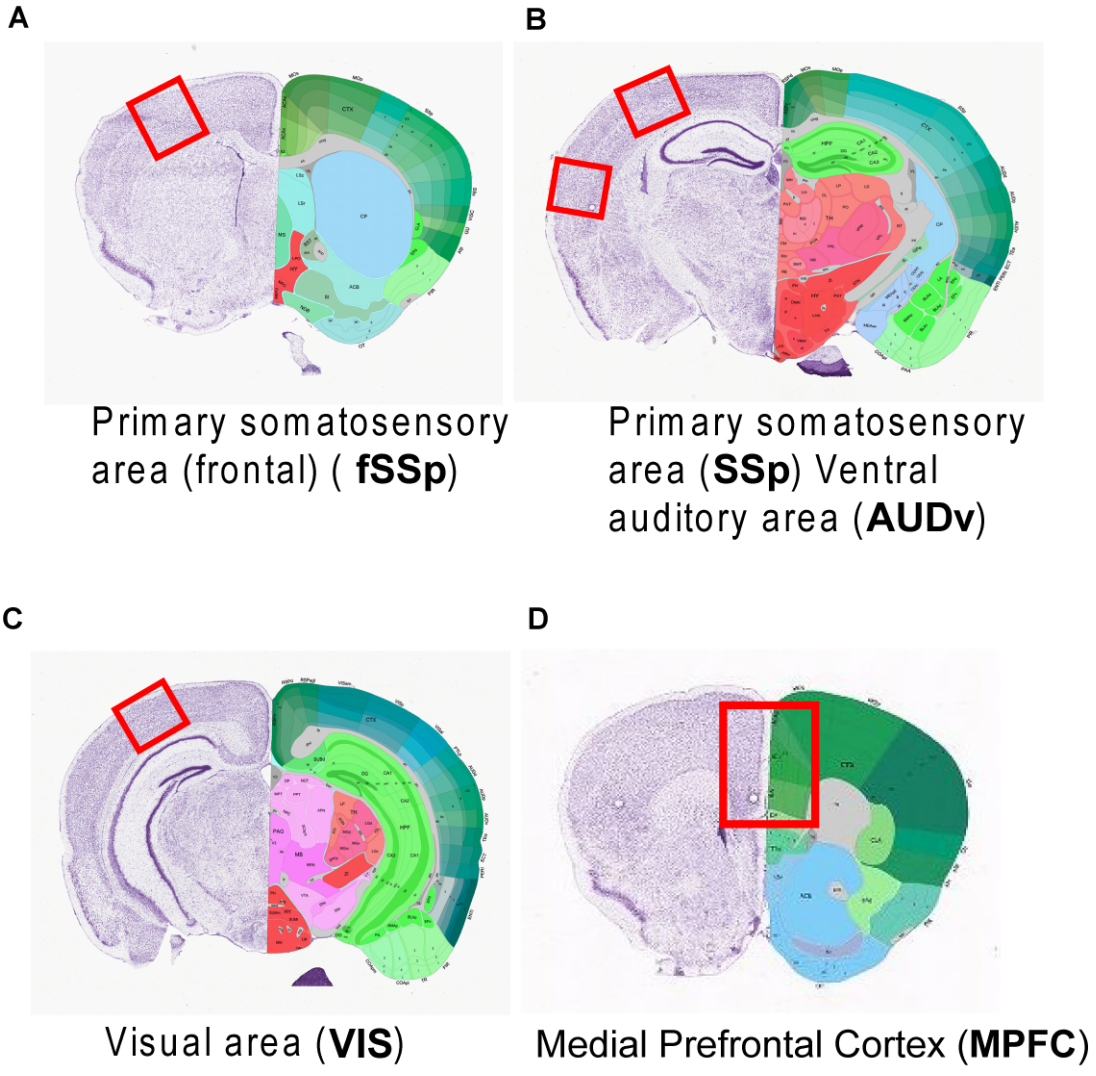

Fig 2.03 Analysis of the *in utero* electroporation of CAGG Disc1-100P IRES GFP into the fSSp at E14.5. Cells positive for GFP and parvalbumin were counted in a 500 µm wide cortical strip and normalised to the area (500 x D) or, for the distribution analysis, to the layer depth in proportion to cortical depth (scale bar: 100 µm).

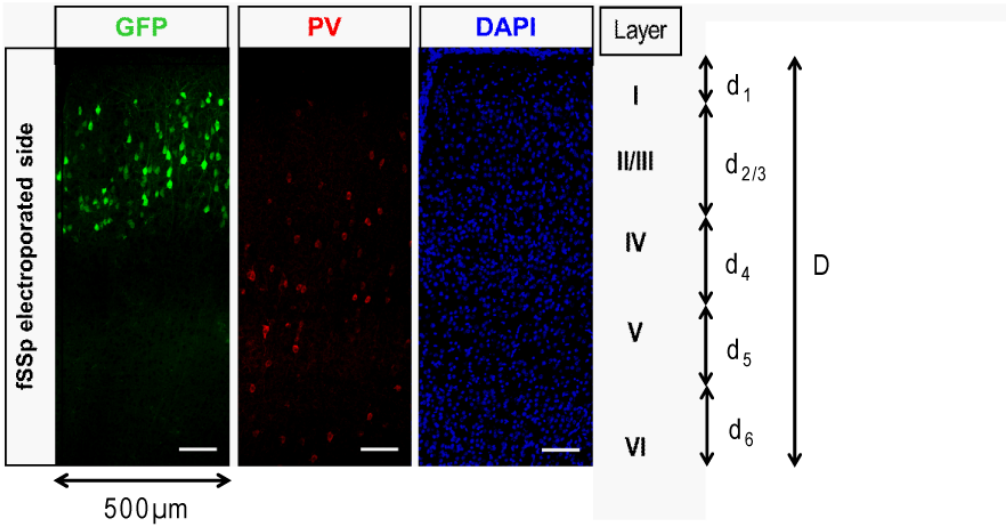

Chapter 3: Investigation of cortical interneuron populations in the cerebral cortex of Disc1 L100P and Q31L mutant mice

3.1 Introduction

A number of Disc1 genetically modified mouse lines have been created to investigate the phenotypic effects of a mutation in this gene. Mice overexpressing human or mouse Disc1 truncated at the position of the t(1:11) translocation breakpoint in the Scottish family, overexpression of the C-terminal part of DISC1, point mutation in exon 2 of mouse Disc1 or a selective knockdown by means of *in utero* electroporation or using a retrovirus showed both structural and behavioural changes that could be translated to those observed in humans affected by psychiatric disorders (Li et al., 2007; Clapcote et al., 2007; Pletnikov et al., 2008; Niwa et al., 2010; Zhou et al., 2013). Disc1 is present in vital brain regions such as the hippocampus and cerebral cortex, known to have a likely role in schizophrenia (Roberts, 2007). There is also evidence of Disc1 taking an active part in both brain development and neuronal function (Porteous and Millar, 2006) as well as outgrowth of neurites, neuronal migration and integration of newborn neurons (Chubb et al., 2008). Moreover, transgenic mice carrying mutated (human or endogenous) Disc1 were found to have traits that can be related to schizophrenia with spatial and working memory anomalies, hyperactivity and reduced sociability (Pletnikov et al., 2008; Kvajo et al., 2008). The structure of Disc1 itself gives some clues to its function. The Disc1 protein consists of multiple putative coiled-coil domains at its carboxy end implying the possibility of interaction with other proteins (Porteous and Millar, 2006). The best known DISC1 interactors are phosphodiesterase 4 (PDE4), especially PDE4B (Camargo et al., 2004), nuclear distribution E-like (NDEL1/NUDEL) and lissencephaly 1 (LIS1) (Brandon et al., 2004). The latter two are part of the centrosome/dynamin motor complex which implies a DISC1 role in neuronal migration. Such implication was made even more plausible by *in vivo* studies in which introduction of either lentiviral or plasmid vectors containing sequence knocking down DISC1 expression in an embryonic mouse brain caused disruption of cortical radial migration (Kamiya et al., 2005; Kubo et al., 2010). Disruption in radial migration was also shown in the ENU L100P and Q31L mice with a point mutation in exon 2 of DISC1 (mice characterised by Clapcote et al., 2007; study cited: Lee et al., 2011). Although the effect Disc1 has on the cortical

projection neurons was studied quite extensively, little attention was paid to the other group of cortical neurons - the GABAergic interneurons.

Unlike projection neurons, interneurons are born primarily in the ganglionic eminence (GE), a structure at the base of the telencephalon (subpallium) in rodents. The GE is a transient structure during development which in adult brain gives rise to the basal ganglia. It can be divided into three distinct parts: medial GE (MGE), caudal GE (CGE) and lateral GE (LGE). The interneurons born in the LGE are mainly destined to migrate rostrally to populate the olfactory bulb in rodents, but also have a minor contribution to the cortical interneuron population (reviewed in Metin et al 2006). A large portion of the CGE-born interneurons will populate the neocortex, though most of them will travel to the caudal parts of the telencephalon. The majority (about 70%) of the cortical interneurons originate in the MGE, from where they migrate laterally and, when reaching the cortex, spreading uniformly according to their birthdate (Miyoshi et al., 2007; Miyoshi et al., 2010; Miyoshi and Fishell, 2011). Similarly to the cortical projection neurons, the birthdates of the interneurons within particular parts of the GE are correlated to their position within the neocortex (Miyoshi and Fishell., 2011). The MGE-derived interneurons follow a similar 'inside-out' pattern to that of the migrating pyramidal cells as well as matching their birthdates. However, the CGE-born cells contribute about 75% of their total number to more superficial layers and approximately 25% to the deeper layers of the cortex (Miyoshi et al. 2010). This phenomenon occurs regardless of the birth time of the CGE-derived interneurons. The birth place of the cortical interneurons also correlates with their neurochemical subgroups. The largest subtype of interneurons in the cortex, the parvalbumin expressing cells, is born exclusively within the MGE. Other types of MGE-derived cortical GABAergic interneurons are those containing somatostatin (mainly generated in the MGE, with a minor contribution from the CGE) and NPY (about half of them generated in the MGE, the other half is produced in the CGE). There is also a minor input from the MGE to the population of calretinin positive cells, which are mainly generated in the dorsal part of the CGE.

The immature interneurons migrate tangentially from the ventral telencephalon to the neocortex. The movement of the future interneurons is directed by extracellular motogenic cues, both attractive and repelling. Generally, the direction of cell motion is based on the polarity of the cell, i.e. the highly polarised part of the cell is a marker of the direction of cell movement. From there a leading process is generated, which generally works similarly to that of the growth cones of the extending axons, i.e. they are a form of probe that reacts to external cues and adjusts their behaviour accordingly. The movement of the neuronal cell as a reaction to the information from the leading process is known as locomotion. There are three distinct steps of locomotion. The first is the extension of the leading process to probe the surroundings. Next, there is translocation of the nucleus in the direction of the leading process, a process known as nucleokinesis (see Metin et al., (2006) for more details regarding proteins and dynamics involved in this process). Here, the centrosome is involved and with it DISC1 acts as a scaffold for NDEL1 and LIS1, genes without which the dynein motor at the centrosome does not work properly (Brandon et al., 2009). Lastly, the remaining 'trailing' process is eliminated and the whole cycle begins again. These three phases of cell locomotion are used in interneuron migration with one difference being that the cell uses two branches of the leading process to search for the migration permissive area (for more details see a review by Marin et al 2010). This greatly increases the area scanned and most probably speeds up interneuron migration so that they can arrive at their final destination in the cortex and mature in time to form connections with other cortical neurons.

Upon arrival into the marginal zone and intermediate zone, the interneurons cease their tangential orientation of migration and switch to radial relocation into their destined cortical layers. This occurs postnatally in mouse neocortex and is in parallel with the final stages of projection neuron migration into the cortex. In general, the immature interneurons that migrated to the cortex via the marginal zone will start a downward motion in the direction of the ventricle, while the interneurons migrating via the intermediate zone will migrate towards the pia in a manner similar to that used by the pyramidal neurons. However, the radial migration of the majority of the

interneurons seems to be independent of reelin signalling which is different to that of the glutamatergic neurons (see a review by Nakajima, 2007). What the interneurons most probably use to find their destination in the cortex is the interaction between them and the simultaneously born projection neurons that have already settled within their destined layers (Hevner et al., 2004).

In this study I investigated the role Disc1 has on the formation of cortical interneurons using two mouse models that have an ENU-generated point mutation in Disc1 - the L100P and Q31L mutants. To see if there is any change in interneuron density and their laminar distribution within the cortex I analysed the interneuron marker glutamate decarboxylase 67 (GAD67) expression in four cortical regions of the 3-week-old mouse brain: frontal primary somatosensory (fSSp), primary somatosensory (SSp), ventral auditory (vAud) and visual (Vis). In these regions I have also assessed the density of parvalbumin, somatostatin and calretinin - neuronal markers of the three major cortical interneuron subgroups. Laminar distribution of parvalbumin expressing cells as well as density of cells with parvalbumin mRNA and parvalbumin protein expression in the medial prefrontal cortex was analysed in the L100P strain once parvalbumin was shown to be downregulated in the four regions mentioned above.

3.2 Results

3.2.1 Analysis of cortical interneuron density and distribution in the adult Disc1 L100P mutant brains

3.2.1.1 Mild decrease in the total cell density in some areas of Disc1 L100P mutant cortex

Since the Disc1 L100P mutants (both homozygous and heterozygous for the mutation) have reduced brain volume (Clapcote et al., 2007) and lower density of NeuN-positive cells (Lee et al., 2011), I firstly assessed if there are any changes in overall cell density and the cortical depth in P21 Disc1 L100P/+ (heterozygous) and L100P/L100P (homozygous) mouse brains when compared to their wild type littermates (WT). Cell density was reduced in the L100P homozygous mutants in the primary somatosensory and visual cortices when compared to the L100P/+ and WT littermates (Fig 3.01 A, B). There was no reduction in the total cell density in the frontal somatosensory and the ventral auditory cortices when compared to the WT controls (Fig 3.01 B). There was no difference in the cortical depth between the WT and L100P/L100P in all of the analysed cortical regions (Fig 3.01 C). A small but significant decrease in the cortical thickness was observed in the L100P/+ primary somatosensory cortex when compared to the WT and L100P/L100P littermates (Fig 3.01 C).

A mild decrease in the cell density observed in the primary somatosensory and visual cortices in the homozygous Disc1 L100P mutant mouse brain was restricted to cortical layer VI (Fig 3.01 E and G). A significant increase in the cell density in the L100P/+ primary somatosensory cortex layer II/III and a decrease in the ventral auditory cortex layer VI was also observed (Fig 3.01 E,F). There was no significant change in the cell density across the frontal somatosensory cortex in the L100P/+ and L100P/L100P mutant brains (Fig 3.01 D).

Fig 3.01 Decrease in total cell density in the visual cortex of P21 Disc1 L100P/L100P mutant brain. DAPI stain was used to distinguish between the cortical layers as well as visualise the nuclei for the total cell count (A1-A4; Scale bar 100 μm). Cell density was significantly reduced in the homozygous mutant when compared to WT (B) with no difference in the cortical thickness between L100P/L100P and WT (C). There was a minor laminar distribution defect in SSp (E), vAud (F) and Vis (G) with none in the fSSp (D). (n = 3 animals per genotype; ANOVA with Bonferroni post hoc test: * $p<0.05$; ** $p<0.01$; *** $p<0.001$)

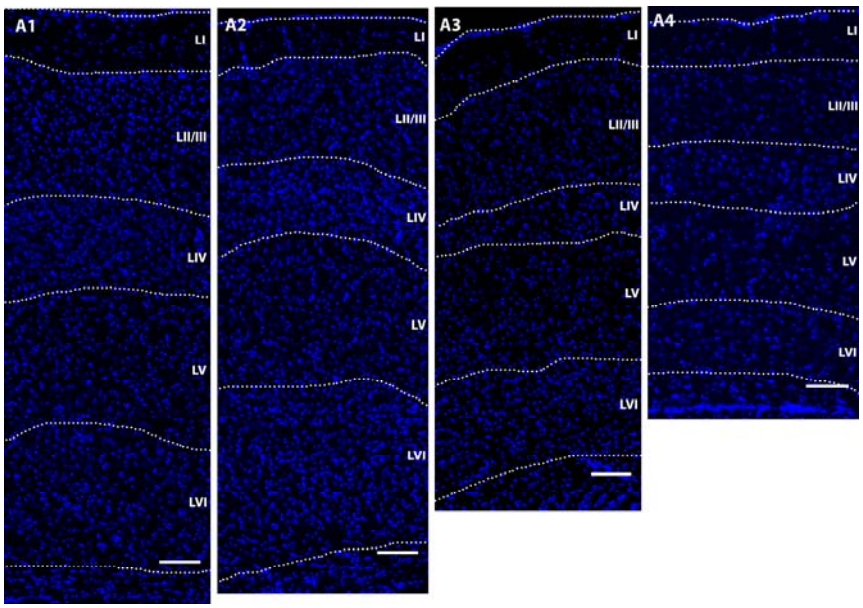
A1
A2
A3
A4
LI
LII/III
LIV
LV
LVI

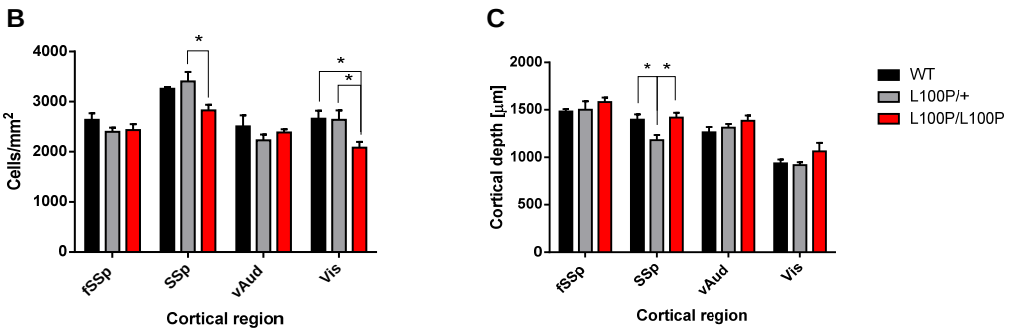
B
Cells/mm2
4000
3000
2000
1000
0
fSSp
SSp
vAud
Vis
Cortical region
C
Cortical depth [µm]
2000
1500
1000
500
0
WT
L100P/+
L100P/L100P

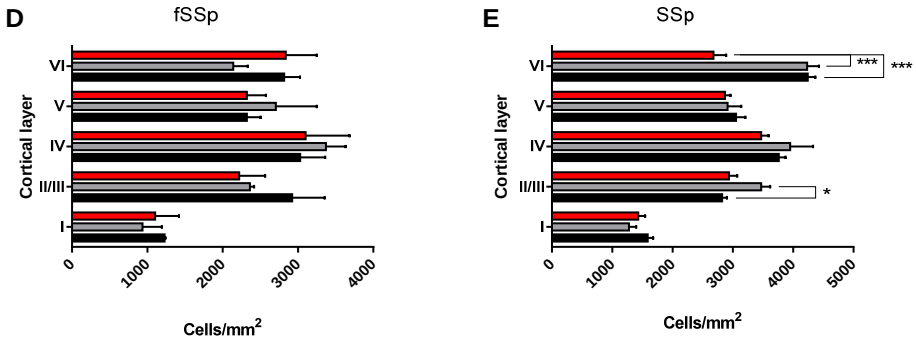
D
fSSp
E
SSp
Cortical layer
VI
V
IV
II/III
I
0
1000
2000
3000
4000
5000
Cells/mm2

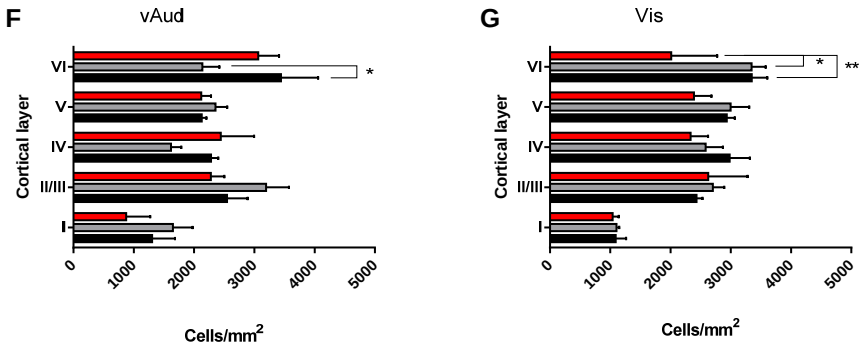
F
vAud
G
Vis
Cortical layer
VI
V
IV
II/III
I
0
1000
2000
3000
4000
5000
Cells/mm2

3.2.1.2 Decrease in parvalbumin expression but not interneuron number across Disc1 L100P mutant mouse cortex

To assess interneuron density in the mouse cerebral cortex I immunoassayed the brain tissue for an interneuron marker, glutamate decarboxylase 67 (GAD67). GAD 67 is an enzyme that synthesises gamma-aminobutyric acid (GABA) from glutamate and is expressed in the soma of all cortical interneurons. There was no change in the interneuron density across the cortex of the L100P+ and L100P/L100P mouse brain when compared to the WT (Fig 3.02 A). Next, I investigated the three major distinct subclasses of cortical interneurons: parvalbumin, somatostatin and calretinin expressing cells (Gonchar and Burkhalter, 1997; Xu et al., 2004). In the L100P/L100P mouse brain there was a striking reduction in parvalbumin expressing cell density when compared to the WT littermate control in all of the cortical regions analysed (Fig 3.02 B, Fig 3.03). Furthermore, parvalbumin cell density was significantly reduced in the ventral auditory and visual cortices of the L100P/+ brain when compared to the WT controls (Fig 3.02 b, Fig 3.03). In order to assess whether this reduction in parvalbumin protein expression is due to a transcription or translation defect I performed an *in situ* hybridisation with the parvalbumin probe designed previously by Tanahira et al. (2009). In all of the cortical regions analysed, parvalbumin mRNA was markedly reduced in the L100P/L100P cortex when compared to the WT (Fig 3.02 c, Fig 3.03) suggesting that the observed downregulation of parvalbumin protein expression in the cells normally expressing this calcium binding protein is most probably due to a decrease in the parvalbumin mRNA in these cells. This in turn strongly suggests that Disc1 has an effect on the transcription of the parvalbumin gene.

Cell densities of the other two subpopulations of interneurons were mostly unaffected. Somatostatin was significantly reduced in the ventral auditory region of the L100P/+ and L100P/L100P brain cortex when compared to the WT controls (Fig. 3.02 E). There was also a significant increase in somatostatin density in the L100P/+ visual cortex when compared to the WT (Fig 3.02 E). No significant changes were

observed in calretinin density across the neocortex in both L100P/+ and L100P/L100P brains (Fig 3.02 D).

3.2.1.3 Minor disruptions in the distribution of interneurons in Disc1 L100P mutant mouse cortex

Since the L100P/L100P mutant exhibits an altered neuronal distribution across the neocortex (Lee et al., 2011) I investigated if there is any disturbance in the cortical distribution of interneurons in these mouse brains. Only layer I of the ventral auditory cortex showed an increase in GAD67 cell density in the L100P/L100P mutant when compared to the WT control and the L100P/+ littermate (Fig 3.04 C). Similarly, there was a significant increase in the density of GAD67 expressing cells in the primary somatosensory cortex in the L100P/+ mouse when compared to the WT and L100P/ L100P (Fig 3.04 B). GAD67 expression seems to be uniform across the cortical layer I in WT cortex. The increase of these cells in more lateral ventral auditory cortex in the mutant could suggest a minor migratory defect. Frontal somatosensory and visual cortices were unaffected by the mutation (Fig 3.04 A and D).

3.2.1.4 Disruption of the parvalbumin positive cell distribution across the neocortex in Disc1 L100P mutant mouse cortex

With no major defect in the cortical interneuron distribution across the cortex and a substantial decrease in parvalbumin expression in the L100P/L100P mouse brain I investigated cortical distribution of parvalbumin cells. There was a substantial reduction in parvalbumin cells in cortical layer IV in the L100P/L100P and L100P/+ when compared to the WT littermates (Fig 3.05 A-D). In the primary somatosensory, ventral auditory and visual cortices there is also a significant decrease in parvalbumin cells in layer V of the L100P/L100P mice when compared to WT or L00P/+ mice (Fig 3.05 B-D). This layer is also affected in the ventral auditory and visual cortices of the heterozygote L100P mutant when compared to WT (Fig 3.05 C-D). Lastly, a similar reduction in parvalbumin cells is observed in layers II/III of

Fig 3.02 Downregulation of parvalbumin in cortical interneurons across the cortex of the P21 Disc1 L100P/L100P mouse brain. No change in the density of the GAD67 expressing cells in all the cortical regions analysed (A). There was a decrease in parvalbumin protein expressing (B) and parvalbumin mRNA expressing (C) cell density across the cortex. There was no change in calretinin positive cell density (D) and only small changes in somatostatin expressing cell density (E) (n = 3-8 animals per genotype; ANOVA with Bonferroni post hoc test: * $p<0.05$; ** $p<0.01$; *** $p<0.001$)

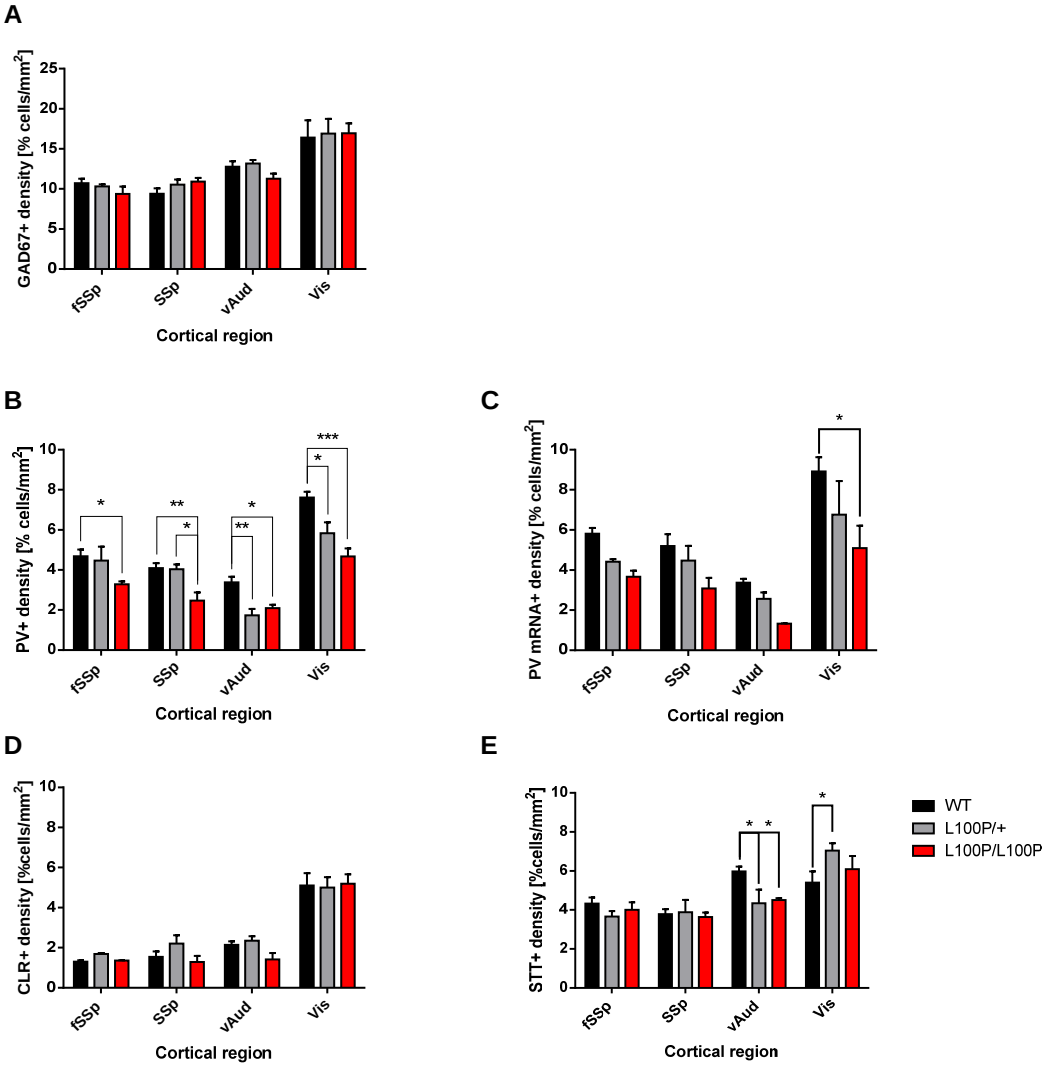

Fig 3.03 Parvalbumin and parvalbumin mRNA expression in the frontal somatosensory cortex of the P21 L100P mutant strain. Parvalbumin expression in the WT (A), L100P/+ (B) and L100P/L100P (C) cortex. Parvalbumin mRNA expression is shown in the WT (D), L100P/+ (E) and L100P/L100P (F) fSSp cortex. Scale bars: A-B, D-F: 200 µm; C: 100 µm.

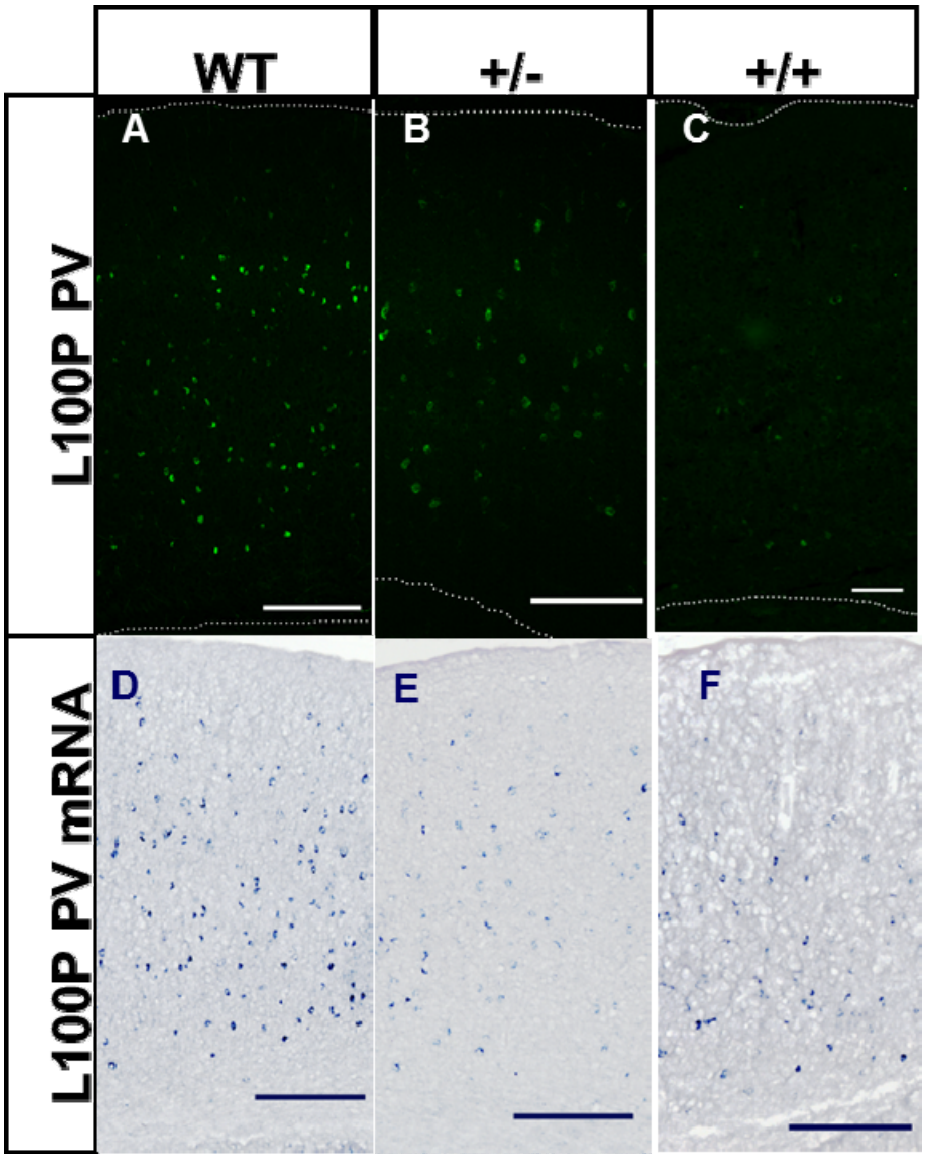

Fig 3.04 Laminar distribution of the cortical interneurons is mildly disrupted in the L100P mutants. GAD67 cell density in the frontal primary somatosensory (A), somatosensory (B), ventral auditory (C) and visual (D) cortices (n=3-4 animals per genotype; ANOVA with Bonferroni post hoc test: * p<0.05; ** p<0.01; *** p<0.001)

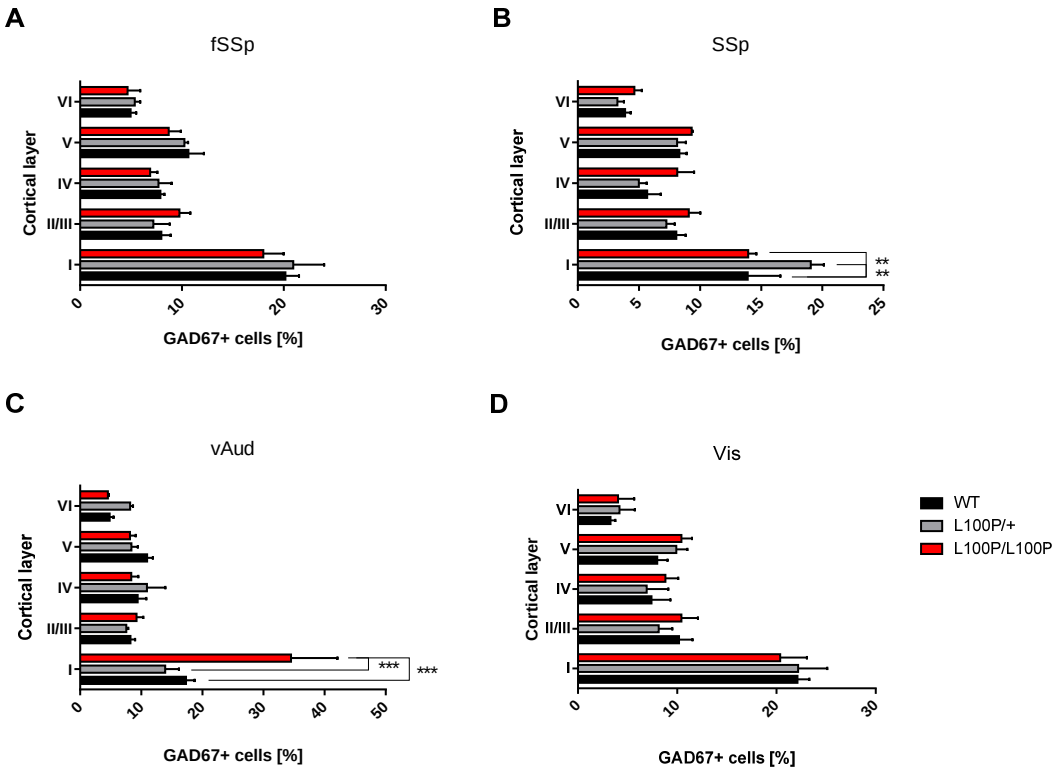

the primary somatosensory cortex in the L100P/+ ($p = 0.06$, $n = 4\text{-}8$; Two-way ANOVA with Bonferroni multiple comparison test) and L100P/L100P when compared to the WT littermate control (Fig 3.05B).

3.2.1.5 No changes in cell density and parvalbumin expression in the medial prefrontal cortex (MPFC) of Disc1 L100P mutant mouse brain.

All of the areas investigated so far are related to the sensory modalities which are affected in most schizoaffective disorders: auditory, visual, sensory (Boksa, 2009). However, the cortical region most studied in these diseases is prefrontal cortex (PFC), a region believed to be responsible for higher cognition (Wood and Grafman, 2003). There is some controversy when it comes to assessing if the rodent equivalent of the human PFC - medial prefrontal cortex (MPFC) has the same functions. Nonetheless, this region has been implicated in attention, learning and decision making in the rodent (Birrell and Brown, 2000; Euston et al., 2012). Although parvalbumin was found to be downregulated across the Disc1 L100P mutant mouse cortex, no such reduction was found in the limbic area (LA; infralimbic area (ILA) plus prelimbic area (PL)), anterior cingulate area (ACA) and MPFC (LA plus ACA) in the L100P mutant brains (Fig 3.06 C). There was also no difference in the total cell density and the cell distribution across the cortical regions in the mutants when compared to the WT (Fig 3.06 A-B, D-E).

Fig 3.05 Laminar distribution of the parvalbumin expressing interneurons is highly disrupted in the L100P/+ and L100P/L100P brains. Parvalbumin cell density in the frontal primary somatosensory (A), somatosensory (B), ventral auditory (C) and visual (D) cortices (n = 3-4 animals per genotype; ANOVA with Bonferroni post hoc test: * p<0.05; ** p<0.01; *** p<0.001

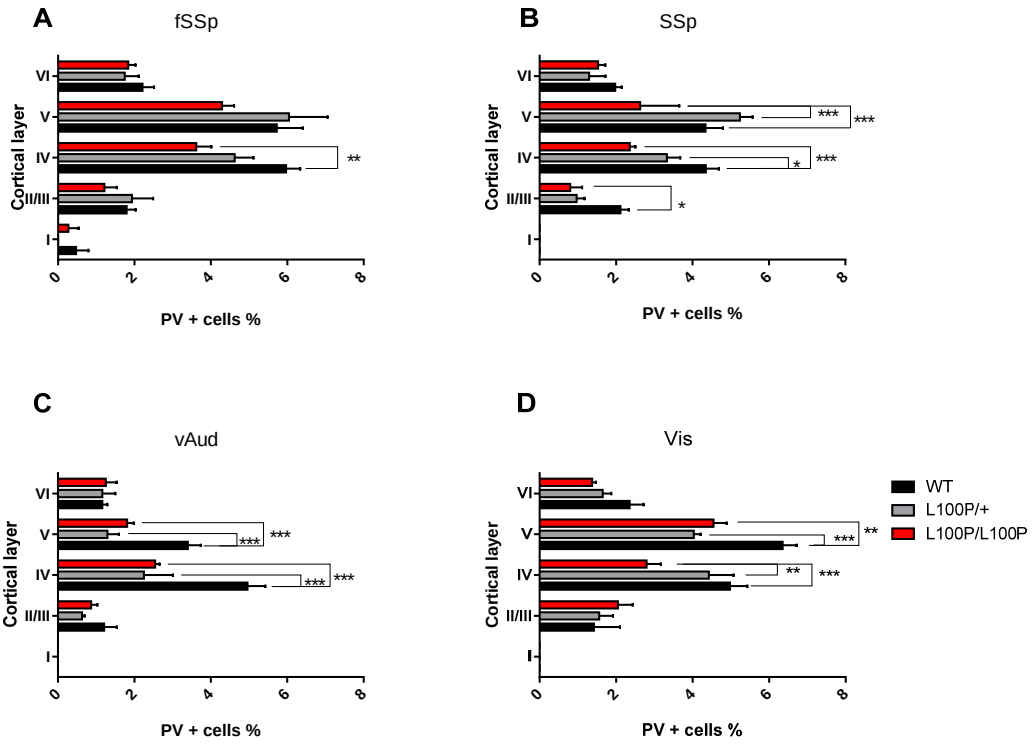

Fig 3.06 Cell density and laminar distribution of the parvalbumin expressing interneurons is not disrupted in the medial prefrontal cortex of the L100P/+ and L100P/L100P brains. Medial prefrontal cortex and the regions within (A). Total cell density (B) and parvalbumin cell density (C) is not affected in the infra- and prelimbic areas (ILA and PLA respectively), anterior cingulate area (ALA) and in medial prefrontal cortex (ILA + PLA + ALA) and limbic system (LA = ILA + PLA). Relative distribution in the LA (D) and MPFC (E) is not disrupted either. (n = 3-5 animals per genotype; ANOVA with Bonferroni post hoc test: * $p<0.05$; ** $p<0.01$; *** $p<0.001$). Scale bar 100 μm.

A

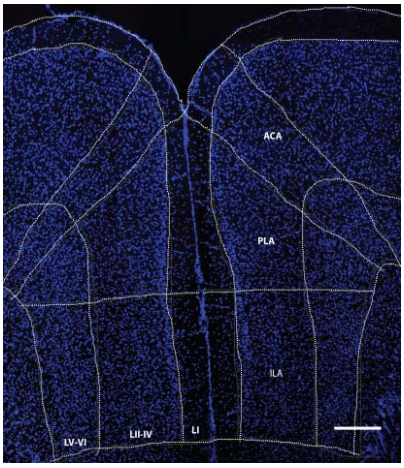
ACA
PLA
ILA
LV-VI
LII-IV
LI

B

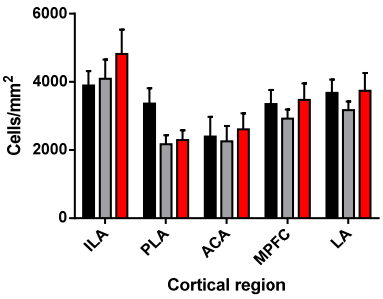
6000
4000
2000
0
Cells/mm2
ILA
PLA
ACA
MPFC
LA
Cortical region

C

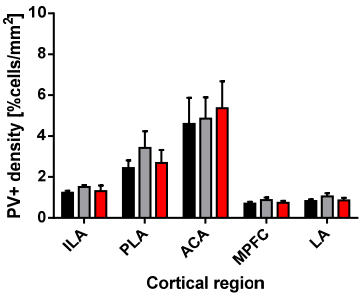
10
8
6
4
2
0
PV+ density [%cells/mm2]
ILA
PLA
ACA
MPFC
LA
Cortical region

D

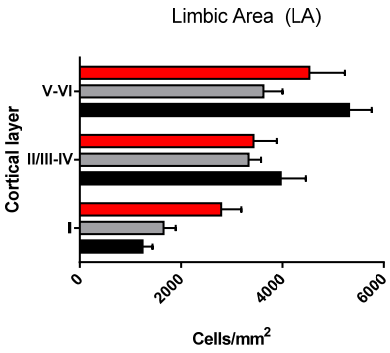
Limbic Area (LA)
V-VI
II/III-IV
I
Cortical layer
0
2000
4000
6000
Cells/mm2

E

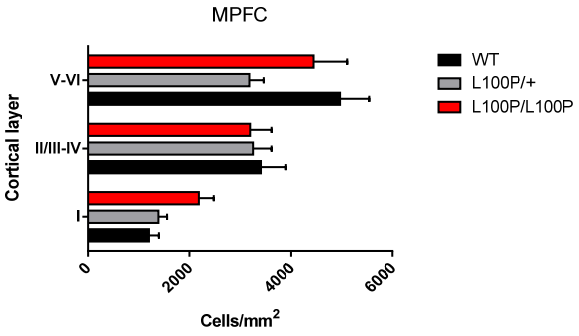
MPFC
V-VI
II/III-IV
I
Cortical layer
0
2000
4000
6000
Cells/mm2
WT
L100P/+
L100P/L100P

3.2.2 Analysis of cortical interneuron density and distribution in the adult Disc1 Q31L mutant brain

3.2.2.1 Decreased cell density in visual cortex of Disc1 Q31L mutant brain

Similar to the Disc1 L000P mouse mutant brain, the Q31L homozygous and heterozygous mutants have reduced brain volume and reduced cortical neuron density (Clapcote et al., 2007; Lee et al., 2011). In Q31L/Q31L mutant brain, there is a significant decrease in the cell density in the visual cortex when compared to the Q31L/+ brain (Fig 3.07 A). This decrease in cell density in the homozygous Q31L mutant visual cortex is also almost significant ($p = 0.0607$, $n = 3\text{-}5$; Two-way ANOVA with Bonferroni multiple comparison test) when compared to the WT littermate controls (Fig 3.07 A). There is a significant increase in the cell density in the primary somatosensory cortex of the Q31L/+ brain when compared to the WT and Q31L/Q31L littermates (Fig 3.07 A). However, it is most probably due to a significant decrease in the cortical depth in this area in the brain of heterozygotes (Fig 3.07 B).

There was no difference in cell distribution in the frontal somatosensory cortex of the Q31L/+ and Q31L/Q31L mouse brains when compared to the WT control (Fig. 3.07 C). In the primary somatosensory cortex, there was a decrease in the cell density in cortical layer IV of the L100P/L100P brain and an increase in layers II/III and V of the Q31L/+ mice (Fig 3.07 D). In the Q31L/+ ventral auditory cortex, cell density in layer IV was markedly reduced when compared to the WT and Q31L/Q31L mice (Fig 3.07 E). It is possible, though unlikely, that this reduction was due to difficulty in distinguishing between layers II/III and IV in this region resulting in a smaller cell number and/or larger layer 4 areas in Q31L/+ group. In the visual cortex - the only region in which the cell density was reduced - there is an increase in the cell density in layer I and decrease in layer V in the Q31L/Q31L cortex when compared to the WT controls (Fig 3.07 F). In layers II/III, there is a further reduction of the cell density in the Q31L/Q31L mutant cortex but this is only significant when compared to the Q31L/+ cortex. Furthermore, there is a significant increase in the cell density

in layer IV in the Q31L/+ mice when compared to the WT and Q31L/Q31L littermates cortex as well as a reduction in the cell density in layer V, though this is not significant ($p = 0.0565$, $n = 3\text{-}5$; Two-way ANOVA with Bonferroni multiple comparison test) (Fig 3.07 F). Taken together, although there is not much difference in the overall cell density between the Q31L/Q31L, Q31L/+ and WT control, there are major disturbances in the cortical layer cell densities, mainly in the primary somatosensory and visual cortices.

3.2.2.2 No major changes in the cortical interneuronal density in Disc1 Q31L mutant mouse cortex

Just as in the case of the Disc1 L100P mutant, there was no difference in GAD67 positive cell density across the cortex (Fig 3.08 A). However, unlike the profound downregulation of parvalbumin expression in the L100P mutant cortex, there was no significant difference in parvalbumin cell density in all of the cortical regions analysed in the Q31L/Q31L and Q31L/+ mice when compared to their WT littermates (Fig 3.08 B-C). The Q31L mutation in Disc1 did not affect the density of calretinin expressing interneurons across the cortex (Fig 3.08D). Interestingly, just as in the L100P line, there was a significant decrease in somatostatin expressing cell density in the ventral auditory cortex of the Q31L/Q31L brain when compared to the WT control (Fig 3.08 E). This effect was not observed in the heterozygote and the difference between the WT and the mutant was much smaller (1.48% /mm^2 and 0.61% /mm^2 for L100P and Q31L respectively) suggesting that the two mutations have either have different effects on the somatostatin expressing cells or similar effect of different magnitude.

Fig 3.07 Decrease in total cell density in the visual cortex of the P21 Disc1 Q31L/Q31L mutant brain. Cell density was significantly reduced in the homozygous mutant when compared to WT (A) with no difference in the cortical thickness between Q31L/Q31L and WT (B). There was a minor laminar distribution defect in SSp (D), vAud (E) and Vis (F) with none in the fSSp (C). (n = 3-5 animals per genotype; ANOVA with Bonferroni post hoc test: * $p<0.05$; ** $p<0.01$; *** $p<0.001$)

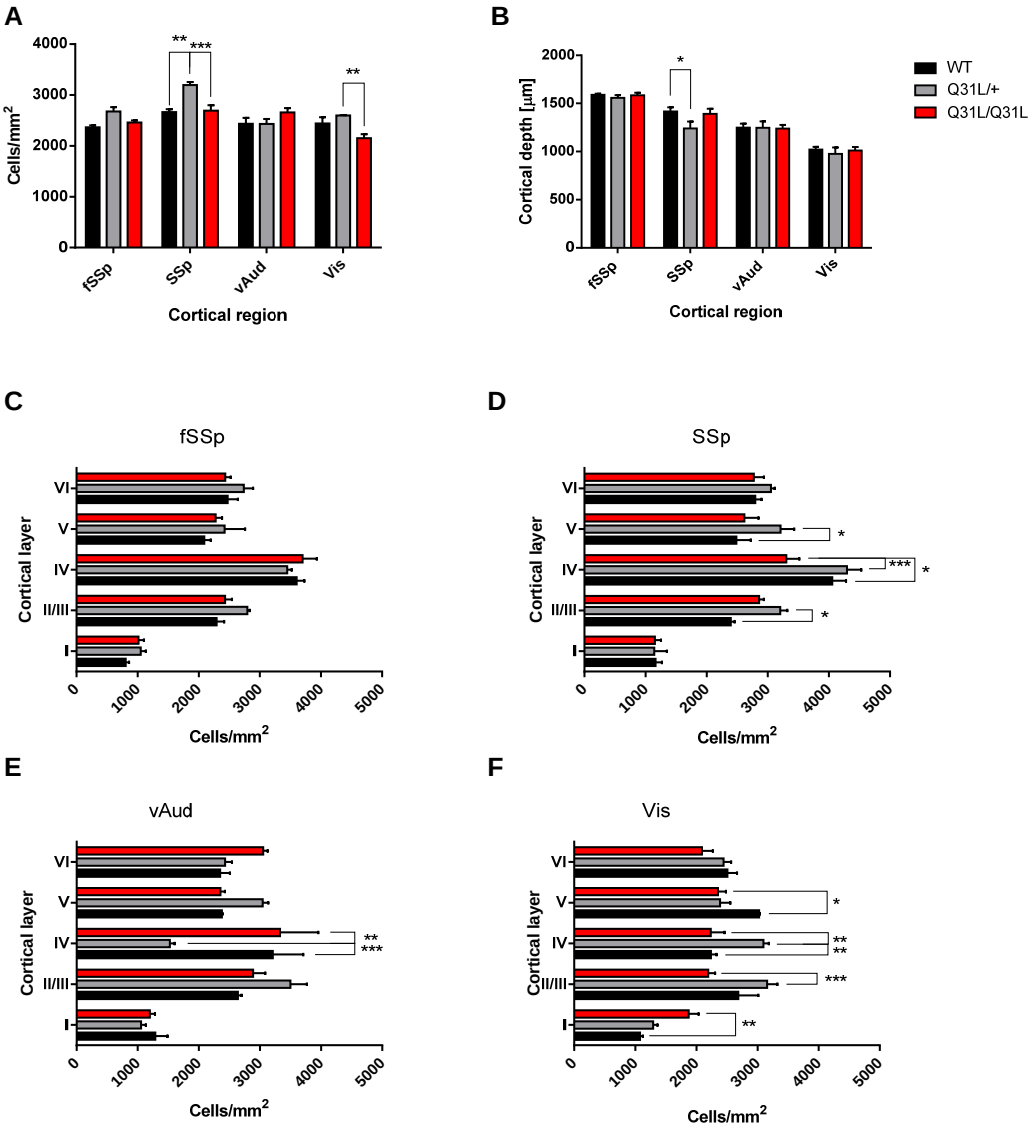

Fig 3.08 No major changes in the cortical interneurons across the cortex of the P21 Disc1 Q31L/Q31L mouse brain. No change in the density of GAD67 expressing cells in all the cortical regions analysed (A) as well as in parvalbumin (B) and calretinin positive cell density (C). A small change in the somatostatin expressing cell density in the ventral auditory cortex was observed (D) (n = 3-9 animals per genotype; ANOVA with Bonferroni post hoc test: * $p<0.05$; ** $p<0.01$; *** $p<0.001$). Scale bar: 200 μm.

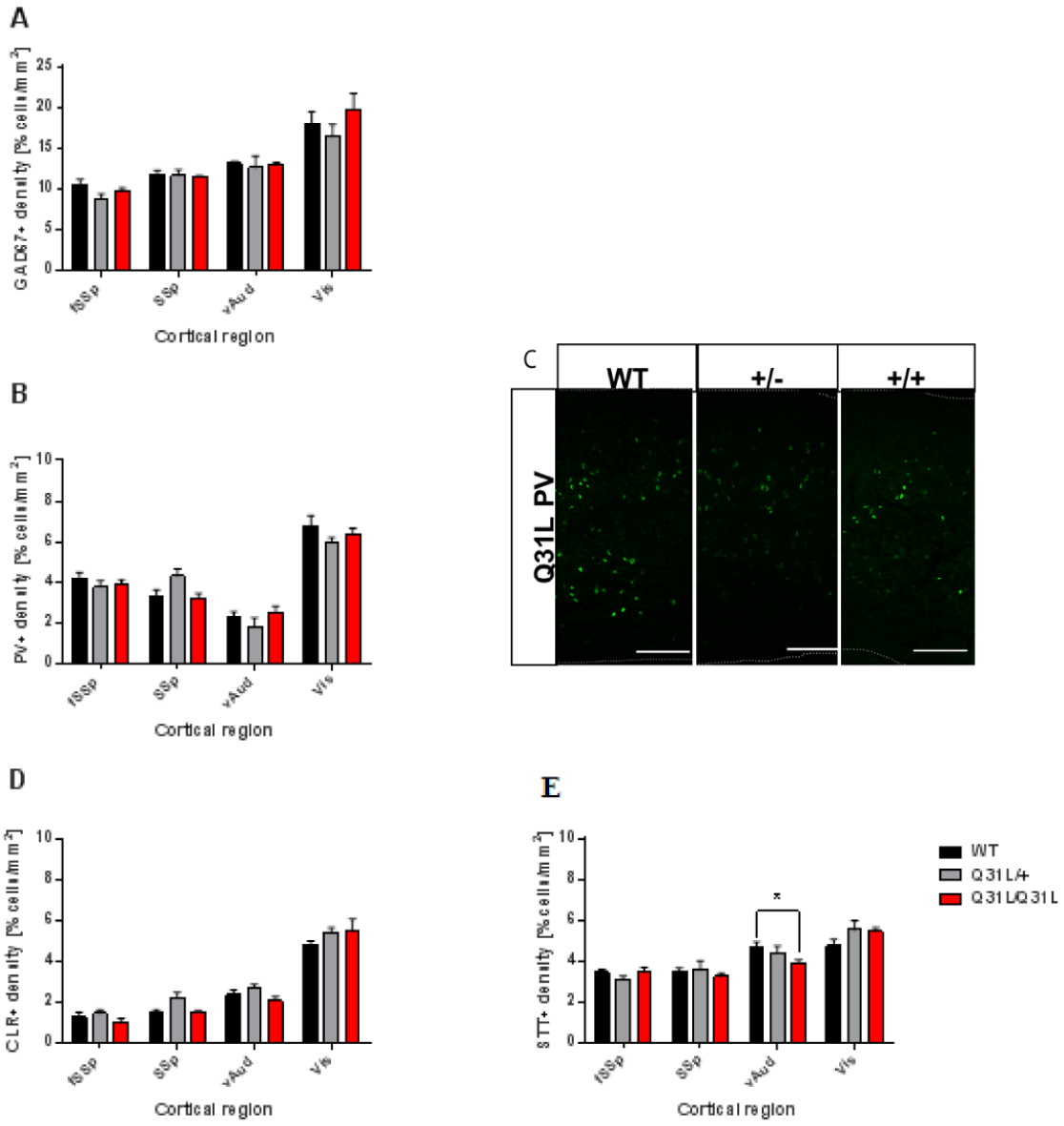

3.2.2.3 Minor disruption in cortical interneuron distribution in the Disc1 Q31L mutant mouse brain.

The distribution of cortical neurons is disrupted in the Disc1 Q31L mutants (Lee et al., 2011). As in the case of the L100P mutant, there was no difference in the interneuron density across the cortex. Interestingly, the few minor disruptions in the distribution of these cells in the Q31L mutants' cortex are observed predominantly in layer II/III of SSp and vAud between Q31L/+ and Q31L/Q31L (Fig 3.09 B, C). In the fSSp, there is a significant increase in layer V of Q31L/Q31L when compared to WT (Fig 3.09 A). Interneuron distribution was not changed in the visual cortex of the Q31L/+ and Q31L/Q31L mice when compared to the WT littermates (Fig 3.09 D).

Fig 3.09 Laminar distribution of the cortical interneurons is mildly disrupted in the Q31L mutants. GAD67 cell density in the frontal primary somatosensory (A), somatosensory (B), ventral auditory (C) and visual (D) cortices (n = 3-4 animals per genotype; ANOVA with Bonferroni post hoc test: * p<0.05; ** p<0.01; *** p<0.001)

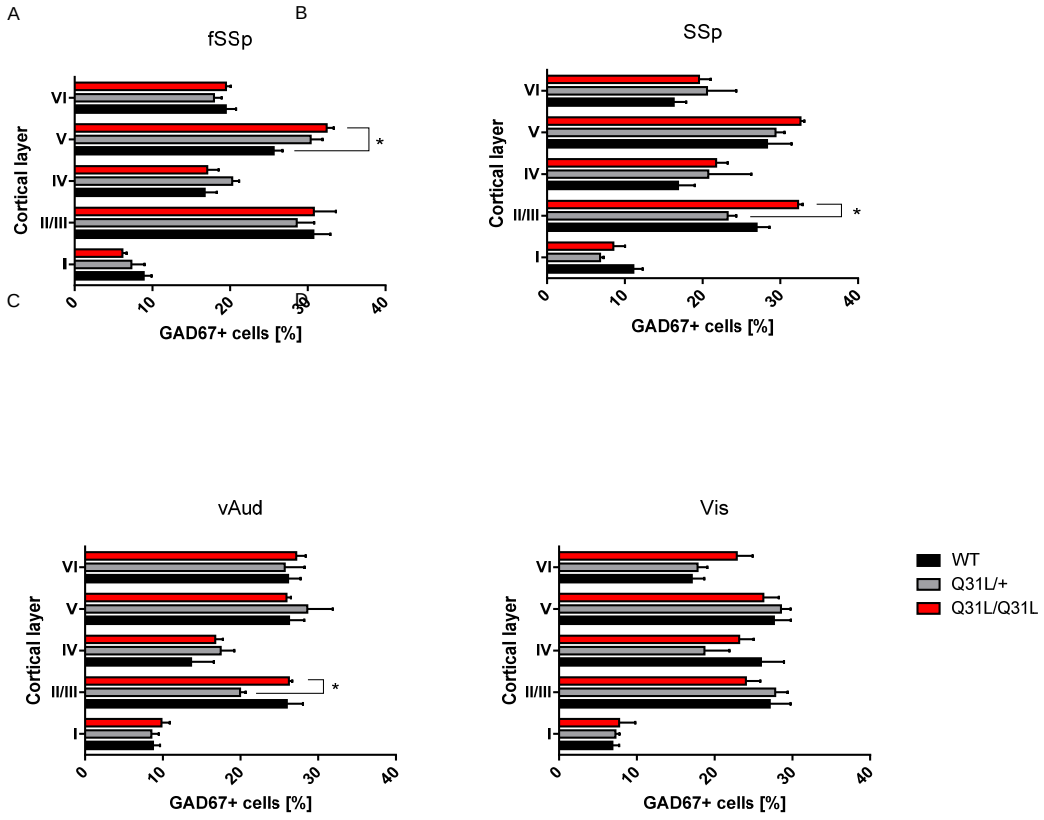

3.3 Discussion

The animals used in this study were Disc1 L100P and Q31L heterozygous and homozygous mutant mice which have a point mutation in exon 2 of the Disc1 gene resulting in a schizophrenia-like and depressive-like phenotype respectively (as characterised by Clapcote et al., 2007). As was recently shown, both mutants show disruption in cortical neuronal migration (Lee et al., 2011) and from previous studies it is known that DISC1 plays a role in radial migration in the cortex (Kamiya et al., 2005; Kubo et al., 2010; Ishizuka et al., 2011) and migration of pyramidal neurons in the hippocampus (Tomita et al., 2011). At the time I started this project there was little data on DISC1 involvement in the development of cortical interneurons. Transgenic mice expressing truncated Disc1 showed a reduced number of parvalbumin cells in the medial prefrontal cortex (MPFC) and hippocampus with a disruption in their distribution in the dorsolateral frontal cortex (DLFC) (Shen et al., 2008). Mice expressing a dominant negative C-terminus truncated form of Disc1 also showed a reduction in parvalbumin interneurons in the MPFC, with no change in the number of calretinin and calbindin neurons (Hikida et al., 2007). However, in another study these mice did not show any decrease in the parvalbumin in the MPFC unless the neonatal mice were injected with the polyriboinosinic-polyribocytidylic acid (polyI:C) to cause an innate immune response (Ibi et al., 2010). This mouse model also showed no changes in the parvalbumin cells in the hippocampus with and without exposure to the polyI:C. Overexpression of mutant human DISC1 (hDISC1-ΔC) both pre- and postnatally also resulted in a decrease in parvalbumin cell number in areas of the frontal cortex (Ayhan et al., 2011). However, none of those papers hinted at any mechanisms behind parvalbumin reduction in Disc1 mutants nor did they assess if Disc1 mutations result in changes in the overall interneuron numbers or, in some cases, other subpopulations of interneurons. So far, only a paper from Jurgen Bolz's group showed *in vitro* and *in silico* that knockdown of Disc1 results in an abnormal migration of the interneurons (Steinecke et al., 2012).

Here, I have addressed the question of whether there are any differences in the density and distribution of the interneurons in cortex of mice hetero- and

homozygous for the L100P and Q31L point mutations in Disc1 when compared to their WT littermates. In both mutants, the interneurons accounted for 10-15% of total cell density per mm^2 of area (depending on the cortical region) which is in line with the interneurons being up to 20% of neurons in the cortex. I found no changes in the density of interneurons across the cortex in both Disc1 mutants. Minor differences in the distribution of the interneurons were found mainly in layer I of primary somatosensory and ventral auditory cortices in both mutants and in frontal somatosensory cortex in the Q31L/Q31L mice. However, in the case of the Q31L line, in all cases but for the layer I frontal somatosensory cortex ($p = 0.0136$, $n = 3\text{-}4$, Two-way ANOVA with Bonferroni multiple comparison test), the significance is marginal ($0.04 < p < 0.05$, $n = 3\text{-}4$; Two-way ANOVA with Bonferroni multiple comparison test) with fairly large variations within the samples judging from the size of the error bars. This means that in the case of the Q31L mutants, a larger sample would be needed to determine if the differences in the layer I interneurons could be biologically relevant. Furthermore, lack of any significant difference in other layers in both homozygous mutants could suggest Disc1 involvement in the switch from the tangential to radial migration that normally occurs perinatally in the marginal zone in the rodent cortex (Nadarajah et al., 2002; Metin et al., 2006).

In both Disc1 mutants, I have also assessed the density of the cells expressing major interneuron markers: parvalbumin, somatostatin and calretinin. In general, in the WT controls of both Q31L and L100P, parvalbumin was present in roughly 3-5% of cells per mm^2 in both somatosensory and ventral auditory cortices and ~7-8% of cells per mm^2 in the visual cortex, which is in agreement with parvalbumin being present in roughly half of the interneurons. Similarly, somatostatin cells contributed around 4% of all cells per mm^2 in somatosensory cortices and ~5-6% of cells per mm^2 in the ventral auditory and visual cortices - around 40% of interneurons across the cortex except for ventral auditory where they contributed to about 60% of cells per mm^2. Calretinin positive cell contribution to the interneuron subpopulation assessed was the lowest - ~1-2% of cells per mm^2 in both somatosensory and ventral auditory cortices and around 5% of cells per mm^2 in the visual cortex (10-30% of total interneurons depending on the region). It can be appreciated that there are more

somatostatin positive cells in the ventral auditory cortex than in other brain regions. Likewise, there are more calretinin positive cells in the visual cortex than in other regions, while parvalbumin is relatively equally distributed in the regions assessed. This is possibly due to different properties of these cells as well as different functions and structure of the particular cortical regions.

The most striking difference between the two Disc1 mutant brains was the selective downregulation of parvalbumin in most of the regions investigated in the L100P but not Q31L mutant brain. This downregulation was also observed in the ventral auditory and visual cortices in the L100P/+ mice suggesting a milder defect in the heterozygous brain. Interestingly, the MPFC in the L100P strain was not affected. Downregulation of parvalbumin in the interneurons in all affected regions was reflected by downregulation of the parvalbumin mRNA, suggesting a transcription defect. There are a few possible mechanisms behind such decrease in the parvalbumin cell density. Firstly, a population of interneurons born in the MGE did not acquire a parvalbumin cells fate, which would result in a decrease in this particular subset. However, with no decrease in the interneuron density across the cortex and no striking change in the density of other major interneurons subsets it is rather unlikely. Secondly, some of the parvalbumin cells could have undergone apoptosis though again lack of difference in the total interneurons density discards such option. On the other hand, since parvalbumin cells constitute approximately 40-50% interneurons (depending on a cortical regions), a 30-50% loss in PV cells might not have been identified as significant in the total interneurons analysis. As the GAD67 analysis has been done on a group of 4 animals, we cannot exclude the possibility of it being underpowered. Thirdly, migration of a subset of future parvalbumin cells could have been disrupted. Such possibility is also unlikely as there was neither any major migratory defects in the areas investigated nor a decrease in the overall cortical interneurons population. Lastly, a point mutation in Disc1 could directly or indirectly affect parvalbumin expression.

Since parvalbumin expression commences in the visual cortex around the end of the second week of life in rodent brain - a time when the eyes open - it has been

suggested that parvalbumin expression in the cortical interneurons might be triggered by the input from the excitatory and/or inhibitory cells (Patz et al., 2004, Sugiyama et al., 2008, Donato et al., 2013). As the L100P mice have altered neuronal distribution in the cortex as well as reduced spine density on the excitatory cells (Lee et al., 2011) it is possible that as a result of disrupted connectivity/transmission, a subset of parvalbumin-expressing interneurons might not mature. One of the molecular factors known to regulate parvalbumin expression in the visual cortex is a homeodomain protein Orthodenticle homeobox 2 (Otx2) (Sugiyama et al., 2008, Beurdeley et al., 2012). Otx2 is a TF that is necessary for forebrain and eye development as well as in the maintenance of the outer retina during adulthood (Beby and Lamonerie, 2013). Interestingly, Otx2 is not expressed endogenously in the parvalbumin cells in the visual cortex prior to the critical period onset (Sugiyama et al., 2008, Beurdeley et al., 2012). It has been shown that upon eye opening, Otx2 is transported via visual pathway from the retina to the visual cortex where its incorporation into parvalbumin cells is facilitated by the perineuronal nets surrounding these cells (Sugiyama et al., 2008, Beurdeley et al., 2012). It is worth noting that other sources of Otx2 could exist in the brain possibly with a similar mechanism of transportation to and uptake by the parvalbumin cells (Spatazza et al., 2013). Nevertheless, it is possible that the incapability of a subset of parvalbumin cells to express parvalbumin could be due to no or decreased levels of Otx2 uptake by these cells either by disrupted transport of this TF or abnormal perineuronal nets formation.

The results obtained in this study stand in contrast with the findings from John Roder's group where they found a significant reduction in parvalbumin cells in the MPFC but not DLFC in 8-week-old mice (Lee et al., 2013). However, the representative image of the MPFC region used for counting presented in the paper is not the one that I have counted from (it seems much more caudal and is possibly not a 'true' MPFC). I have also performed my analysis on 3 weeks old mice which could explain why I see downregulation of the parvalbumin in the frontal somatosensory cortex - a region that could correspond to the DLFC from the Lee et al. (2013) paper. This could suggest a delay in parvalbumin expression in the L100P mutant mice. Furthermore, Lee et al. (2013) found mild differences in the laminar distribution of

the parvalbumin cells but due to a lack of layer-specific quantification it is impossible to assess which layer was affected. Judging from the images provided it would be layers I and V/VI in the DLFC. In the frontal somatosensory cortex of the P21 L100P mouse brain I found a significant decrease in layer IV parvalbumin density and this region was the least affected of the four. This layer, together with layer V, was affected by the parvalbumin density decrease in L100P and L100P/+ in other brain regions. Parvalbumin cells seem to be mostly present in layers densely populated by excitatory cells like pyramidal neurons (layer V and II/III) or spiny stellates (layer IV) (Packer et al., 2013). Moreover, they are believed to form local connections onto the soma and dendrites of the neuron (basket cells) or onto the initial segment of the axon (chandelier cells) (Somogoyi et al., 1977; DiCristo et al., 2004). Since there is no defect in the interneuron density in these layers and knowing that proper connectivity between interneurons and excitatory cells is necessary for parvalbumin expression it is possible to suggest a cell non-autonomous effect of the L100P mutant on this subset of cortical interneurons.

In both L100P and Q31L mutants there was no difference in the density of calretinin expressing cells. In the Q31L/Q31L, L100P/L100P and L100P/+ brains, there was a significant reduction in the somatostatin positive cells in the ventral auditory cortex but not in any other region of the brain. In the L100P/+ visual cortex there was a significant increase in the somatostatin cell density but none in the L100P homozygous mutant. Since there is no increase in any other major interneuron subpopulation, no reduction in the cortical interneurons and only ventral auditory cortex is affected by both mutants, this could suggest that the mutated Disc1 could have caused either a defect in the migration to this brain region or a decrease in the cells destined to be somatostatin positive cells in this region.

Chapter 4: Investigation of a cell non-autonomous effect of Disc1 L100P mutation on parvalbumin expression in a subset of cortical interneurons

4.1 Introduction

The cerebral cortex consists of two main groups of neurons: the excitatory projection neurons (70-80% of neurons) and the inhibitory interneurons (around 30% of cortical neurons). The projection neurons originate from the neural stem cells found at the ventricular zone, a neuroepithelial layer lining the ventricle of the anterior part of the telencephalon (Malatesta et al., 2000; Noctor et al., 2002; Anderson et al., 2002). Initially, symmetrical divisions of the neural stem cells at the ventricular zone that result in the production of two daughter cells identical to the original cell sustain and enlarge the proliferative pool. With the beginning of neurogenesis (around embryonic day 11.5 (E11.5) in the rodent brain) these cells will start to divide asymmetrically to give rise to, and ultimately be replaced by, two distinctive cell types - the radial glia cells and the basal (intermediate) progenitors (Noctor et al., 2004; Haubensak et al., 2004; Miyata et al., 2004). Through a further series of asymmetric divisions, radial glia cells give rise to one identical daughter cell and an intermediate progenitor which moves to the newly formed structure called the subventricular zone to divide symmetrically and form two immature neurons (Noctor et al., 2004; Haubensak et al., 2004; Miyata et al., 2004). These neuronal cells migrate radially towards the superficial parts of the dorsal telencephalon and form the neocortex in an inside-out manner: the cells born at earlier stages of proliferation (mostly in the ventricular zone) will form deeper cortical layers while those born later (subventricular zone) will populate superficial layers (Rakic and Lombroso, 1998; Nadarajah et al., 2002). Hence, neurons born at E11.5-E13.5 will form layers VI and V, while those born at E13.5-E16.5 contribute to layer IV and II/III (Hevner et al., 2003). Radial migration of the cortical projection cells is concluded by the end of the first postnatal week in a rodent brain.

Neurogenesis of the interneurons in the ganglionic eminences of the ventral telencephalon starts earlier, around E9.5 in the rodent brain (Xu et al., 2004). By the time the first born immature interneurons reach their correct position in the cortex and switch from the tangential to radial migration to populate a correct layer (around birth) (Miyoshi and Fishell, 2011), the immature excitatory cells of layers V-VI

already have or are about to reach their final destination. With the interneurons mimicking the inside-out fashion of populating the cortex to that of the projection neurons, it is possible that the latter guide the former to their correct position within the cortex. There is some evidence suggesting that the migrating interneurons could be using the basal processes of the radial glia to migrate to their final destination within the neocortex, most probably with the help of gap junction proteins (Yokota et al., 2007; Elias et al., 2010). Upon reaching their destination (around P7) the interneurons up-regulate a potassium/chloride co-transporter KCC2, which in turn changes the responsiveness of the cell to GABA resulting in a reduction in their motility (Bortone and Polleux, 2009; Inamura et al., 2012). It has been suggested that the KCC2 regulation could be cell-intrinsic but the external cues are also believed to play a role in the slowing down of the migrating interneurons (Inamura et al., 2012). It is possible that these cues could be the excitatory cells as embryonic neurons growing on postnatal neurons in culture had a markedly reduced motility (Inamura et al., 2012).

Cortical interneurons, though much lower in number than their excitatory counterparts, exhibit a wide range of morphological, molecular and physiological properties (DeFelipe et al., 2013). Approximately half of the cortical interneurons express a calcium-binding protein - parvalbumin. Unlike other calcium binding proteins in the interneurons, parvalbumin has a strong affinity to both calcium and magnesium ions, being bound to the latter during the resting state (Li-Smerin et al., 2002). However, upon influx of calcium, magnesium dissociates slowly from the parvalbumin making it the slow-onset buffer and allowing biexponential decay of the calcium transients, with an accelerated initial rate of this transient (Lee et al., 2000). This in turn has an effect on the paired-pulse ratio - a measurement of synaptic plasticity. It has been shown that parvalbumin acts as a potent inhibitor of facilitation (Callard et al., 2000). Parvalbumin is not expressed in the rodent brain until late in the second postnatal week where it starts to be expressed in the visual cortex around the time of the eye opening (Alcantara et al., 1993; Patz et al., 2004). It has been suggested that the expression of parvalbumin in the interneurons might be regulated by the formation of functional synapses with the excitatory cell (Sugiyama et al.,

2008; Donato et al., 2013). In my previous chapter I reported a decrease in parvalbumin protein and mRNA, with no change in other interneuronal markers including GAD67, in the somatosensory, visual and auditory cortices of P21 Disc1 L100P heterozygote and homozygote mice when compared to their wild type littermates. Based on these findings and the nature of the parvalbumin regulation I formed a hypothesis that this decrease in parvalbumin expression in a subset of interneurons was due to cell-extrinsic effects. Since parvalbumin cells are born in the proliferative zones of the ventral telencephalon, I introduced the Disc1-100P variant exclusively into a subpopulation of pyramidal neurons born at E14.5 in the dorsal telencephalon of wild-type mice and investigated if the Disc1-100P variant expression in these cells would affect the expression of parvalbumin in the neighbouring wild-type interneurons. To achieve that, I sub-cloned the Flag-tagged mouse Disc1-WT and Disc1-100P long variants (ORF only; the first codon was substituted with the tag) into a CAGG-IRES-GFP vector (Fig 4.01 A) and overexpressed both the wild type and mutated versions in a small subpopulation of superficial layer excitatory cells at E14.5 (the peak of Disc1 expression (Mao et al., 2009)) by means of *in utero* electroporation. I have investigated the correlation between the cells overexpressing the constructs and parvalbumin expressing cells, as well as analysed the mean densities and distributions of the parvalbumin cells in the frontal and primary somatosensory (fSSp and SSP respectively), ventral auditory (vAud) and visual (Vis) areas of the P21 mouse brain cortex.

4.2 Results

4.2.1 Transfection efficacy of the Disc1-WT and Disc1-100P IRES-GFP vectors *in vitro* and *in utero*

Initial attempts to overexpress Flag-tagged long variants of the Disc-WT and Disc1-100P cloned into pcDNA4/TO (Invitrogen) *in utero* failed (Fig 4.01 A, C). The constructs easily expressed *in vitro*, though not with a very good efficiency (Fig 4.01 B). Thus, I concluded that the inability to detect the Flag-tagged Disc1-WT and Disc1-100 was due to the CMV promoter being silenced when the differentiating cell matures into a neuron, hence preventing the constructs' expression during postnatal ages (Tabata and Nakajima, 2001). Due to the necessity of co-electroporating the Disc1 constructs with a GFP-expressing vector (pTP6 plasmid expressing tauGFP; Pratt et al., 2000) to enable screening for successful electroporations and assessing the electroporation efficiency, I subcloned the Disc1 variants (keeping the Flag-tag) into a CAGG-IRES-GFP vector (a kind gift from Dr Thomas Theil). Both Disc1-WT and Disc1-100P IRES-GFP constructs were highly expressed *in vitro* with the Flag and GFP signals overlapping (Fig 4.01 D). When overexpressed *in utero* a weak Flag signal was detected in most but not all GFP-expressing cells 4 weeks after electroporation (P21) (Fig 4.01 E). This might be due to the antibody against Flag not working particularly well on cryosections. However, since the Disc1 ORF is the first message in the cloned CAGG-IRES-GFP it is safe to assume that the subcloned Disc1-WT and Disc1-100P are expressed after *in utero* electroporation (Fig 4.01 A). In the analysis of the data in this chapter, Disc1-WT overexpression is treated as a control for the Disc1-100P overexpression as both constructs result in an increase in the Disc1 protein in the electroporated cells. The empty vector GFP expression analysis was included to see if the electroporation itself has an effect on the parvalbumin expression and to see if there is potential effect of overexpression of the WT construct.

Fig 4.01 Expression of Disc1 constructs *in vitro* and *in utero*. (A) Original pcDNA4/TO vector with the CMV promoter and the CAGG-IRES-GFP vector with the Flag-tagged Disc1 and L100P Disc1. (B) Expression of the CMV Flag-Disc1 and pTP6 (tauGFP) vectors 48h after co-transfection in HEK 293 cells (scale bar 50μm). (C) Undetectable Flag-tag expression in the P21 somatosensory cortex after co-electroporation of CMV Flag-Disc1 and pTP6 (tauGFP) vectors at E14.5 (scale bar 250μm). (D) Expression of the CAGG-Flag-Disc1-WT-IRES-GFP constructs 48h after transfection in HEK 293 cells (scale bar 50μm). (E) Flag-tag expression overlaps with that of GFP in the electroporated cells in layers II/III (boundary showed by white dotted line) of the P21 primary somatosensory cortex after *in utero* electroporation with a CAGG-Flag-Disc1-IRES-GFP at E14.5 (scale bar 100μm).

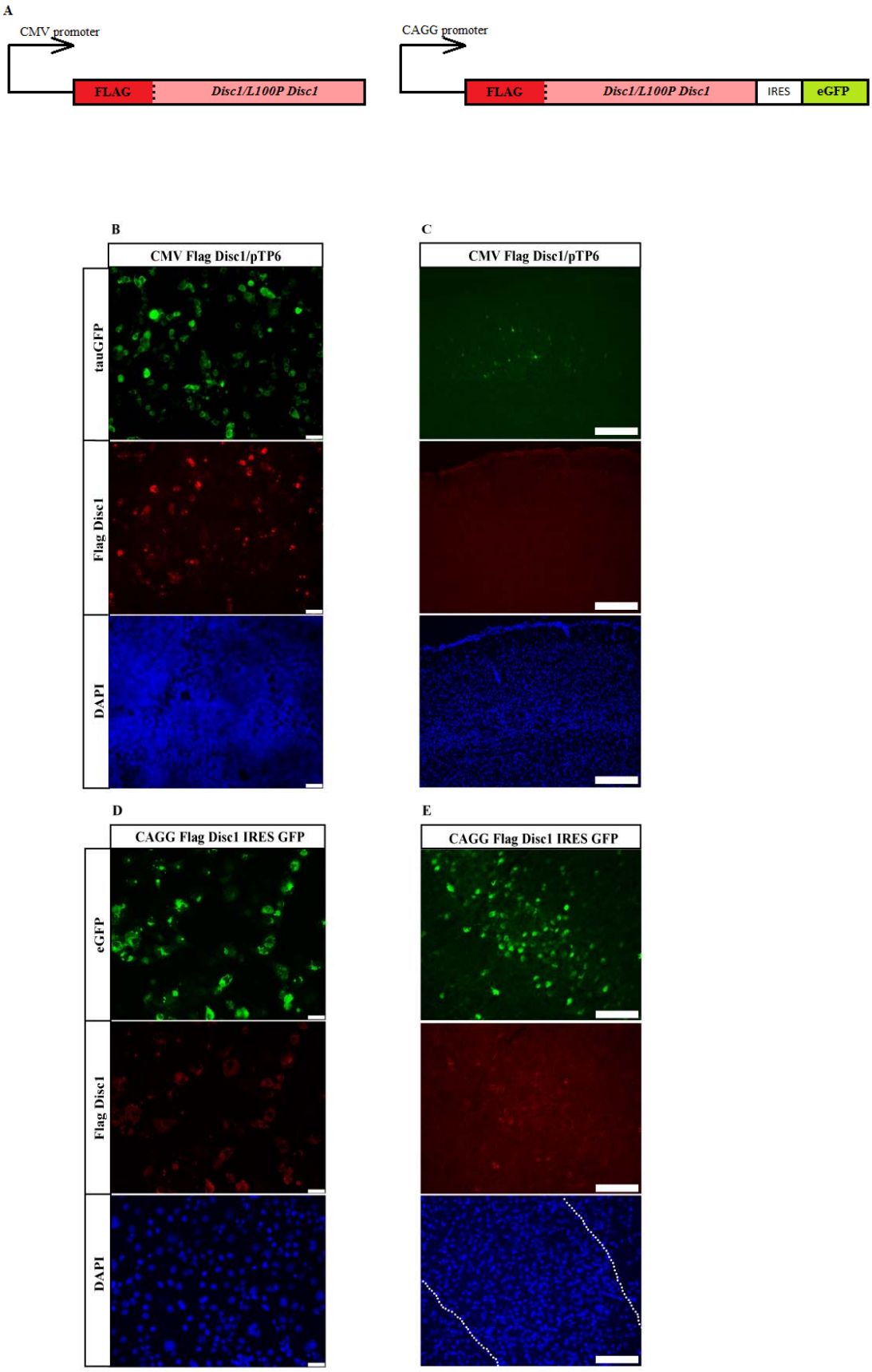
A
CMV promoter
FLAG
Disc1/L100P Disc1
CAGG promoter
FLAG
Disc1/L100P Disc1
IRES
eGFP
B
CMV Flag Disc1/pTP6
tauGFP
Flag Disc1
DAPI
C
CMV Flag Disc1/pTP6
D
CAGG Flag Disc1 IRES GFP
eGFP
Flag Disc1
DAPI
E
CAGG Flag Disc1 IRES GFP

Although plasmids concentrations were 2mg/ml and the plasmids' volumes injected were kept as identical as possible, I have observed a range of different efficiencies in different regions of the cortex (Fig 4.02 A-B). This is mainly due to technical issues like the needle diameter at the break point influencing the volume injected, the orientation of the electrodes during electroporation as well as variation in numbers of cells that incorporated the plasmid. Furthermore, the size of the plasmid with the WT and L100P mutant Disc1 was approximately 2.5kb larger than that of the empty vector which could explain the lower transfection efficiency than that of the empty vector. Lastly, my main aim was to introduce the plasmid into the somatosensory cortices, as those were the regions where I observed the highest decrease in the parvalbumin expressing cells. This means that the cells in the ventral auditory and visual cortex were hit due to the size of the electrodes used or purely by chance.

Disc1 is known to have a role in neuronal migration and the L100P homozygous mice exhibit disrupted cortical migration with cells destined for more superficial layers being found in deeper layers (Lee et al., 2011). Surprisingly, overexpression of the Disc1-100P or Disc1-WT constructs did not cause a similar pattern; on the contrary, it seems that more Disc1-100P overexpressing cells migrate preferentially to the more superficial layers than their wild type Disc1 expressing control in primary somatosensory and visual cortices (Fig 4.02 D, F) but not in frontal primary somatosensory and ventral auditory cortices (Fig 4.02 C, E). One explanation could be that the differences in the migration in these areas could be due to region-specific effects, for example difference in external cues or timing of the migrating cells. On the other hand this could be an artifact due to the timing of the procedure. Although all the embryos were electroporated at E14.5 there might have been some variation in the actual electroporation time, most possibly due to variable mating time or the time difference between multiple surgeries performed on the same day.

Fig 4.02 Density and relative distribution of cells expressing GFP across the brain cortex of the P21 mouse after *in utero* electroporation at E14.5. (A) Variation in the density of GFP expressing cells in the somatosensory cortex of the P21 mouse brain electroporated with CAGG Disc1-WT-IRES-GFP vector. (B) GFP expressing cell density in the four cortical areas electroporated with Disc1 constructs. The majority of the cells that express the IRES-GFP constructs migrated to the superficial layers of each of the targeted regions: frontal somatosensory (C), primary somatosensory (D), ventral auditory (E) and visual (F) cortices. The differences in the distribution are more probably related to the timing of electroporation rather than a migration defect. (n=3-10 animals per genotype; error bars - SEM; ANOVA with Bonferroni post hoc test: * $p<0.05$; ** $p<0.01$; *** $p<0.001$)

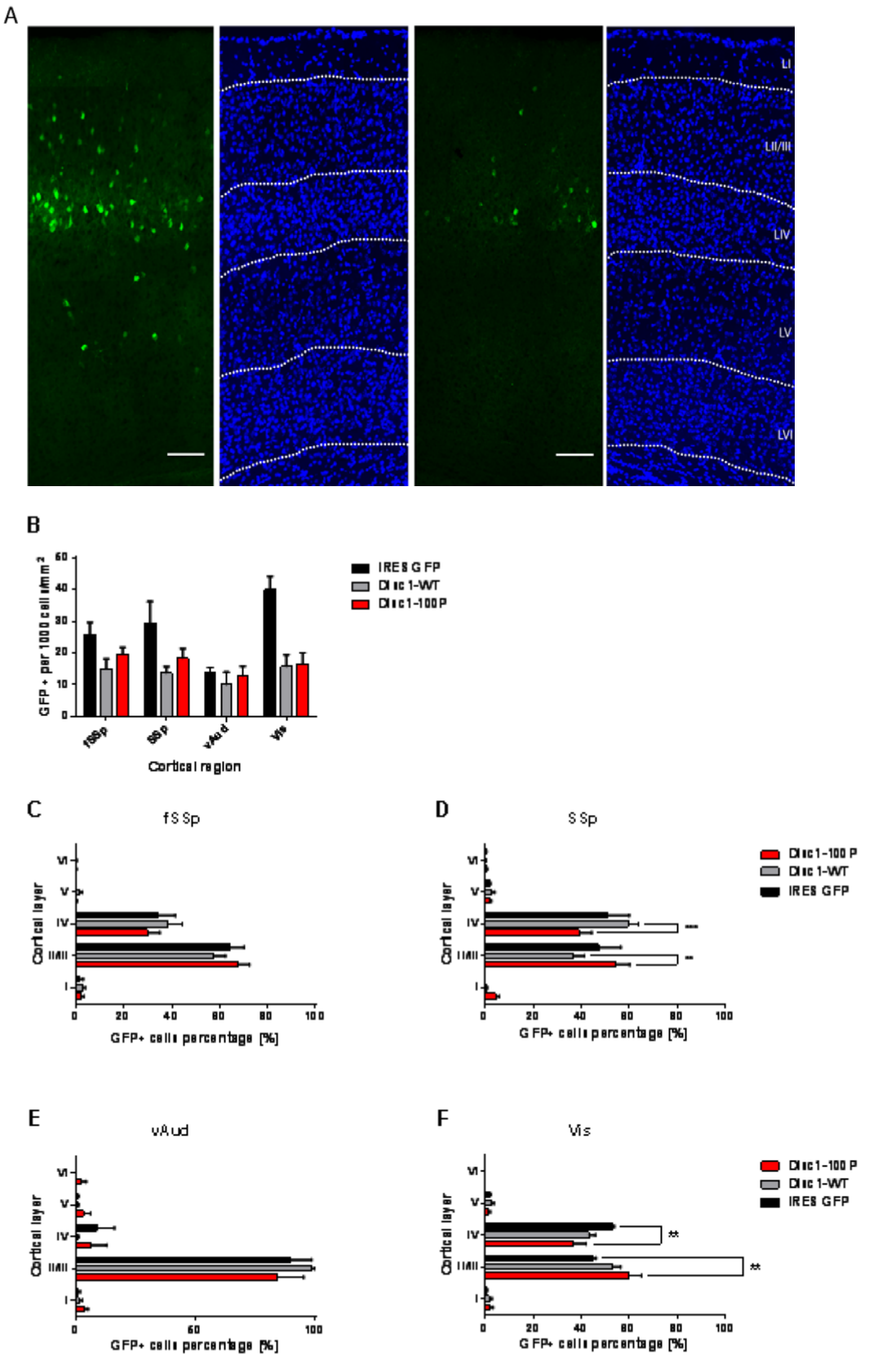
A
LI
LII/III
LIV
LV
LVI
B
IRES GFP
Dlic1-WT
Dlic1-100P
GFP + per 1000 cell/mm²
Cortical region
fSSp
SSp
vAud
Vis
C
fSSp
D
SSp
E
vAud
F
Vis
Cortical layer
GFP+ cells percentage [%]

4.2.2 Increased cell density in the adult mouse cerebral cortex with overexpression of wild type Disc1

Disc1 is known to play a role in progenitor proliferation - knocking down mouse Disc1 *in utero* results in a decrease of the cycling cells in the ventricular and subventricular zone while overexpression of Disc1 increased the number of proliferating cells in these regions (Mao et al., 2009). Before analysing the effect of the overexpression of both variants of the mouse Disc1 on the parvalbumin-expressing subpopulation of interneurons, I examined whether the electroporation of these constructs resulted in any changes in cortical thickness as well as layer and cortical cell density in the chosen areas of the P21 mouse brain. No difference in cortical thickness was observed on ipsilateral or contralateral side of the cortex after electroporation with any of the three vectors (Fig 4.03 A, B). However, overexpression of wild type Disc1 construct resulted in a significant increase in the density of cells in the frontal and primary somatosensory cortices as well as in the visual cortex, but not in the ventral auditory cortex (Fig 4.03 C). The possible reasons for lack of the effect in the ventral auditory cortex are: lower density of overexpressing cells due to targeting of the neighbouring somatosensory cortices or low number of brains used for analysis (n=3) and possible inconsistency in establishing the location of this region based on morphological cues (indentation in the cortical surface, lower cell density in layer IV, etc). The increased cell density was not observed when Disc1-100P variant or empty IRES GFP vectors were electroporated at the same time point during brain development (Fig 4.03 C). Since this increase in cell density was also not observed on the contralateral side of the cortex upon either Disc1 construct overexpression (Fig 4.03 D) it seems that the Disc1-100P variant most likely has no effect on the cell proliferation and the wild type Disc1 overexpression is the causative agent for the increased cortical cell density. Interestingly, the density of the cells upon the Disc1-WT overexpression was increased in layers II/III, IV and VI in the frontal and primary somatosensory areas (Fig 4.04 A-B), layers IV and VI in ventral auditory cortex (Fig 4.04 C) and layers II/III and IV in visual cortex (Fig 4.04 D).

Fig 4.03 Overexpression of WT and mutant form of mouse Disc1 results in changes in the total cells density across the P21 mouse cortex. Overexpression of neither the Disc1-100P nor the mouse Disc1-WT affects the cortical depth on either ipsi- (A) or contralateral (B) sides to the electroporation. However, overexpression of Disc1-WT, but not mutant Disc1-100P, resulted in an increase in total cell density in both the somatosensory and visual cortices on the ipsilateral (C) but not contralateral hemisphere (D). (n=3-10 animals per genotype; ANOVA with Bonferroni post hoc test: * $p<0.05$; ** $p<0.01$; *** $p<0.001$).

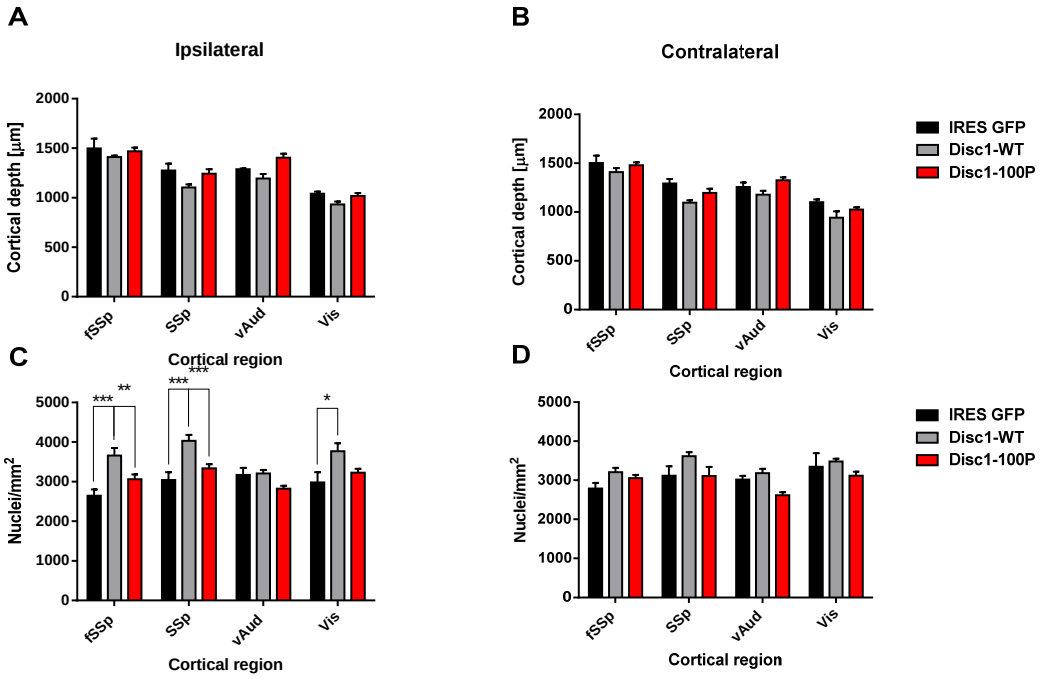

Fig 4.04 Increased cell density in layers II/III, IV and VI across the P21 mouse cortex. Overexpression of Disc1-WT at E14.5 resulted in an increased cell density in the cortical layers formed by the affected cell population in all four cortical regions on the ipsilateral side: fSSp (A), SSp (B), vAud (C) and Vis (D). Similar effect was observed in layer VI across all the cortical regions. No such effect was observed for the Disc1-100P overexpression (n=3-10 animals per genotype; ANOVA with Bonferroni post hoc test: * p<0.05; ** p<0.01; *** p<0.001).

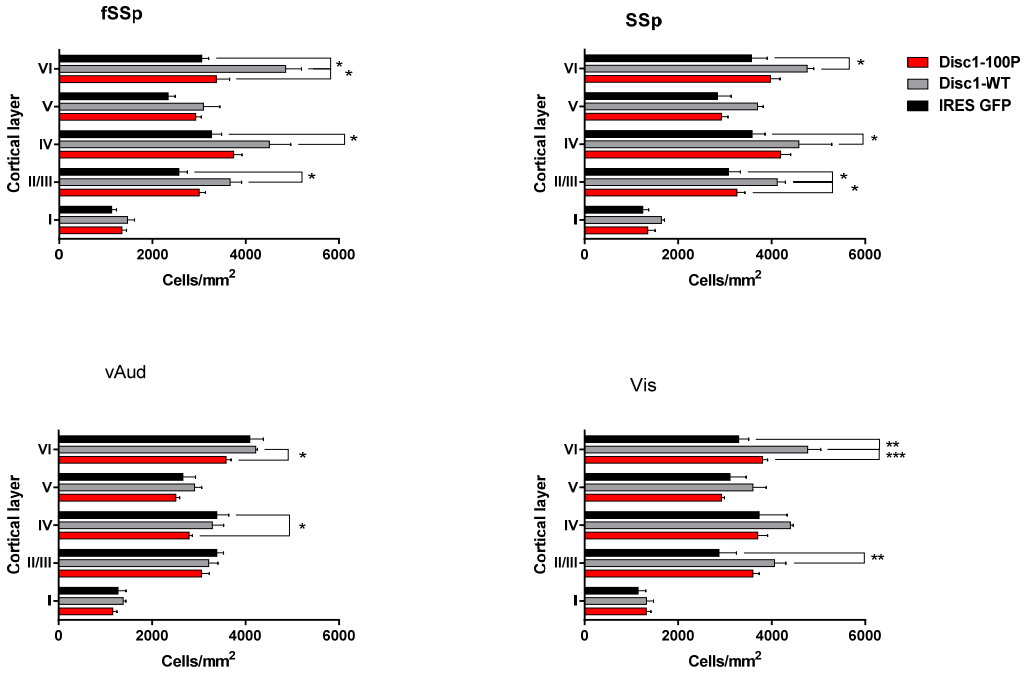

4.2.3 Decreased density of the parvalbumin expressing cells following Disc1-100P overexpression in the adult mouse cortex

In order to assess parvalbumin cell density as well as any correlation between the electroporation efficiency and parvalbumin expression, all GFP-positive cells and parvalbumin expressing cells were counted in a 500μm wide region of the chosen cortical area, and normalised to the area they occupy (as seen in Fig 4.02 A). I performed analysis of means for each of the affected cortical regions and found a significant decrease in the density of the parvalbumin cells in all of the cortical regions expressing Disc1-100P when compared to Disc1-WT overexpression (Fig 4.05 A). Furthermore, similar reductions were observed in the primary somatosensory and visual cortices on the contralateral side (Fig 4.05 B), where the cells overexpressing Disc1 variants send their axons. This strongly suggests that the Disc1-100P has a cell non-autonomous effect on parvalbumin expression, and supports the possibility that the proper connection between excitatory and inhibitory cells could play a role in parvalbumin expression.

4.2.4 No correlation between the proportion of cells overexpressing the Disc1 constructs and parvalbumin positive cells

The *in utero* electroporation efficiency varies regardless of the type of construct overexpressed. This enabled testing the possibility that the decrease in the parvalbumin expressing cells might be correlated to the proportion of the excitatory cells overexpressing the Disc1-100P construct. Since overexpression of Disc1-WT results in an increase in cell density in most of the chosen cortical regions, no normalisation to the cell density was performed as this could potentially mask any cell extrinsic effect of overexpressing Disc1-100P variant on the parvalbumin cells. The scatter plots of the density of the GFP-positive cells to parvalbumin cells density in somatosensory areas initially suggested a possible correlation between the two in the Disc1-100P overexpression. However, an increase of the data points for the somatosensory area and addition of the ventral auditory and visual cortices showed

Fig 4.05 Overexpression of the WT and mutant forms of mouse Disc1 results in changes in the density of PV expressing cells across the P21 mouse cortex. Overexpression of the Disc1-100P results in a decrease in PV expressing cell density across the cortex when compared to the control overexpression with the mouse Disc1-WT (A). A similar effect is observed in the SSp and Vis cortices contralateral to the overexpression area suggesting an effect of the callosal projection neurons on the PV expressing interneurons (B). (n=3-10 animals per genotype; ANOVA with Bonferroni post hoc test: * $p<0.05$; ** $p<0.01$; *** $p<0.001$)

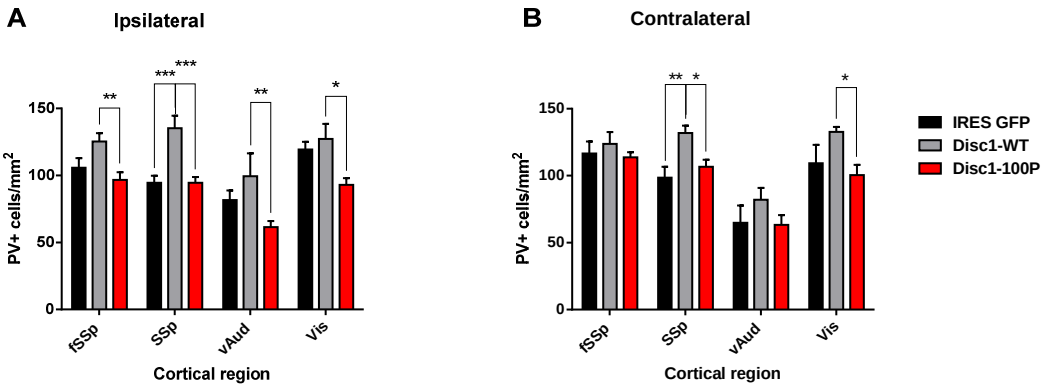

no correlation between parvalbumin expression and the GFP positive cell density based on the Pearson's coefficient calculation (Fig 4.06 A-D). Since the cells born at E14.5 are callosal projecting neurons destined to populate layer II/III and send axons to the contralateral side, correlation analysis was performed to see if there is any difference in the density of the parvalbumin cells on the area contralateral to the electroporated side. Similarly to the ipsilateral side, there was no correlation between the density of the GFP-positive cells and the density of the parvalbumin expressing cells (Fig 4.06 E-H). However, it is quite clear from the scatter plots that in most of the regions overexpression of mouse Disc1-WT resulted in an increase in the parvalbumin expressing cell density which was not observed when overexpressing the Disc1-100P variant (Fig 4.06) which is what was observed through analysis of means, as described in the previous paragraph.

4.2.5 Layer-specific changes in the parvalbumin positive cell density and distribution in different areas of the adult mouse brain cortex overexpressing L100P Disc1

Overexpression of Disc1-100P resulted in an overall reduction in parvalbumin cell density in all of the electroporated regions when compared to the Disc1-WT overexpression. Since parvalbumin cells are present in all cortical layers but for layer I, the observed decrease might be either uniform, or some of the layers might be more affected than others. To investigate that possibility, I have analysed the parvalbumin expressing cell density in each of the layers.

Interestingly, the parvalbumin cell density was significantly reduced in layers IV and V in both somatosensory cortices where Disc1-100P was overexpressed, when compared to Disc1-WT overexpression control (Fig 4.07 A and C). Since there was no effect on the parvalbumin cell density in the frontal somatosensory cortex on the contralateral side to electroporation it is not surprising that there is no difference in the distribution of these cells in cortex (Fig 4.07 B). Conversely, the contralateral primary somatosensory cortex showed a similar decrease in the parvalbumin density

Fig 4.06 No correlation between the densities of GFP positive cells and parvalbumin positive cells in the electroporated regions. Different doses of overexpression of the Disc1-100P and the Disc1-WT did not correlate with parvalbumin cell density in the fSSp (A), SSp (B), vAud (C) and Vis (D) cortices. Similar lack of correlation between the two was observed on the contralateral sides to the electroporation in the fSSp (E), SSp (F), vAud (G) and Vis (H) cortices. (n=3-10 animals per genotype; Pearson's Coefficient with two-tailed t-test to refute null hypothesis).

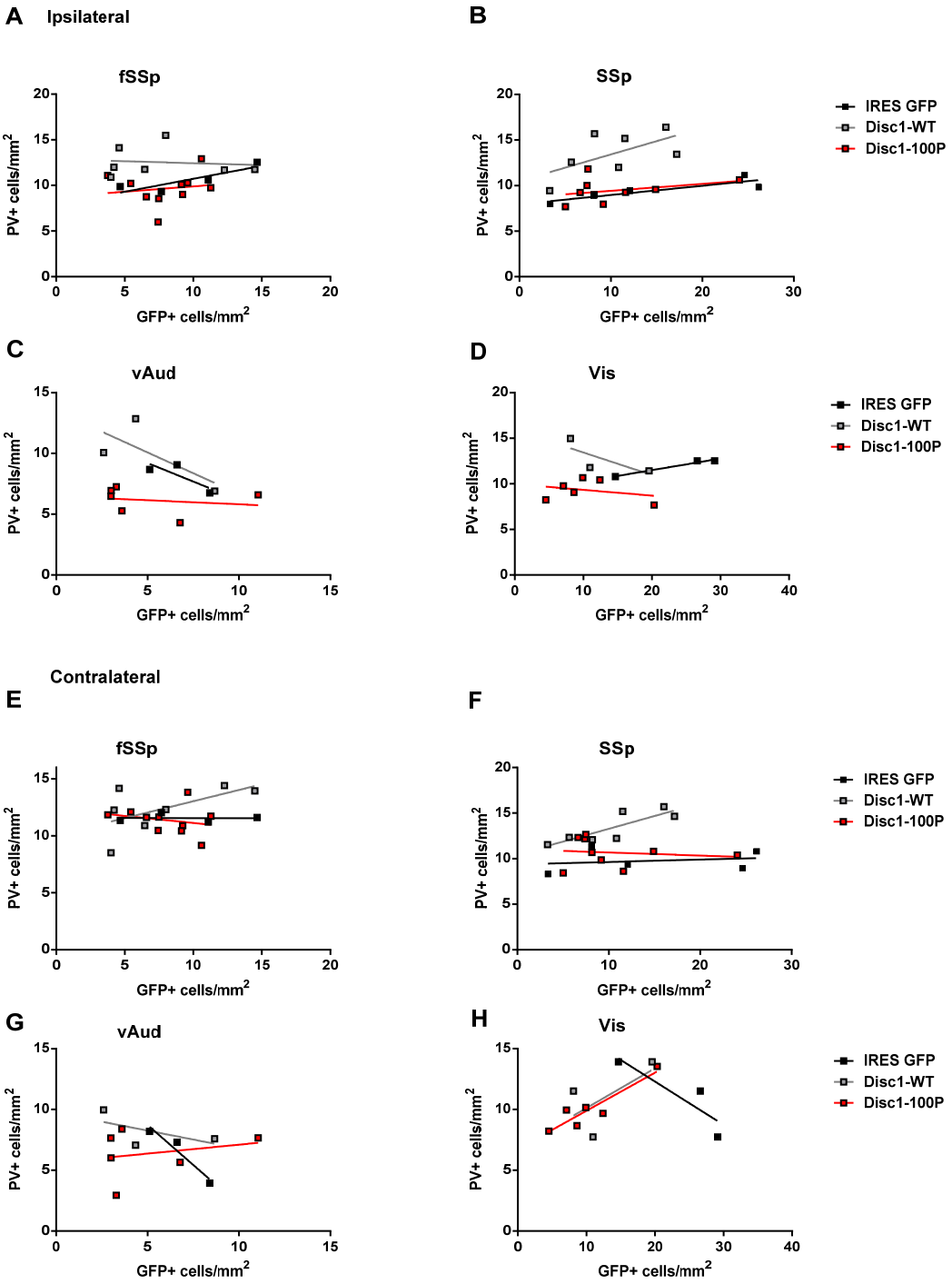
A
Ipsilateral
fSSp
B
SSp
C
vAud
D
Vis
Contralateral
E
fSSp
F
SSp
G
vAud
H
Vis
PV+ cells/mm2
GFP+ cells/mm2
IRES GFP
Disc1-WT
Disc1-100P

to that of the ipsilateral side. Interestingly, the most affected layers were layers II/III and VI where the parvalbumin cell density was significantly decreased when the Disc1-100P was overexpressed in comparison to Disc1-WT overexpression (Fig 4.07 D).

Most of the cells expressing GFP in the ventral auditory cortex ended up in layers II/III (Fig 4.02 D) but, curiously, these are the only layers unaffected by Disc1-100P overexpression in comparison to the wild type Disc1 overexpression (Fig 4.08 A). Similarly, the layers in the visual cortex affected by the L100P Disc1 overexpression were layers V and VI (Fig 4.08 C) where there were virtually no GFP positive cells (Fig 4.02 E). What is more, overexpression of the L100P Disc1 in the ventral auditory cortex did not disrupt the parvalbumin cell distribution on the contralateral side to the electroporation (Fig 4.08 B). In the visual cortex, only layer V parvalbumin cells density was decreased in the contralateral side to the L100P Disc1 overexpression when compared to the wild type Disc1 control (Fig. 4.08 D) suggesting a possible indirect effect of the callosal projection cells overexpressing L100P Disc1. Taken together, there seems to be no migratory defect due to overexpression of the L100P Disc1 when compared to the wild type Disc1 control and the observed decrease in the parvalbumin cells density is most probably due to improperly formed connections between the affected excitatory cells and the unaffected parvalbumin expressing inhibitory cells.

Fig 4.07 Changes in the density of the PV expressing cells in layers IV and V in the frontal and primary somatosensory cortices after the overexpression of Disc1-100P and Disc1-WT at E14.5. (A) Overexpression of Disc1-100P resulted in a decrease in the PV cells density in layer IV and V when compared to Disc1-WT overexpression in frontal somatosensory cortex. No changes in parvalbumin cell density were observed on the contralateral side after introduction of either of the constructs (B). (n=4-10 animals per genotype; ANOVA with Bonferroni post hoc test: * $p<0.05$; ** $p<0.01$; *** $p<0.001$). Overexpression of the Disc1-100P in primary somatosensory cortex resulted in a decrease in PV cell density in layers IV and V when compared to the Disc1-WT overexpression (C). Disc1-100P variant overexpression resulted in a decrease in PV cell density in all layers (significant only in layers II/III and VI) on the contralateral side when compared to the WT Disc1 overexpression (D) (n=5-9 animals per genotype; ANOVA with Bonferroni post hoc test: * $p<0.05$; ** $p<0.01$; *** $p<0.001$)

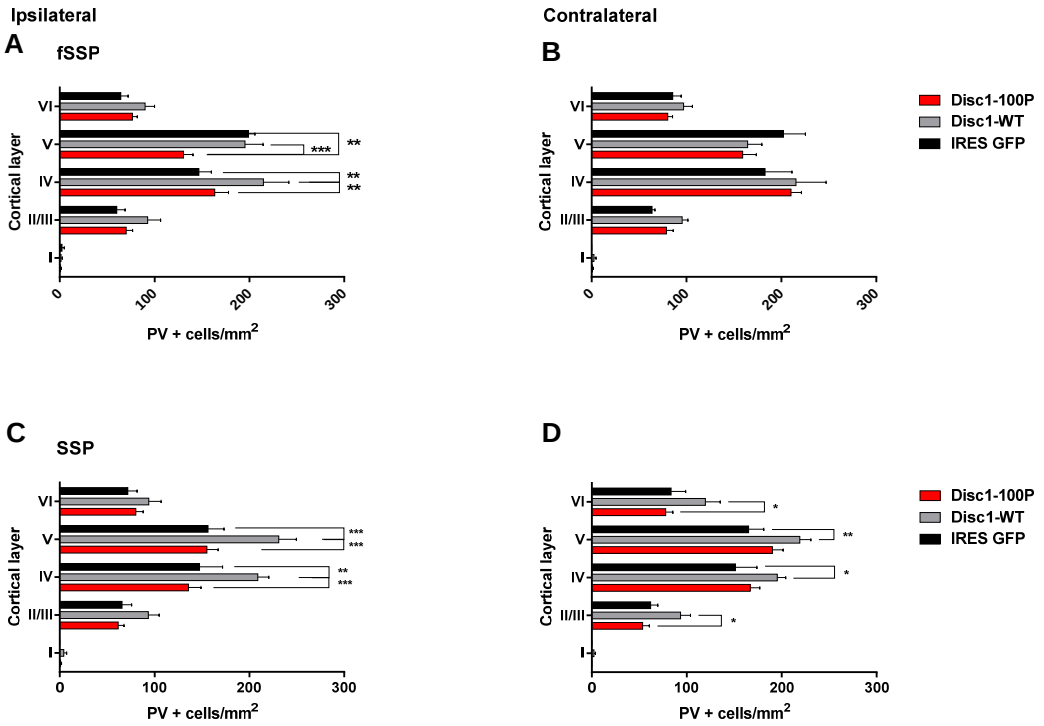

Fig 4.08 Decrease in the density of PV expressing cells in the deeper cortical layers in the ventral auditory and visual cortices after the overexpression of the Disc1-100P at E14.5. Overexpression of the Disc1-100P resulted in a decrease in the PV cell density in layers IV, V and VI when compared to Disc1-WT overexpression (A). PV cell density on the contralateral side remained unaffected by overexpression of either of the Disc1 versions (B). (n=3-6 animals per genotype; ANOVA with Bonferroni post hoc test: * $p<0.05$; ** $p<0.01$; *** $p<0.001$). Overexpression of Disc1-100P resulted in a decrease in the PV expressing cell density in layers V and VI (A) and in layer V on the contralateral side (B) when compared to Disc1-WT overexpression. (n=3-6 animals per genotype; ANOVA with Bonferroni post hoc test: * $p<0.05$; ** $p<0.01$; *** $p<0.001$)

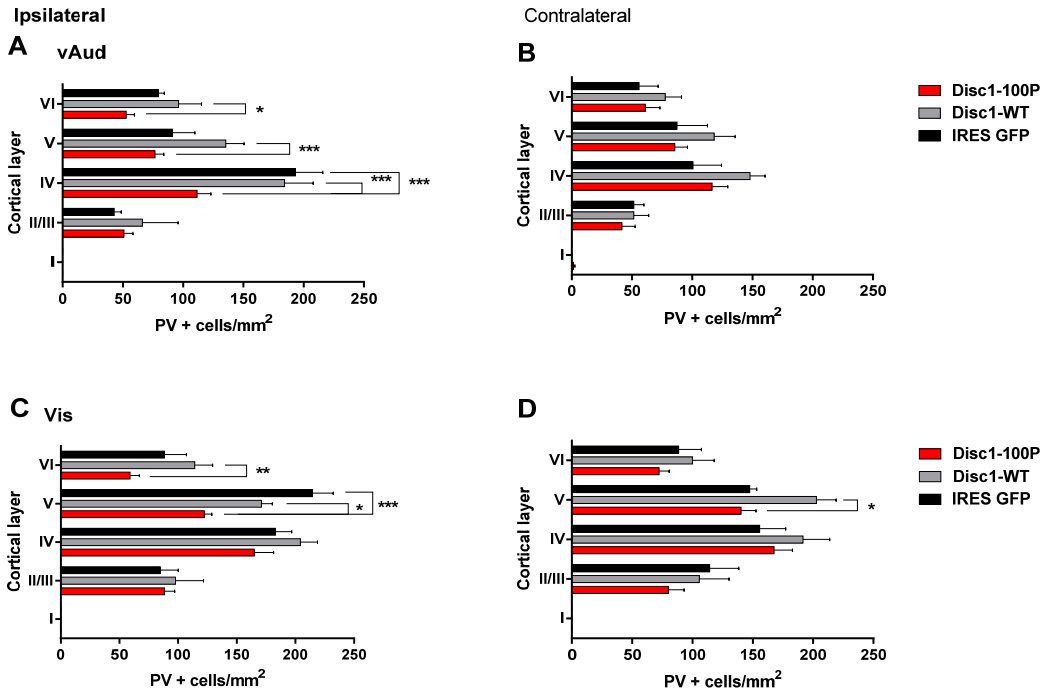

4.3 Discussion

Maintaining the correct excitation/inhibition (E/I) balance in the activity of neuronal networks is essential in the proper functioning of the brain. Disruption of this fine balance is becoming more recognised as one of the underlying causes of a wide range of neurodevelopmental disorders, spanning from epilepsy through schizophrenia to autism spectrum disorders (Žiburkus et al., 2013, Yizhar et al., 2011). The mechanisms enabling maintenance of the system's homeostasis are acquired during development and implemented throughout adulthood (for a review see Turigiano and Nelson, 2004). One of those mechanisms is feedback excitation and inhibition where the excitatory cell not only makes a connection with another excitatory cell, but also with an inhibitory one, which in turn connects back to the original cell and regulates its output (Rutherford et al., 1997). Since parvalbumin expressing cells are the largest subtype of cortical interneurons and they are responsible for feed-forward inhibition, they play a major role in information processing. Thus it is highly possible that even a subtle change in these cells' number or their properties could have an observable impact on the E/I balance.

In the previous chapters, I described how the inability of a substantial proportion of interneruons to express parvalbumin was found across the cortex of a mouse Disc1 L100P point mutant but not the Q31L mutant. Since parvalbumin expression is believed to be regulated by signals received from other cells, such a deficit would imply a potential disruption in the network's connectivity, either due to misconnection of the inputs coming from the excitatory cells, or due to inability of the parvalbumin interneuron to receive signal from said cells. Disc1 involvement in axonal outgrowth (Chen et al., 2011; Kvajo et al., 2011) and synaptic transmission (Holley et al., 2013) has been established, thus both processes could be affected by Disc1 L100P mutation resulting in parvalbumin downregulation. When overexpressing the mouse Disc1-100P variant or wild type mouse Disc1 during brain development in the wild type mouse cortex, I have found that even a relatively minor change in Disc1 levels has a considerable impact on parvalbumin expression in this particular subset of interneurons. Interestingly, these changes were not confined to

the ipsilateral side. In some cases this effect was clearly observed on the contralateral side probably due to the axonal projections of the callosal neurons expressing either of the Disc1 variants.

The observed decrease in parvalbumin expressing cells seemed consistent across the cortex but was not uniform within the cortical column. In specific regions, particular layers were more affected than others. Conversely, both somatosensory regions showed similar layer-specific changes in the parvalbumin cell density on the ipsilateral side. Since these two regions exist on approximately the same rostro-caudal axis (with frontal somatosensory cortex being more rostral) it could be possible that they share intra-cortical connection patterns. This in turn could further support the non-cell autonomous effect the Disc1 L100P variant has on parvalbumin expression in a subset of cortical interneurons.

Parvalbumin cells in layer IV receive connections from the thalamus (primary somatosensory cortex) as well as from locally residing excitatory spiny neurons in rat (Aqmon and Connors 1991; Koelbl et al., 2013). In both electroporated frontal somatosensory and primary somatosensory cortices there were small proportions of GFP positive cells in layer IV. If the cells overexpressing Disc1-100P do not form a proper connection with the parvalbumin cells, and these cells in turn cannot express parvalbumin, it could possibly explain a decrease in PV cell density in layer IV. Similar explanation of the observed decrease in the parvalbumin cells could be applied to layer V as it receives connections from the layers II/III excitatory cells (at least in visual and primary somatosensory cortex) and it is possible that some of those cells form connections with the local population of parvalbumin cells (Kenan-Vaknin et al., 1992). Layer II/III callosal projecting neurons send their axons to the contralateral hemisphere and densely populate mainly layer II/III in the primary somatosensory cortex, and layer V at the border of primary and secondary somatosensory cortex (Wang et al., 2007). The defect observed in the contralateral somatosensory cortex following Disc1-100P overexpresssion could possibly be due to improper connection of the callosal projections either directly onto the inhibitory cells (layers II/III) or indirectly through other excitatory cells (layers II/III and VI

connection). In the visual cortex, callosal projections densely populate layers II/III and V (Mizuno et al., 2007) which in turn could explain lower parvalbumin cell density in layer V of the contralateral side to the Disc1-100P overexpression when compared to the WT.

As observed in the previous chapter, the homozygous L100P Disc1 mouse cortex exhibits minor disruptions in the laminar distribution of both the parvalbumin cells and interneurons in general, suggesting a subtle migratory defect. In the electroporation experiments, since the overexpression of the L100P Disc1 not only occurred in a relatively small proportion of the cells, but also these affected cells have already been expressing endogenous wild-type Disc1, it is unsurprising that there was no obvious migratory defect of the electroporated nor parvalbumin expressing cells. Since the parvalbumin cells are not affected by the electroporation, their tangential migration from the ventral telencephalon should not be affected either. However, there is an increase in parvalbumin cell density following wild type Disc1 overexpression when compared to the empty vector control electroporation. The most probable reason for this occurrence could be some kind of a change in the termination signal sensed by the tangentially migrating parvalbumin cells resulting in the migrating cells either prolonging this phase of migration or prematurely entering the cortex. At present, it is not known what regulates the switch between the two types of migration in the interneurons, but it is believed to correlate with the loss of sensitivity to CxC112, a chemoattractant that enables the interneurons to form the migratory stream by reducing their branching rate (Li et al., 2008; Lesko et al., 2011). Another potential regulator of the switch could be an unknown chemokine present in the cortical plate (future layer VI at this time-point) which, despite being receptive towards interneurons throughout development, is being avoided by the interneurons until they switch off their responsiveness to CxCl12 (Li et al., 2008; Lopez-Bendito et al., 2008). After wild type Disc1 overexpression there is an increase in the cell density in layer VI in most of the affected regions, which in turn could provide an increased amount of the chemoattractant, and an increase in radial migration into the affected region. This possibility could be further supported with a decrease in the cell density and parvalbumin cells' density in the cortex when Disc1-

100P is overexpressed. Taken together, it could be another mechanism through which Disc1 could have a non cell autonomous effect on the parvalbumin expressing cells.

When overexpressing wild-type Disc1 in the developing mouse cortex, I observed a significant increase in the cell density which was not observed following Disc1-100P variant overexpression. One possibility is that the overexpression of the Disc1-100P variant decreases proliferation when compared to the Disc1 overexpression, which would be in agreement with previous findings (Lee et al., 2011). However, in my analysis of the L100P line. I have found no difference in the cell density in the Disc1 L100P homozygous and heterozygous mice when compared to their wild type littermates. Thus it is possible that the overexpression of the Disc1-100P simply has no effect on the proliferation and hence no change in the cell density. The cells born at E14.5 that incorporated the wild type Disc1 plasmid became more proliferative but did not have any migratory defect. Thus it could be assumed that they follow the migratory pattern assigned to them at their birthdate and populate the superficial layers which in turn explain the increase in the cell density in these layers. Layer VI is generated between E11.5 and E16.5 (proliferation and migration) hence an increase in the cell density observed in the WT Disc1 overexpression in this layer might be due to some proportion of the over-proliferating cells expressing wild type Disc1 differentiating and migrating earlier than they should. Another interesting observation is that despite increase in the cell density across the cortex when WT Disc1 was overexpressed at E14.5, there was no increase in the GFP-positive cells. Since Disc1 overexpression *in utero* has been shown to increase cell proliferation 2-fold (Mao et al., 2009), the most probable explanation is that the plasmid is not incorporated into the genome.

Chapter 5: General Discussion

5.1 Overview

In this work I investigated the role that Disc1 plays in the development of cortical interneurons in the murine brain. To achieve this, I analysed the density and distribution of the three largest interneuron subpopulations: parvalbumin, somatostatin and calretinin expressing cells; in five cortical regions of P21 brains in two ENU-mutant Disc1 mice: L100P and Q31L.

Analysis of interneurons in Disc1 L100P and Q31L homozygote and heterozygote mice revealed a decrease in parvalbumin interneuron density in all cortical regions investigated, except for medial prefrontal cortex, in the L100P Disc1 heterozygous and homozygous mice. No such defect was observed in any cortical region of the Q31L Disc1 mutant mice. With no difference in overall cortical interneuron density and the observed decrease in the parvalbumin mRNA-expressing cells, I have concluded that this defect is due to downregulation of parvalbumin in the interneurons programmed to express it. Another two cortical interneuronal subpopulations were largely unaffected by either the L100P or Q31L Disc1 mutation in all cortical regions except for ventral auditory cortex. Here there was a significant reduction in somatostatin expressing interneurons in Q31L and L100P homozygous and in L100P heterozygous mutant brains. The presence of this deficiency in both Disc1 mutants could suggest a potential defect related to fate-acquisition in the MGE.

In chapter 4 I followed up on the results from parvalbumin interneurons analysis. I investigated a possible cell non-autonomous mechanism behind the parvalbumin downregulation defect observed in the Disc1 L100P cortex, basing this hypothesis on the activity-dependent nature of parvalbumin expression regulation. To test it, I overexpressed the Disc1-100P variant in the developing cortical projection neurons *in utero* at E14.5 and assessed the density of parvalbumin-expressing interneurons. Parvalbumin cell density was lower in all cortical regions that had excitatory neurons expressing the Disc1 L100P variant when compared to control overexpression with

wild type Disc1. This result strongly suggests Disc1 involvement in regulation of parvalbumin in a cell non-autonomous fashion.

In this chapter I will discuss how the observations reported fit with the current understanding of cortical interneuron development and how these findings add to the understanding of the Disc1's role in cortical development.

5.2 Discussion

5.2.1 Role of Disc1 in the development of cortical interneurons

Little is known about Disc1's role in the development of cortical interneurons. Previous studies have shown that Disc1 is highly expressed in the proliferative zones of the LGE, MGE and POA in the mouse brain at E14.5, suggesting its role in the late proliferation of interneuron precursor cells (Steinecke et al., 2012). However, none of the studies using Disc1 mutant mice or Disc1 knockdown studies investigated its effect on the proliferation of future interneurons. Unlike proliferation, migration of interneurons from the ventral telencephalon to the forming cortex has been studied to some extent. Disc1 has been shown to be expressed in the cell cytoplasm and in the tips of the leading processes in interneurons tangentially migrating from the MGE (Steinecke et al., 2012). What is more, in some cases Disc1 is expressed at the trailing edge of the cell, binding to CAMDI (coiled-coil protein associated with myosin II and DISC1) (Fukuda et al., 2010). Since myosin II is required for the movement of the nucleus during the nucleokinesis step of the tangential migration, Disc1 forming a complex with the CAMDI suggests its role in migration. Disc1 knockdown in the E14.5 MGE resulted in disruption of tangential migration of the affected cells (Steincke et al., 2012). A similar defect was shown in the L100P Disc1 mice (Lee et al., 2013). However, Disc1 seems not to have a role in the migration of interneurons from LGE to olfactory bulb (rostral migratory stream) via Girdin regulation (Wang et al., 2011). Other Disc1 partners that are known to

affect tangential migration (for example Lis1/Nde1/dynactin complex) should be investigated to get a better picture of potential Disc1 regulation of this process.

Disc1's effect on radial migration of interneurons, and their final laminar positioning in the cortex, has not been investigated. In this study I have found minor defects in the distribution of the interneurons across the cortex. In the L100P Disc1 mutants the affected cortical region was ventral auditory cortex where I found increased interneuron density in layer I in the mutants when compared to the wild type brain. This implies that L100P Disc1 mutation seems to be playing a small role in the tangential and radial migration of interneurons.

5.2.2 Cell non-autonomous effect of Disc1 upon maturation of parvalbumin interneurons

Once the cortical interneurons reach their correct laminar position, they need to be integrated into the neuronal network and become functional. Functional integration and maturation of the largest subpopulation of interneurons, the parvalbumin expressing basket and chandelier cells, is hallmarked by the expression of this calcium binding protein. Many Disc1 mutant mouse models have shown decreased numbers of parvalbumin cells in MPFC and DLFC (Shen et al., 2008; Hikida et al., 2007; Ibi et al., 2010; Ayhan et al., 2011). A study by Lee et al. (2013) showed lower numbers of parvalbumin expressing neurons in the MPFC but not DLFC in 8-week-old L100P Disc1 mutant mice. This stands in contradiction with my findings – in P21 L100P Disc1 mutant cortex I found decreased parvalbumin cell density across the cortex but not in the MPFC. Nonetheless, both studies agree that the observed decrease in parvalbumin is due to its downregulation in the interneurons, and not due to a decreased numbers of parvalbumin-expressing interneurons. I have also shown that a milder downregulation of parvalbumin exists in the L100P heterozygous mice. All in all, this suggests that the L100P mutation in mouse Disc1 does not have an effect on the generation of the cortical interneurons as such, but that it does have an effect on their maturation.

How exactly Disc1 affects parvalbumin interneuron maturation was not previously investigated. In this study I have shown that in the L100P Disc1 mouse cortex, together with downregulation of parvalbumin protein, there is a decrease in parvalbumin mRNA, suggesting that the observed defect could be due to a transcriptional rather than a translational defect. What is more, by overexpressing the mouse Disc1-100P variant in a small population of cortical projection neurons born at E14.5, and investigating the parvalbumin expression in wild type interneurons, I have shown that parvalbumin downregulation is, at least in part, due to extrinsic factors rather than being a cell autonomous effect. This notion was strengthened by the observation of parvalbumin downregulation on the contralateral side to the electroporation as well as by an increase in parvalbumin expression in the WT-Disc1 overexpression.

An example of possible regulation of parvalbumin expression by the Disc1-100P overexpressing layer II/III callosal projecting neurons in the barrel cortex is shown in Fig 5.01. Interestingly, the affected parvalbumin cells were not those present in layer II/III, but in layer IV and V on the ipsilateral side. Parvalbumin downregulation in the basket and/or chandelier interneurons (pale red) in the two latter cortical layers could be due to the defective connections the callosal axon makes with these cells. Parvalbumin cells in layer IV could be affected by connections from a proportion of cells expressing the mutant Disc1 construct in this layer (e.g. spiny stellate cells shown in light green). Parvalbumin was downregulated in the layer II/III interneurons on the contralateral side possibly due to incorrect input from the Disc1-100P overexpressing layer II/III callosal projecting neurons. Another possibility for these cells not expressing parvalbumin properly could be lack of proper connection of the pyramidal cells residing in this layer that have received abnormal input from the affected callosal projection cells. Lastly, the parvalbumin expression defect observed in layer VI on the contralateral side could be an effect of improper cortico-cortical connection of the callosal projecting neurons from the electroporated side.

Curiously, overexpression of the wild-type Disc1 constructs resulted in an increased parvalbumin cell density suggesting that the fate of a particular interneuronal subtype acquired at birth can be changed by the environment. Another possible explanation is that the apoptosis of a subset of interneurons that should happen once they finish their cortical lamination without making connections with the excitatory cells did not happen as more cells have formed such connections.

Fig 5.01 Cortico-cortical callosally projecting neurons expressing Disc1 L100P variant form incorrect connections with the cortical parvalbumin interneurons in P21 mouse primary somatosensory cortex. The callosally projecting axon sent by the projection neuron expressing Disc1 L100P variant (green triangle) forms connections onto the parvalbumin cells (red circles) along its route to the contralateral cortex. Formation of an incorrect connection results in downregulation of parvalbumin in a subset of interneurons (light red circle). This defect could either be due to weakened connection (light blue-red cross) or improper synaptic transmission (blue-red cross). Downregulation of parvalbumin could occur through direct connection with the affected neuron or, less likely, indirectly with intermediate unaffected cell(s) in the circuit. L – cortical layer.

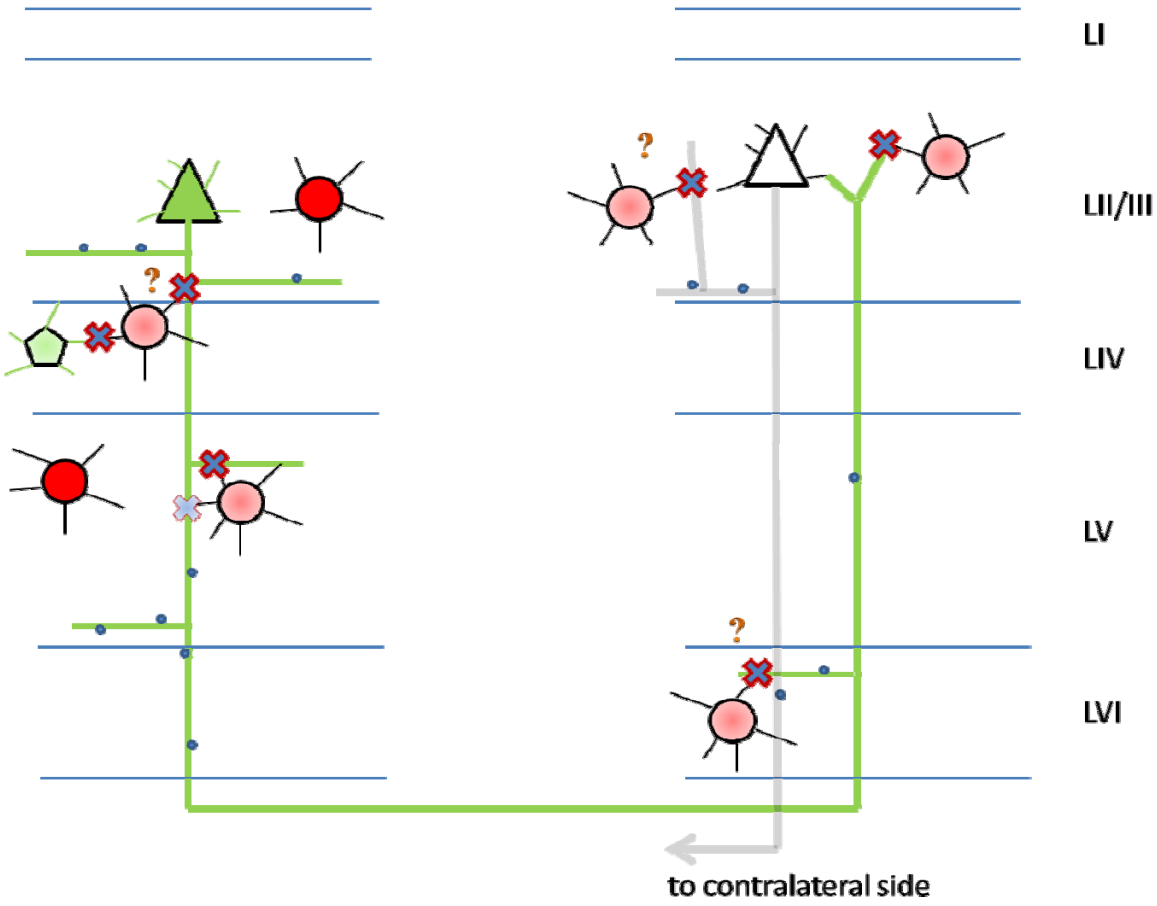

5.2.3 Disc1's role in circuit formation and/or signal transduction

Disc1 has been shown to be necessary for proper axonal projection and spine formation suggesting its role in the correct physical formation of the neuronal circuit (Koike et al., 2006; Duan et al., 2007; Kvajo et al., 2008; Hayashi-Takagi et al., 2010; Lee et al., 2011;). What is more, Disc1 also seems to be needed for proper neurotransmission, both glutamatergic and GABAergic (Holley et al., 2013). It has been shown to have a presynaptic function in the glutamatergic synapse (Maher and LoTurco, 2012) and possibly postsynaptic functions at GABAergic synapses as a partner for another scaffold protein, Dact1 (Arguello et al., 2013). Downregulation of parvalbumin upon Disc1-100P expression was observed in different cortical layers on both ipsilateral and contralateral sides, implying disruption in the intracortical and cortico-cortical connectivity. With that in mind, possible mechanism behind this cell non-autonomous effect in parvalbumin cells could be related to an abnormal formation of processes and/or connections in both Disc1-L100P mosaics and WT-Disc1 overexpressing excitatory cells. Possible explanations for this disruption due to Disc1-100P variant overexpression are:

1) The axons of the affected cells did not properly contact the targeted parvalbumin interneurons and these cells died;
2) Some of the axons from the Disc1-100P mosaics formed connections onto the parvalbumin interneuron, but these connections were not strong enough to make the inhibitory cells mature i.e. express parvalbumin;
3) The connection was properly formed but the glutamatergic synapse (presynaptic) was not transducing the signals necessary for maturation of the parvalbumin cells (e.g. Otx2) properly, resulting in inactivity and downregulation of parvalbumin expression.

Since the number of interneurons in the Disc1 L100P heterozygote was not altered it is possible that the pyramidal cells expressing endogenous mouse Disc1 and the exogenous Disc1 L100P did not cause death of the interneurons they failed to connect to. Thus either improperly active synapses, weak connection of the affected excitatory neurons due to Disc1 mutation or reduced probability of mutant cells connecting to the WT PV-cell would cause an altered input and reduction in PV.

If the connectivity between these cells is disrupted, it would indicate that the extrinsic factors responsible for parvalbumin expression are not properly transported into the parvalbumin cells. For example, Otx2, TF responsible for parvalbumin expression in the cortex, is not expressed in the parvalbumin cells but is incorporated from the surrounding neurons (Sugiyama et al., 2008). Subsequently, measuring a change in the levels of this transcription factor in affected parvalbumin cells could also indicate disrupted connectivity.

5.3 Summary and future perspectives

The observations presented and discussed in this thesis have shed some light on the role of Disc1 in the development of cortical interneurons and their integration into the cortical network. The most intriguing result was my demonstration that Disc1 regulates the maturation of the cortical parvalbumin-expressing cells in a cell non-autonomous manner. My results from the analysis of cortical interneurons of the Disc1 L100P and Q31L mutant mice have also shown further differences between these two lines, as parvalbumin expression in the cortical interneurons was unaffected in the Q31L cerebral cortex. Lastly, mice heterozygous for the Disc1 L100P mutation showed an intermediate phenotype in parvalbumin cell density suggesting a dose-dependent effect of Disc1 upon parvalbumin expression.

From this, a few more questions arise. Since Disc1 has a role in the outgrowth of projecting axons and the formation of dendritic spines (Koike et al., 2006; Duan et al., 2007; Kvajo et al. 2008; Faulkner et al., 2009) as well as formation of functional inhibitory and excitatory synapses (Maher and LoTurco, 2012; Arguello et al., 2013; Holley et al., 2013) it would be interesting to establish which of these processes is responsible for the parvalbumin interneurons' defect observed upon overexpression of the Disc1-100P mutant in the projecting interneurons. Further to this, I would also be interested in overexpressing the Disc1-100P mutant in the developing projection neurons at different stages of development. In this thesis I was investigating the effect projection neurons born at E14.5 have on parvalbumin expression. The Disc1 expression peak falls between E14.5-E16.5 in the mouse brain, and that was the

reason behind overexpression of the mutant variant at this stage. Overexpressing both mutant and wild-type Disc1 variants could potentially have different effects on parvalbumin interneurons at earlier stages (E11.5-E13.5). What is more, it would be interesting to investigate which population of parvalbumin expressing interneurons (for example: large basket cells, nested basket cells, chandelier cells) is affected in both the Disc1 L100P variant *in utero* overexpression model and the ENU-induced Disc1 L100P mutant mice. With this knowledge, it would be possible not only to predict potential effects on cortical neural network activity, but also to obtain further insight into the specification of cortical interneurons.

Further investigation of the development of the cortical parvalbumin interneurons in the Disc1 L100P mutant mouse could shed more light on the nature of this defect. The results from the mutant analysis presented in this thesis are to some extent contradictory to those reported by Lee et al. (2013). However, there was a difference in the developmental timing of these two analyses which could explain the lack of parvalbumin downregulation in the dorsolateral cortex when analysed at an older age (Lee et al., 2013). To further investigate a possible developmental delay in parvalbumin interneurons maturation in the cortex it would be worth analysing other features associated with parvalbumin cells maturation. An example of such markers could be the expression of Otx2 in the PV cells and formation of peri-neuronal nets that surround parvalbumin interneurons - a process that is also experience dependent (Sugiyama et al., 2008; Ye and Miao, 2013). This lattice-like structure maintains ion homeostasis in highly active neurons like the mature parvalbumin interneurons and plays a role in neuroprotection and synaptic plasticity (for a review see Bitanihirwe and Woo, 2014). Interestingly, it has been suggested that defects in the peri-neuronal nets could be linked to the pathophysiology of schizophrenia (Bitanihirwe and Woo, 2014). Lastly, since the largest subpopulation of cortical interneurons is most severely affected by the Disc1 L100P mutation it would be interesting to show how it affects the phenotype of mice heterozygous and homozygous for the mutation. Such investigation could also be performed in combination with the environmental factors (infection, maternal stress) that were shown to trigger the parvalbumin

downregulation in the medial prefrontal cortex of the dominant-negative Disc1 mutant mouse (Ibi et al., 2010).

Altered parvalbumin expression in a subset of interneurons in the Disc1 L100P mutant strain will ultimately lead to behavioural changes in these animals. Parvalbumin fast spiking cells are highly interconnected, forming large number of electrical synapses with other neurons, and are responsible for a precise control of the stimulus propagation mainly through feed-forward inhibition and fast GABA release (Galarreta and Hestrin, 2002, Hu et al., 2014). Parvalbumin expressing cells have been involved in regulation of synaptic plasticity and learning, gain of sensory responses and generation of network oscillations (Hu et al., 2014), all of which could potentially be tested in a mouse. Downregulation of parvalbumin across cerebral cortex of L100P mice could result in a disruption in the fast inhibition resulting in loss of fine-tuning in the neuronal circuitry and potential changes in the behaviours such as learning or sensory responses. Thus appropriate behavioural study combined with electrophysiological investigation of the functionality of the affected parvalbumin cells is needed.

5.4 Conclusions

Cortical interneuron development is a complex and multistage process in which each step needs to be completed with the highest precision for correct functioning of the cortical neuronal network. A cocktail of molecules ranging from transcription factors to cytoskeletal proteins is required for the correct formation of a vast variety of cortical interneurons. Disc1 is but one of those proteins yet its disruption was shown to strongly affect this process.

Here I have shown that a point mutation in the N-terminus of Disc1 has a dramatic effect on the largest subpopulation of cortical interneurons, the parvalbumin-expressing cells. The Disc1 L100P mutant causes downregulation of parvalbumin at the transcriptional level in up to one half of cortical interneurons fated to express this calcium binding protein. This effect is milder in the cerebral cortex of mice heterozygous for the mutation. In my study this effect was not present in the medial prefrontal cortex. In the second part of my thesis, I showed that the effect the Disc1-100P mutant has on parvalbumin expression is cell non-autonomous and is most probably due to either incorrect connectivity of the projection cells onto the inhibitory neurons or due to disruption in signal transduction. Either way, this further supports the proposal that Disc1 is necessary for proper functioning of the neuronal connections in the cortex.

Bibliography

Agmon, A., Connors, B.W. (1991). Thalamocortical responses of mouse somatosensory (barrel) cortex *in vitro*. *Neuroscience* **41**: 365-379.

Alcantara, S., Ferret, I., Soriano, E. (1993). Postnatal development of parvalbumin and calbindin D28K immunoreactivities in the cerebral cortex of the rat. *Anatomy and Embryology* **188**: 63–73.

Anderson, S. A., Eisenstat, D.D., Shi, L., Rubenstein, J.L.R. (2001). Interneuron migration from basal forebrain to neocortex: dependence on Dlx genes. *Science* **278**: 474-476.

Anderson, S. A, Kaznowski, C.E., Horn, C., Rubenstein, J.L.R., McConnell, S.K. (2002). Distinct origins of neocortical projection neurons and interneurons in vivo. *Cereb. Cortex* **12**: 702–9.

Arguello, A., Yang, X., Vogt, D., Stanco, A., Rubenstein, J.L.R., Cheyette, B.N.R. (2013). Dapper antagonist of catenin-1 cooperates with Dishevelled-1 during postsynaptic development in mouse forebrain GABAergic interneurons. *PLoS One* **8**: 1-13.

Ascoli, G.A., Alonso-Nanclares, L., Anderson, S.A., Barrionuevo, G., Benavides-Piccione, R., Burkhalter, A., Buzsáki, G., Cauli, B., Defelipe, J., Fairén, A., Feldmeyer, D., Fishell, G., Fregnac, Y., Freund, T.F., Gardner, D., Gardner, E.P., Goldberg, J.H., Helmstaedter, M., Hestrin, S., Karube, F., Kisvárday, Z.F., Lambolez, B., Lewis, D. A., Marin, O., Markram, H., Muñoz, A., Packer, A., Petersen, C.C.H., Rockland, K.S., Rossier, J., Rudy, B., Somogyi, P., Staiger, J.F., Tamas, G., Thomson, A.M., Toledo-Rodriguez, M., Wang, Y., West, D.C., Yuste, R. (2008). Petilla terminology: nomenclature of features of GABAergic interneurons of the cerebral cortex. *Nat. Rev. Neurosci.* **9**: 557–68.

Austin, C.P., Ky, B., Ma, L., Morris, J. a, Shughrue, P.J. (2004). Expression of Disrupted-In-Schizophrenia-1, a schizophrenia-associated gene, is prominent in the mouse hippocampus throughout brain development. *Neuroscience* **124**: 3–10.

Ayhan, Y., Abazyan, B., Nomura, J., Kim, R., Ladenheim, B., Krasnova, I.N., Sawa, A., Margolis, R.L., Cadet, J.L., Mori, S., Vogel, M.W., Ross, C. A., Pletnikov, M. V. (2011). Differential effects of prenatal and postnatal expressions of mutant human DISC1 on neurobehavioral phenotypes in transgenic mice: evidence for neurodevelopmental origin of major psychiatric disorders. *Mol. Psychiatry* **16**: 293–306.

Bartolini, G., Ciceri, G., Marín, O. (2013). Integration of GABAergic interneurons into cortical cell assemblies: lessons from embryos and adults. *Neuron* **79**: 849–64.

Beby, F., Lamonerie, T. (2013) The homeobox gene Otx2 in development and disease. *Exp Eye Res.* **111**: 9-16.

Behar, T.N., Tran, H.T., Ma, W. (1996). GABA Stimulates Cortical Neurons Chemotaxis and Chemokinesis of Embryonic via Calcium-Dependent Mechanisms. *J. Neurosci.* **16**: 1808–1818.

Behar, T.N., Schaffner, A. E., Scott, C. A., O'Connell, C., Barker, J.L. (1998). Differential response of cortical plate and ventricular zone cells to GABA as a migration stimulus. *J. Neurosci.* **18**: 6378–87.

Behar, T.N., Schaffner, A. E., Scott, C. A., Greene, C.L., Barker, J.L. (2000). GABA receptor antagonists modulate postmitotic cell migration in slice cultures of embryonic rat cortex. *Cereb. Cortex* **10**: 899–909.

Beurdeley, M., Spatazza, J., Lee, H.H., Sugiyama, S., Bernard, C., Di Nardo, A.A., Hensch, T.K., Prochiantz, A. (2012) Otx2 binding to perineuronal nets persistently regulates plasticity in the mature visual cortex. *J Neurosci.* **32**(27): 9429-37.

Billing-Marczak, K., Ziemińska, E., Leśniak, W., Łazarewicz, J.W., Kuźnicki, J. (2004). Calretinin gene promoter activity is differently regulated in neurons and cancer cells. Role of AP2-like cis element and zinc ions. *Biochim. Biophys. Acta* **1678**: 14–21.

Birrell, J.M., Brown, V.J. (2000). Medial frontal cortex mediates perceptual attentional set shifting in the rat. *J. Neurosci.* **20**: 4320–4.

Bitanihirwe, B.K.Y., Woo, T.-U.W. (2014). Perineuronal nets and schizophrenia: The importance of neuronal coatings. *Neurosci. Biobehav. Rev.* **45**: 1–14.

Blackwood, D.H., Fordyce, a, Walker, M.T., St Clair, D.M., Porteous, D.J., Muir, W.J. (2001). Schizophrenia and affective disorders--cosegregation with a translocation at chromosome 1q42 that directly disrupts brain-expressed genes: clinical and P300 findings in a family. *Am. J. Hum. Genet.* **69**: 428–33.

Boksa, P. (2009) On the neurobiology of hallucinations. *J Psychiatry Neurosci.* **34**(4): 260-262.

Bortone, D., Polleux, F. (2009). KCC2 expression promotes the termination of cortical interneuron migration in a voltage-sensitive calcium-dependent manner. *Neuron* **62**: 53–71.

Bradshaw, N.J., Hennah, W., Soares, D.C. (2013) NDE1 and NDEL1: twin neurodevelopmental proteins with similar 'nature' but different 'nurture' *Biomol Concepts* **4**(5): 447-464.

Brandon, N.J., Handford, E.J., Schurov, I., Rain, J.-C., Pelling, M., Duran-Jimeniz, B., Camargo, L.M., Oliver, K.R., Beher, D., Shearman, M.S., Whiting, P.J. (2004). Disrupted in Schizophrenia 1 and Nudel form a neurodevelopmentally regulated protein complex: implications for schizophrenia and other major neurological disorders. *Mol. Cell. Neurosci.* **25**: 42–55.

Brandon, N.J., Millar, J.K., Korth, C., Sive, H., Singh, K.K., Sawa, A. (2009). Understanding the role of DISC1 in psychiatric disease and during normal development. *J. Neurosci.* **29**: 12768–75.

Brown, K.N., Chen, S., Han, Z., Lu, C.-H., Tan, X., Zhang, X.-J., Ding, L., Lopez-Cruz, A., Saur, D., Anderson, S. A., Huang, K., Shi, S.-H. (2011). Clonal production and organization of inhibitory interneurons in the neocortex. *Science* **334**: 480–6.

Butt, S.J.B., Fuccillo, M., Nery, S., Noctor, S., Kriegstein, A., Corbin, J.G., Fishell, G. (2005). The temporal and spatial origins of cortical interneurons predict their physiological subtype. *Neuron* **48**: 591–604.

Bystron, I., Molnár, Z., Otellin, V., Blakemore, C. (2005). Tangential networks of precocious neurons and early axonal outgrowth in the embryonic human forebrain. *J. Neurosci.* **25**: 2781–92.

Caillard, O., Moreno, H., Schwaller, B., Llano, I., Celio, M.R., Marty, A (2000). Role of the calcium-binding protein parvalbumin in short-term synaptic plasticity. *Proc. Natl. Acad. Sci. U. S. A.* **97**: 13372–7.

Cannon T.D., Kaprio J., Lönnqvist J., Huttunen M., Koskenvuo M. (1998) The genetic epidemiology of schizophrenia in a Finnish twin cohort. A population-based modeling study. *Arch Gen Psychiatry* **55**: 67-74.

Camargo, L.M., Collura, V., Rain, J.-C., Mizuguchi, K., Hermjakob, H., Kerrien, S., Bonnert, T.P., Whiting, P.J., Brandon, N.J. (2007). Disrupted in Schizophrenia 1 Interactome: evidence for the close connectivity of risk genes and a potential synaptic basis for schizophrenia. *Mol. Psychiatry* **12**: 74–86.

Cardno, A.G., Gottesman, I.I. (2000) Twin studies of schizophrenia: from bow-and-arrow concordances to star wars Mx and functional genomics. *Am J Med Genet*. **97**(1): 12-7.

Chen, S.-Y., Huang, P.-H., Cheng, H.-J. (2011). Disrupted-in-Schizophrenia 1-mediated axon guidance involves TRIO-RAC-PAK small GTPase pathway signaling. *Proc. Natl. Acad. Sci. U. S. A.* **108**: 5861–6.

Chubb, J.E., Bradshaw, N.J., Soares, D.C., Porteous, D.J., Millar, J.K. (2008). The DISC locus in psychiatric illness. *Mol. Psychiatry* **13**: 36–64.

Ciceri, G., Dehorter, N., Sols, I., Huang, Z.J., Maravall, M., Marín, O. (2013). Lineage-specific laminar organization of cortical GABAergic interneurons. *Nat. Neurosci.* **16:** 1199–210.

Clapcote, S.J., Lipina, T. V, Millar, J.K., Mackie, S., Christie, S., Ogawa, F., Lerch, J.P., Trimble, K., Uchiyama, M., Sakuraba, Y., Kaneda, H., Shiroishi, T., Houslay, M.D., Henkelman, R.M., Sled, J.G., Gondo, Y., Porteous, D.J., Roder, J.C. (2007). Behavioral phenotypes of Disc1 missense mutations in mice. *Neuron* **54**: 387–402.

Cobos, I., Calcagnotto, M.E., Vilaythong, A.J., Thwin, M.T., Noebels, J.L., Baraban, S.C., Rubenstein, J.L.R. (2005). Mice lacking Dlx1 show subtype-specific loss of interneurons, reduced inhibition and epilepsy. *Nat Neurosci* **8**: 1059-1068.

Costas, J., Suárez-Rama, J.J., Carrera, N., Paz, E., Páramo, M., Agra, S., Brenlla, J., Ramos-Ríos, R., Arrojo, M. (2013) Role of DISC1 interacting proteins in schizophrenia risk from genome-wide analysis of missense SNPs. *Ann Hum Genet.* **77**(6): 504-512.

Cross, D.A., Alessi, D.R., Cohen, P., Andjelkovich, M., Hemmings, B.A. (1995) Inhibition of glycogen synthase kinase-3 by insulin mediated by protein kinase B. *Nature* **378**(6559): 785-789.

Cross-Disorder Group of the Psychiatric Genomics Consortium (2013) Identification of risk loci with shared effects on five major psychiatricdisorders: a genome-wide analysis. *Lancet* **381**(9875): 1371-1379.

Duan, X., Chang, J.H., Ge, S., Faulkner, R.L., Kim, J.Y., Kitabatake, Y., Liu, X., Yang, C.-H., Jordan, J.D., Ma, D.K., Liu, C.Y., Ganesan, S., Cheng, H.-J., Ming, G., Lu, B., Song, H. (2007). Disrupted-In-Schizophrenia 1 regulates integration of newly generated neurons in the adult brain. *Cell* **130**: 1146–58.

Cuzon, V.C., Yeh, P.W., Cheng, Q., Yeh, H.H. (2006). Ambient GABA promotes cortical entry of tangentially migrating cells derived from the medial ganglionic eminence. *Cereb. Cortex* **16**: 1377–88.

Dargan, S.L., Schwaller, B., Parker, I. (2004). Spatiotemporal patterning of IP3-mediated Ca2+ signals in Xenopus oocytes by Ca2+-binding proteins. *J. Physiol.* **556**: 447–61.

DeFelipe, J., López-Cruz, P.L., Benavides-Piccione, R., Bielza, C., Larrañaga, P., Anderson, S., Burkhalter, A., Cauli, B., Fairén, A., Feldmeyer, D., Fishell, G., Fitzpatrick, D., Freund, T.F., González-Burgos, G., Hestrin, S., Hill, S., Hof, P.R., Huang, J., Jones, E.G., Kawaguchi, Y., Kisvárday, Z., Kubota, Y., Lewis, D. A., Marín, O., Markram, H., McBain, C.J., Meyer, H.S., Monyer, H., Nelson, S.B., Rockland, K., Rossier, J., Rubenstein, J.L.R., Rudy, B., Scanziani, M., Shepherd, G.M., Sherwood, C.C., Staiger, J.F., Tamás, G., Thomson, A., Wang, Y., Yuste, R., Ascoli, G. A. (2013). New insights into the classification and nomenclature of cortical GABAergic interneurons. *Nat. Rev. Neurosci.* **14**: 202–16.

Di Cristo, G., Wu, C., Chattopadhyaya, B., Ango, F., Knott, G., Welker, E., Svoboda, K., Huang, Z.J. (2004). Subcellular domain-restricted GABAergic innervation in primary visual cortex in the absence of sensory and thalamic inputs. *Nat. Neurosci.* **7**: 1184–6.

Donato, F., Rompani, S.B., Caroni, P. (2013). Parvalbumin-expressing basket-cell network plasticity induced by experience regulates adult learning. *Nature* **504**: 272–6.

Elias, L. A. B., Turmaine, M., Parnavelas, J.G., Kriegstein, A.R. (2010). Connexin 43 mediates the tangential to radial migratory switch in ventrally derived cortical interneurons. *J. Neurosci.* **30**: 7072–7.

Enomoto, A., Asai, N., Namba, T., Wang, Y., Kato, T., Tanaka, M., Tatsumi, H., Taya, S., Tsuboi, D., Kuroda, K., Kaneko, N., Sawamoto, K., Miyamoto, R., Jijiwa, M., Murakumo, Y., Sokabe, M., Seki, T., Kaibuchi, K., Takahashi, M. (2009). Roles of disrupted-in-schizophrenia 1-interacting protein girdin in postnatal development of the dentate gyrus. *Neuron* **63**: 774–87.

Esclapez, M., Tillakaratne, N.J., Kaufman, D.L., Tobin, A. J., Houser, C.R. (1994). Comparative localization of two forms of glutamic acid decarboxylase and their mRNAs in rat brain supports the concept of functional differences between the forms. *J. Neurosci.* **14**: 1834–55.

Euston, D.R., Gruber, A.J., McNaughton, B.L. (2012). The role of medial prefrontal cortex in memory and decision making. *Neuron* **76**: 1057–70.

Faas, G.C., Schwaller, B., Vergara, J.L., Mody, I. (2007). Resolving the fast kinetics of cooperative binding: Ca2+ buffering by calretinin. *PLoS Biol.* **5**: e311.

Faulkner, R.L., Jang, M.-H., Liu, X.-B., Duan, X., Sailor, K. A., Kim, J.Y., Ge, S., Jones, E.G., Ming, G., Song, H., Cheng, H.-J. (2008). Development of hippocampal mossy fiber synaptic outputs by new neurons in the adult brain. *Proc. Natl. Acad. Sci. U. S. A.* **105**: 14157–62.

Faux, C., Rakic, S., Andrews, W., Britto, J.M. (2012). Neurons on the move: migration and lamination of cortical interneurons. *Neurosignals*. **20**: 168–89.

Feng, Y., Walsh, C.A. (2004). Mitotic Spindle Regulation by Nde1 Controls Cerebral Cortical Size. *Neuron* **44**: 279–293.

Fukuda, T., Sugita, S., Inatome, R., Yanagi, S. (2010). CAMDI, a novel disrupted in schizophrenia 1 (DISC1)-binding protein, is required for radial migration. *J. Biol. Chem.* **285**: 40554–61.

Galarreta, M., Hestrin, S. (2002) Electrical and chemical synapses among parvalbumin fast-spiking GABAergic interneurons in adult mouse neocortex. *Proc. Natl. Acad. Sci. U. S. A.* **99**(19): 12438-43

Ge, S., Sailor, K. A., Ming, G., Song, H. (2008). Synaptic integration and plasticity of new neurons in the adult hippocampus. *J. Physiol.* **586**: 3759–65.

Gonchar, Y., Burkhalter, A. (1997). Three distinct families of GABAergic neurons in rat visual cortex. *Cereb. Cortex* **7**: 347–58.

Haiech, J., Derancourt, J., Pechère, J.F., Demaille, J.G. (1979). Magnesium and calcium binding to parvalbumins: evidence for differences between parvalbumins and an explanation of their relaxing function. *Biochemistry* **18**: 2752–8.

Haque, F.N., Lipina, T.V., Roder, J.C., Wong, A.H. (2012) Social defeat interacts with Disc1 mutations in the mouse to affect behavior. *Behav Brain Res.* **233**(2): 337-44.

Haubensak, W., Attardo, A., Denk, W., Huttner, W.B. (2004). Neurons arise in the basal neuroepithelium of the early mammalian telencephalon: a major site of neurogenesis. *Proc. Natl. Acad. Sci. U. S. A.* **101**: 3196–201.

Hayashi-Takagi, A., Takaki, M., Graziane, N., Seshadri, S., Murdoch, H., Dunlop, A.J., Makino, Y., Seshadri, A.J., Ishizuka, K., Srivastava, D.P., Xie, Z., Baraban, J.M., Houslay, M.D., Tomoda, T., Brandon, N.J., Kamiya, A., Yan, Z., Penzes, P., Sawa, A. (2010). Disrupted-in-Schizophrenia 1 (DISC1) regulates spines of the glutamate synapse via Rac1. *Nat. Neurosci.* 13: 327–32.

Heiss, J.E., Katz, Y., Ganmor, E., Lampl, I. (2008) Shift in the balance between excitation and inhibition during sensory adaptation of S1 neurons. *J Neurosci*. **28**(49): 13320-30.

Herculano-Houzel, S., Watson, C., Paxinos, G. (2013) Distribution of neurons in functional areas of the mouse cerebral cortex reveals quantitatively different cortical zones. *Front Neuroanat*. 7: 35.

Hernández-Miranda, L.R., Parnavelas, J.G., Chiara, F. (2010). Molecules and mechanisms involved in the generation and migration of cortical interneurons. *ASN Neuro* **2**: 75-86.

Hevner, R.F., Daza, R. A. M., Englund, C., Kohtz, J., Fink, A. (2004). Postnatal shifts of interneuron position in the neocortex of normal and reeler mice: evidence for inward radial migration. *Neuroscience* **124**: 605–18.

Hevner, R.F., Daza, R. a. M., Rubenstein, J.L.R., Stunnenberg, H., Olavarria, J.F., Englund, C. (2003). Beyond Laminar Fate: Toward a Molecular Classification of Cortical Projection/Pyramidal Neurons. *Dev. Neurosci.* **25**: 139–151.

Hikida, T., Jaaro-Peled, H., Seshadri, S., Oishi, K., Hookway, C., Kong, S., Wu, D., Xue, R., Andradé, M., Tankou, S., Mori, S., Gallagher, M., Ishizuka, K., Pletnikov, M., Kida, S., Sawa, A. (2007). Dominant-negative DISC1 transgenic mice display schizophrenia-associated phenotypes detected by measures translatable to humans. *Proc. Natl. Acad. Sci. U. S. A.* **104**: 14501–6.

Hippenmeyer, S., Youn, Y.H., Moon, H.M., Miyamichi, K., Zong, H., Wynshaw-Boris, A., Luo, L. (2010). Genetic mosaic dissection of Lis1 and Ndel1 in neuronal migration. *Neuron* **68**: 695–709.

Holley, S.M., Wang, E. A., Cepeda, C., Jentsch, J.D., Ross, C. A., Pletnikov, M. V, Levine, M.S. (2013). Frontal cortical synaptic communication is abnormal in Disc1 genetic mouse models of schizophrenia. *Schizophr. Res.* **146**: 264–72.

Howes, O.D., Kapur, S. (2009) The dopamine hypothesis of schizophrenia: version III--the final common pathway. *Schizophr Bull.* **35**(3): 549-62.

Hu, H., Gan, J., Jonas, P. (2014) Interneurons. Fast-spiking, parvalbumin^{+} GABAergic interneurons: from cellular design to microcircuit function. *Science* **345**(6196): 1255263.

Ibi, D., Nagai, T., Koike, H., Kitahara, Y., Mizoguchi, H., Niwa, M., Jaaro-Peled, H., Nitta, A., Yoneda, Y., Nabeshima, T., Sawa, A., Yamada, K. (2010). Combined effect of neonatal immune activation and mutant DISC1 on phenotypic changes in adulthood. *Behav. Brain Res.* **206**: 32–7.

Inada, H., Watanabe, M., Uchida, T., Ishibashi, H., Wake, H., Nemoto, T., Yanagawa, Y., Fukuda, A., Nabekura, J. (2011). GABA regulates the multidirectional tangential migration of GABAergic interneurons in living neonatal mice. *PLoS One* **6**: e27048.

Inamura, N., Kimura, T., Tada, S., Kurahashi, T., Yanagida, M., Yanagawa, Y., Ikenaka, K., Murakami, F. (2012). Intrinsic and extrinsic mechanisms control the termination of cortical interneuron migration. *J. Neurosci.* **32**: 6032–42.

Isaacson, J.S., Scanziani, M. (2011) How inhibition shapes cortical activity. *Neuron* **72**(2): 231-43.

Ishizuka, K., Kamiya, A., Oh, E.C., Kanki, H., Seshadri, S., Robinson, J.F., Murdoch, H., Dunlop, A.J., Kubo, K., Furukori, K., Huang, B., Zeledon, M., Hayashi-Takagi, A., Okano, H., Nakajima, K., Houslay, M.D., Katsanis, N., Sawa, A. (2011). DISC1-dependent switch from progenitor proliferation to migration in the developing cortex. *Nature* **473**: 92–6.

Jacobs, P.A., Brunton, M., Frackiewicz A., Newton, M., Cook, P.J.L., Robson E.B. (1970) Studies on a family with three cytogenetic markers. *Ann Hum Genet* **33**: 325-336.

Jia, P., Wang, L., Fanous, A.H., Pato, C.N., Edwards, T.L., International Schizophrenia Consortium, Zhao Z. (2012) Network-assisted investigation of combined causal signals from genome-wide association studies in schizophrenia. *PLoS Comput Biol.* **8**(7): e1002587.

Justice, M.J., Noveroske, J.K., Weber, J.S., Zheng, B., Bradley, A. (1999) Mouse ENU mutagenesis. *Hum Mol Genet.* **8**(10): 1955-63.

Kamiya, A., Kubo, K., Tomoda, T., Takaki, M., Youn, R., Ozeki, Y., Sawamura, N., Park, U., Kudo, C., Okawa, M., Ross, C. A. Hatten, M.E., Nakajima, K., Sawa, A. (2005). A schizophrenia-associated mutation of DISC1 perturbs cerebral cortex development. *Nat. Cell Biol.* **7**: 1167–78.

Kas, M.J.H., Gelegen, C., Schalkwyk, L.C., Collier, D. A. (2009). Interspecies comparisons of functional genetic variations and their implications in neuropsychiatry. *Am. J. Med. Genet. B. Neuropsychiatr. Genet.* **150B**: 309–17.

Kenan-Vaknin, G., Malach, R., Segal, M. (1992). Excitatory inputs to layer V pyramidal cells of rat primary visual cortex revealed by acetylcholine activation. *Brain Res.* **574**: 147–56.

Kepecs, A., Fishell, G. (2014). Interneuron cell types are fit to function. *Nature* **505**: 318–26.

Kessaris, N., Magno, L., Rubin, A.N., Oliveira, M.G. (2014). Genetic programs controlling cortical interneuron fate. *Curr. Opin. Neurobiol.* **26C**: 79–87.

Kim, J.Y., Duan, X., Liu, C.Y., Jang, M.-H., Guo, J.U., Pow-anpongkul, N., Kang, E., Song, H., Ming, G. (2009). DISC1 regulates new neuron development in the adult brain via modulation of AKT-mTOR signaling through KIAA1212. *Neuron* **63**: 761–73.

Kim, J.Y., Liu, C.Y., Zhang, F., Duan, X., Wen, Z., Song, J., Feighery, E., Lu, B., Rujescu, D., St Clair, D., Christian, K., Callicott, J.H., Weinberger, D.R., Song, H., Ming, G. (2012). Interplay between DISC1 and GABA signaling regulates neurogenesis in mice and risk for schizophrenia. *Cell* **148**: 1051–64.

Koelbl, C., Helmstaedter, M., Lübke, J., Feldmeyer, D. (2013). A Barrel-Related Interneuron in Layer 4 of Rat Somatosensory Cortex with a High Intrabarrel Connectivity. *Cereb. Cortex.* [Epub ahead of print].

Koike, H., Arguello, P.A., Kvajo, M., Karayiorgou, M., Gogos, J. A. (2006). Disc1 is mutated in the 129S6/SvEv strain and modulates working memory in mice. *Proc. Natl. Acad. Sci. U. S. A.* **103**: 3693–7.

Kringlen, E. (2000) Twin studies in schizophrenia with special emphasis on concordance figures. *Am J Med Genet.* **97**(1): 4-11.

Kubo, K.-I., Tomita, K., Uto, A., Kuroda, K., Seshadri, S., Cohen, J., Kaibuchi, K., Kamiya, A., Nakajima, K. (2010). Migration defects by DISC1 knockdown in C57BL/6, 129X1/SvJ, and ICR strains via in utero gene transfer and virus-mediated RNAi. *Biochem. Biophys. Res. Commun.* **400**: 631–7.

Kubota, Y. (2014). Untangling GABAergic wiring in the cortical microcircuit. *Curr. Opin. Neurobiol.* **26C**: 7–14.

Kvajo, M., McKellar, H., Arguello, P.A., Drew, L.J., Moore, H., MacDermott, A.B., Karayiorgou, M., Gogos, J. A. (2008). A mutation in mouse Disc1 that models a schizophrenia risk allele leads to specific alterations in neuronal architecture and cognition. *Proc. Natl. Acad. Sci. U. S. A.* **105**: 7076–81.

Kvajo, M., McKellar, H., Drew, L.J., Lepagnol-Bestel, A.-M., Xiao, L., Levy, R.J., Blazeski, R., Arguello, P.A., Lacefield, C.O., Mason, C. A., Simonneau, M., O'Donnell, J.M., MacDermott, A.B., Karayiorgou, M., Gogos, J. A. (2011). Altered axonal targeting and short-term plasticity in the hippocampus of Disc1 mutant mice. *Proc. Natl. Acad. Sci. U. S. A.* **108**: E1349–58.

Lam, C., Vergnolle, M. a S., Thorpe, L., Woodman, P.G., Allan, V.J. (2010). Functional interplay between LIS1, NDE1 and NDEL1 in dynein-dependent organelle positioning. *J. Cell Sci.* **123**: 202–12.

Lee, S.H., Rosenmund, C., Schwaller, B., Neher, E. (2000). Differences in Ca2+ buffering properties between excitatory and inhibitory hippocampal neurons from the rat. *J. Physiol*. **525** Pt 2: 405–18.

Lee, F.H.F., Fadel, M.P., Preston-Maher, K., Cordes, S.P., Clapcote, S.J., Price, D.J., Roder, J.C., Wong, A.H.C. (2011). Disc1 point mutations in mice affect development of the cerebral cortex. *J. Neurosci.* **31**: 3197–206.

Lee, F.H.F., Zai, C.C., Cordes, S.P., Roder, J.C., Wong, A.H.C. (2013). Abnormal interneuron development in disrupted-in-schizophrenia-1 L100P mutant mice. *Mol. Brain* **6**: 20.

Lewis, D.A., Hashimoto, T., Volk, D.W. (2005) Cortical inhibitory neurons and schizophrenia. *Nat Rev Neurosci.* **6**(4): 312-24.

Lewis, D.A., Curley, A.A., Glausier, J.R., Volk, D.W. (2012) Cortical parvalbumin interneurons and cognitive dysfunction in schizophrenia. *Trends Neurosci*. **35**(1): 57-67.

Li, W., Zhou, Y., Jentsch, J.D., Brown, R. a M., Tian, X., Ehninger, D., Hennah, W., Peltonen, L., Lönnqvist, J., Huttunen, M.O., Kaprio, J., Trachtenberg, J.T., Silva, A.J., Cannon, T.D. (2007). Specific developmental disruption of disrupted-in-schizophrenia-1 function results in schizophrenia-related phenotypes in mice. *Proc. Natl. Acad. Sci. U. S. A.* **104**: 18280–5.

Li, G., Adesnik, H., Li, J., Long, J., Nicoll, R. a, Rubenstein, J.L.R., Pleasure, S.J. (2008). Regional distribution of cortical interneurons and development of inhibitory tone are regulated by Cxcl12/Cxcr4 signaling. *J. Neurosci.* **28**: 1085–98.

Lipina, T.V., Niwa, M., Jaaro-Peled, H., Fletcher, P.J., Seeman, P., Sawa, A., Roder, J.C. (2010) Enhanced dopamine function in DISC1-L100P mutant mice: implications for schizophrenia. *Genes Brain Behav.* **9**(7): 777-789.

Lipina, T.V., Fletcher, P.J., Lee, F.H., Wong, A.H., Roder, J.C. (2013) Disrupted-in-schizophrenia-1 Gln31Leu polymorphism results in social anhedonia associated with monoaminergic imbalance and reduction of CREB and β-arrestin-1,2 in the nucleus accumbens in a mouse model of depression. *Neuropsychopharmacology* **38**(3): 423-436.

Lipina, T.V., Zai, C., Hlousek, D., Roder, J.C., Wong, A.H. (2013) Maternal immune activation during gestation interacts with Disc1 point mutation to exacerbate schizophrenia-related behaviors in mice. *J Neurosci.* **33**(18): 7654-66.

Lisman, J. (2011) Excitation, inhibition, local oscillations, or large-scale loops: what causes the symptoms of schizophrenia? *Curr Opin Neurobiol* **3**: 537-544.

Lodge, D.J., Behrens, M.M., Grace, A.A. (2009) A loss of parvalbumin- containing interneurons is associated with diminished oscillatory activity in an animal model of schizophrenia. *J Neurosci.* **29**(8): 2344-54.

López-Bendito, G., Luján, R., Shigemoto, R., Ganter, P., Paulsen, O., Molnár, Z. (2003). Blockade of GABA(B) receptors alters the tangential migration of cortical neurons. *Cereb. Cortex* **13**: 932–42.

López-Bendito, G., Sánchez-Alcañiz, J.A., Pla, R., Borrell, V., Picó, E., Valdeolmillos, M., Marín, O. (2008). Chemokine signaling controls intracortical migration and final distribution of GABAergic interneurons. *J. Neurosci.* **28**: 1613–24.

Ma, Y., Hu, H., Berrebi, A.S., Mathers, P.H., Agmon, A. (2006). Distinct subtypes of somatostatin-containing neocortical interneurons revealed in transgenic mice. *J. Neurosci.* **26**: 5069–82.

Maher, B.J., LoTurco, J.J. (2012). Disrupted-in-schizophrenia (DISC1) functions presynaptically at glutamatergic synapses. *PLoS One* **7**: 1-9.

Malatesta, P., Hartfuss, E., Götz, M. (2000). Isolation of radial glial cells by fluorescent-activated cell sorting reveals a neuronal lineage. *Development* **127**: 5253–63.

Mao, Y., Ge, X., Frank, C.L., Madison, J.M., Koehler, A.N., Doud, M.K., Tassa, C., Berry, E.M., Soda, T., Singh, K.K., Biechele, T., Petryshen, T.L., Moon, R.T., Haggarty, S.J., Tsai, L.-H. (2009). Disrupted in schizophrenia 1 regulates neuronal progenitor proliferation via modulation of GSK3beta/beta-catenin signaling. *Cell* **136**: 1017–31.

Marín, O., Rubenstein, J.L. (2001). A long, remarkable journey: tangential migration in the telencephalon. *Nat. Rev. Neurosci.* **2**: 780–90.

Marín, O., Valiente, M., Ge, X., Tsai, L.-H. (2010). Guiding neuronal cell migrations. *Cold Spring Harb. Perspect. Biol.* **2**: a001834.

Markram, H., Toledo-Rodriguez, M., Wang, Y., Gupta, A., Silberberg, G., Wu, C. (2004). Interneurons of the neocortical inhibitory system. *Nat. Rev. Neurosci.* **5**: 793–807.

Martínez-Cerdeño, V., Noctor, S.C., Espinosa, A., Ariza, J., Parker, P., Orasji, S., Daadi, M.M., Bankiewicz, K., Alvarez-Buylla, A., Kriegstein, A.R. (2010). Embryonic MGE precursor cells grafted into adult rat striatum integrate and ameliorate motor symptoms in 6-OHDA-lesioned rats. *Cell Stem Cell* 6: 238–50.

Mathieson, I., Munafò, M.R., Flint, J. (2012) Meta-analysis indicates that common variants at the*DISC1* locus are not associated with schizophrenia. *Mol Psych* **17**: 634-641.

McManus, M.F., Nasrallah, I.M., Pancoast, M.M., Wynshaw-Boris, A., Golden, J. A. (2004). Lis1 is necessary for normal non-radial migration of inhibitory interneurons. *Am. J. Pathol.* **165**: 775–84.

Métin, C., Godement, P. (1996). The ganglionic eminence may be an intermediate target for corticofugal and thalamocortical axons. *J. Neurosci* **16**(10): 3219-3235.

Métin, C., Baudoin, J.-P., Rakić, S., Parnavelas, J.G. (2006). Cell and molecular mechanisms involved in the migration of cortical interneurons. *Eur. J. Neurosci.* **23**: 894–900.

Meyer, K.D., Morris, J. A. (2008). Immunohistochemical analysis of Disc1 expression in the developing and adult hippocampus. *Gene Expr. Patterns* **8**: 494–501.

Millar, J.K., Wilson-Annan, J.C., Anderson, S., Christie, S., Taylor, M.S., Semple, C. a, Devon, R.S., St Clair, D.M., Muir, W.J., Blackwood, D.H., Porteous, D.J. (2000). Disruption of two novel genes by a translocation co-segregating with schizophrenia. *Hum. Mol. Genet.* **9**: 1415–23.

Millar, J.K., Pickard, B.S., Mackie, S., James, R., Christie, S., Buchanan, S.R., Malloy, M.P., Chubb, J.E., Huston, E., Baillie, G.S., Thomson, P. a, Hill, E. V, Brandon, N.J., Rain, J.-C., Camargo, L.M., Whiting, P.J., Houslay, M.D., Blackwood, D.H.R., Muir, W.J., Porteous, D.J. (2005). DISC1 and PDE4B are interacting genetic factors in schizophrenia that regulate cAMP signaling. *Science* **310**: 1187–91.

Millar, J.K., Mackie, S., Clapcote, S.J., Murdoch, H., Pickard, B.S., Christie, S., Muir, W.J., Blackwood, D.H., Roder, J.C., Houslay, M.D., Porteous, D.J. (2007). Disrupted in schizophrenia 1 and phosphodiesterase 4B: towards an understanding of psychiatric illness. *J. Physiol.* **584**: 401–5.

Miyata, T., Kawaguchi, A., Saito, K., Kawano, M., Muto, T., Ogawa, M. (2004). Asymmetric production of surface-dividing and non-surface-dividing cortical progenitor cells. *Development* **131**: 3133–45.

Miyoshi, K., Asanuma, M., Miyazaki, I., Diaz-Corrales, F.J., Katayama, T., Tohyama, M., Ogawa, N. (2004). DISC1 localizes to the centrosome by binding to kendrin. *Biochem. Biophys. Res. Commun.* **317**: 1195–9.

Miyoshi, G., Butt, S.J.B., Takebayashi, H., Fishell, G. (2007). Physiologically distinct temporal cohorts of cortical interneurons arise from telencephalic Olig2-expressing precursors. *J. Neurosci.* **27**: 7786–98.

Miyoshi, G., Hjerling-Leffler, J., Karayannis, T., Sousa, V.H., Butt, S.J.B., Battiste, J., Johnson, J.E., Machold, R.P., Fishell, G. (2010). Genetic fate mapping reveals that the caudal ganglionic eminence produces a large and diverse population of superficial cortical interneurons. *J. Neurosci.* **30**: 1582–94.

Miyoshi, G., Fishell, G. (2011). GABAergic interneuron lineages selectively sort into specific cortical layers during early postnatal development. *Cereb. Cortex* **21**: 845–52.

Mizuno, H., Hirano, T., Tagawa, Y. (2007). Evidence for activity-dependent cortical wiring: formation of interhemispheric connections in neonatal mouse visual cortex requires projection neuron activity. *J. Neurosci.* **27**: 6760–70.

Murray, J.D., Anticevic, A., Gancsos, M., Ichinose, M., Corlett, P.R., Krystal, J.H., Wang, X.J. (2014) Linking microcircuit dysfunction to cognitive impairment: effects of disinhibition associated with schizophrenia in a cortical working memory model. *Cereb Cortex* **24**(4): 859-72.

Nadarajah, B., Alifragis, P., Wong, R.O.L., Parnavelas, J.G. (2002). Ventricle-directed migration in the developing cerebral cortex. *Nat. Neurosci.* **5**: 218–24.

Nakajima, K. (2007). Control of tangential/non-radial migration of neurons in the developing cerebral cortex. *Neurochem. Int.* **51**: 121–31.

Namba, T., Ming, G.-L., Song, H., Waga, C., Enomoto, A., Kaibuchi, K., Kohsaka, S., Uchino, S. (2011). NMDA receptor regulates migration of newly generated neurons in the adult hippocampus via Disrupted-In-Schizophrenia 1 (DISC1). *J. Neurochem.* **118**: 34–44.

Niwa, M., Kamiya, A., Murai, R., Kubo, K., Gruber, A.J., Tomita, K., Lu, L., Tomisato, S., Jaaro-Peled, H., Seshadri, S., Hiyama, H., Huang, B., Kohda, K., Noda, Y., O'Donnell, P., Nakajima, K., Sawa, A., Nabeshima, T. (2010). Knockdown of DISC1 by in utero gene transfer disturbs postnatal dopaminergic maturation in the frontal cortex and leads to adult behavioral deficits. *Neuron* **65**: 480–9.

Noctor, S.C., Flint, A.C., Weissman, T. a, Wong, W.S., Clinton, B.K., Kriegstein, A.R. (2002). Dividing precursor cells of the embryonic cortical ventricular zone have morphological and molecular characteristics of radial glia. *J. Neurosci.* **22**: 3161–73.

Noctor, S.C., Martínez-Cerdeño, V., Ivic, L., Kriegstein, A.R. (2004). Cortical neurons arise in symmetric and asymmetric division zones and migrate through specific phases. *Nat. Neurosci.* **7**: 136–44.

Packer, A.M., McConnell, D.J., Fino, E., Yuste, R. (2013). Axo-dendritic overlap and laminar projection can explain interneuron connectivity to pyramidal cells. *Cereb. Cortex* **23**: 2790–802.

Patz, S. Grabert J., Gorba, T., Wirth, M.J., Wahle, P. (2004). Parvalbumin Expression in Visual Cortical Interneurons Depends on Neuronal Activity and TrkB Ligands during an Early Period of Postnatal Development. *Cereb. Cortex* **14**: 342–351.

Pi, H.-J., Hangya, B., Kvitsiani, D., Sanders, J.I., Huang, Z.J., Kepecs, A. (2013). Cortical interneurons that specialize in disinhibitory control. *Nature* **503**: 521–4.

Pla, R., Borrell, V., Flames, N., Marín, O. (2006). Layer acquisition by cortical GABAergic interneurons is independent of Reelin signaling. *J. Neurosci.* **26**: 6924–34.

Pletnikov, M. V, Ayhan, Y., Nikolskaia, O., Xu, Y., Ovanesov, M. V, Huang, H., Mori, S., Moran, T.H., Ross, C. A. (2008). Inducible expression of mutant human DISC1 in mice is associated with brain and behavioral abnormalities reminiscent of schizophrenia. *Mol. Psychiatry* **13**: 173–86, 115.

Polleux, F., Whitford, K.L., Dijkhuizen, P. a, Vitalis, T., Ghosh, A. (2002). Control of cortical interneuron migration by neurotrophins and PI3-kinase signaling. *Development* **129**, 3147–60.

Porteous, D.J., Millar, J.K. (2006). Disrupted in schizophrenia 1: building brains and memories. *Trends Mol. Med.* **12**: 255–61.

Pouille, F., Scanziani, M. (2001**)** Enforcement of temporal fidelity in pyramidal cells by somatic feed-forwardinhibition. *Science* **293**(5532): 1159-63.

Powell, E.M., Mars, W.M., Levitt, P. (2001). Hepatocyte growth factor/scatter factor is a motogen for interneurons migrating from the ventral to dorsal telencephalon. *Neuron* **30**: 79–89.

Rajagopalan, S., Nicolas, E., Vivancos, V., Berger, J., Dickson B.J. (2000) Crossing the midline: roles and regulation of Robo receptors. *Neuron* **28**: 767-777.

Rakic, P., Lombroso, P.J. (1998). Development of the cerebral cortex: I. Forming of the cortical structure. *J. Am. Acad. Child Adolesc. Psychiatry* **37(1)**: 116-117.

Ramamoorthi, K., Lin, Y. (2011) The contribution of GABAergic dysfunction to neurodevelopmental disorders. *Trends Mol Med.* **17**(8):452-62.

Roberts, R.C. (2007). Schizophrenia in translation: disrupted in schizophrenia (DISC1): integrating clinical and basic findings. *Schizophr. Bull.* **33**: 11–5.

Rudy, B., Fishell, G., Lee, S., Hjerling-Leffler, J. (2011). Three groups of interneurons account for nearly 100% of neocortical GABAergic neurons. *Dev. Neurobiol.* **71**: 45–61.

Rubenstein, J.L. (2010) Three hypotheses for developmental defects that may underlie some forms of autism spectrum disorder. *Curr Opin Neurol.* **3**(2):118-23.

Russell, W.L., Kelly, E.M., Hunsicker, P.R., Bangham, J.W., Maddux, S.C., Phipps, E.L. (1979) Specific-locus test shows ethylnitrosourea to be the most potent mutagenin the mouse. *Proc. Natl. Acad. Sci. U. S. A.* **76**(11): 5818-9

Rutherford, L.C., Nelson, S.B., Turrigiano, G.G. (1998). BDNF has opposite effects on the quantal amplitude of pyramidal neuron and interneuron excitatory synapses. *Neuron* **21**: 521–30.

Sasaki, S., Mori, D., Toyo-oka, K., Chen, A., Garrett-beal, L., Muramatsu, M., Miyagawa, S., Hiraiwa, N., Yoshiki, A., Wynshaw-boris, A., Sasaki, S., Mori, D., Toyo-oka, K., Chen, A., Garrett-beal, L., Muramatsu, M., Miyagawa, S., Hiraiwa, N., Yoshiki, A., Wynshaw-boris, A., Hirotsune, S. (2005). Complete loss of Ndel1 results in neuronal migration defects and early embryonic lethality. *Mol. Cell. Biol.* 25: 7812-27

Schizophrenia Psychiatric Genome-Wide Association Study (GWAS) Consortium (2011) Genome-wide association study identifies five new schizophrenia loci. *Nat Genet.* **43**(10): 969-976

Schurov, I.L., Handford, E.J., Brandon, N.J., Whiting, P.J. (2004). Expression of disrupted in schizophrenia 1 (DISC1) protein in the adult and developing mouse brain indicates its role in neurodevelopment. *Mol. Psychiatry* **9**: 1100–10.

Shen, S., Lang, B., Nakamoto, C., Zhang, F., Pu, J., Kuan, S.-L., Chatzi, C., He, S., Mackie, I., Brandon, N.J., Marquis, K.L., Day, M., Hurko, O., McCaig, C.D., Riedel, G., St Clair, D. (2008). Schizophrenia-related neural and behavioral phenotypes in transgenic mice expressing truncated Disc1. *J. Neurosci.* **28**: 10893–904.

Shu, T., Ayala, R., Nguyen, M., Xie, Z., Gleeson, J.G., Tsai, L. (2004). Ndel1 Operates in a Common Pathway with LIS1 and Cytoplasmic Dynein to Regulate Cortical Neuronal Positioning. *Neuron* **44**: 263–277.

Singh, K.K., Ge, X., Mao, Y., Drane, L., Meletis, K., Samuels, B. A., Tsai, L.-H. (2010). Dixdc1 is a critical regulator of DISC1 and embryonic cortical development. *Neuron* **67**: 33–48.

Singh, K.K., De Rienzo, G., Drane, L., Mao, Y., Flood, Z., Madison, J., Ferreira, M., Bergen, S., King, C., Sklar, P., Sive, H., Tsai, L.-H. (2011). Common DISC1 polymorphisms disrupt Wnt/GSK3β signaling and brain development. *Neuron* **72**: 545–58.

Soares, D.C., Carlyle, B.C., Bradshaw, N.J., Porteous, D.J. (2011). DISC1: Structure, Function, and Therapeutic Potential for Major Mental Illness. *ACS Chem. Neurosci.* **2**: 609–632.

Sohal, V.S., Zhang, F., Yizhar, O., Deisseroth, K. (2009). Parvalbumin neurons and gamma rhythms enhance cortical circuit performance. *Nature* **459**: 698–702.

Southwell, D.G., Froemke, R.C., Alvarez-Buylla, A., Stryker, M.P., Gandhi, S.P. (2010). Cortical plasticity induced by inhibitory neuron transplantation. *Science* **327**: 1145–8.

Southwell, D.G., Paredes, M.F., Galvao, R.P., Jones, D.L., Froemke, R.C., Sebe, J.Y., Alfaro-Cervello, C., Tang, Y., Garcia-Verdugo, J.M., Rubenstein, J.L., Baraban, S.C., Alvarez-Buylla, A. (2012). Intrinsically determined cell death of developing cortical interneurons. *Nature* **491**: 109–13.

Spatazza, J., Lee, H.H., Di Nardo, A.A., Tibaldi, L., Joliot, A., Hensch, T.K., Prochiantz, A. (2013) Choroid-plexus-derived Otx2 homeoprotein constrains adult cortical plasticity. *Cell Rep.* **3**(6): 1815-23.

St Clair, D., Blackwood, D., Muir, W., Carothers, A., Walker, M., Spowart, G., Gosden, C., Evans, H.J. (1990) Association within a family of balanced autosomal translocation with major mental illness. *The Lancet* **336**: 13-16.

Steinecke, A., Gampe, C., Valkova, C., Kaether, C., Bolz, J. (2012). Disrupted-in-Schizophrenia 1 (DISC1) is necessary for the correct migration of cortical interneurons. *J. Neurosci.* **32**: 738–45.

Stevens, J., Rogers, J.H. (1997). Chick calretinin: purification, composition, and metal binding activity of native and recombinant forms. *Protein Expr. Purif.* **9**: 171–81.

Su, P., Li, S., Chen, S., Lipina, T.V., Wang, M., Lai, T.K., Lee, F.H., Zhang, H., Zhai, D., Ferguson, S.S., Nobrega, J.N., Wong, A.H., Roder, J.C., Fletcher, P.J., Liu, F. (2014) A Dopamine D2 Receptor-DISC1 Protein Complex may Contribute to Antipsychotic-Like Effects. *Neuron* **84**: 1-15.

Sugiyama, S., Di Nardo, A. a, Aizawa, S., Matsuo, I., Volovitch, M., Prochiantz, A., Hensch, T.K. (2008). Experience-dependent transfer of Otx2 homeoprotein into the visual cortex activates postnatal plasticity. *Cell* **134**: 508–20.

Sultan, K.T., Shi, W., Shi, S.-H. (2014). Clonal origins of neocortical interneurons. *Curr. Opin. Neurobiol.* **26C**: 125–131.

Tabata, H., Nakajima, K. (2001). Efficient in utero gene transfer system to the developing mouse brain using electroporation: visualization of neuronal migration in the developing cortex. *Neuroscience* **103**: 865–72.

Tanahira, C., Higo, S., Watanabe, K., Tomioka, R., Ebihara, S., Kaneko, T., Tamamaki, N. (2009). Parvalbumin neurons in the forebrain as revealed by parvalbumin-Cre transgenic mice. *Neurosci. Res.* **63**: 213–23.

Tanaka, D.H., Mikami, S., Nagasawa, T., Miyazaki, J., Nakajima, K., Murakami, F. (2010). CXCR4 is required for proper regional and laminar distribution of cortical somatostatin-, calretinin-, and neuropeptide Y-expressing GABAergic interneurons. *Cereb. Cortex* **20**: 2810–7.

Taub, A.H., Katz, Y., Lampl, I. (2013) Cortical balance of excitation and inhibition is regulated by the rate of synaptic activity. *J Neurosci.* **33**(36): 14359-68.

Thomson, P.A., Malavasi, E.L. V, Grünewald, E., Soares, D.C., Borkowska, M., Millar, J.K. (2013). DISC1 genetics, biology and psychiatric illness. *Front. Biol. (Beijing).* **8**: 1–31.

Tomioka, R., Okamoto, K., Furuta, T., Fujiyama, F., Iwasato, T., Yanagawa, Y., Obata, K., Kaneko, T., Tamamaki, N. (2005). Demonstration of long-range GABAergic connections distributed throughout the mouse neocortex. *Eur. J. Neurosci.* **21**: 1587–600.

Tomita, K., Kubo, K., Ishii, K., Nakajima, K. (2011). Disrupted-in-Schizophrenia-1 (Disc1) is necessary for migration of the pyramidal neurons during mouse hippocampal development. *Hum. Mol. Genet.* **20**: 2834–45.

Tomppo, L., Ekelund, J., Lichtermann, D., Veijola, J., Järvelin, M.R., Hennah, W. (2012) DISC1 conditioned GWAS for psychosis proneness in a large Finnish birth cohort. *PLoS One* **7**(2): e30643

Trevelyan, A.J., Watkinson, O. (2005) Does inhibition balance excitation in neocortex? Prog. *Biophys. Mol. Biol.* **87**: 109–143.

Tsuang, M. (2000) Schizophrenia: genes and environment. *Biol Psych* **47**(3): 210-220.

Turrigiano, G.G., Nelson, S.B. (2004). Homeostatic plasticity in the developing nervous system. *Nat. Rev. Neurosci.* **5**: 97–107.

Volante, M., Rosas, R., Allìa, E., Granata, R., Baragli, a, Muccioli, G., Papotti, M. (2008). Somatostatin, cortistatin and their receptors in tumours. *Mol. Cell. Endocrinol.* **286**: 219–29.

Wang, Y., Toledo-Rodriguez, M., Gupta, A., Wu, C., Silberberg, G., Luo, J., Markram, H. (2004). Anatomical, physiological and molecular properties of Martinotti cells in the somatosensory cortex of the juvenile rat. *J. Physiol.* **561**: 65–90.

Wang, C.-L., Zhang, L., Zhou, Y., Zhou, J., Yang, X.-J., Duan, S., Xiong, Z.-Q., Ding, Y.-Q. (2007). Activity-dependent development of callosal projections in the somatosensory cortex. *J. Neurosci.* **27**: 11334–42.

Wang, Y., Kaneko, N., Asai, N., Enomoto, A., Isotani-Sakakibara, M., Kato, T., Asai, M., Murakumo, Y., Ota, H., Hikita, T., Namba, T., Kuroda, K., Kaibuchi, K., Ming, G., Song, H., Sawamoto, K., Takahashi, M. (2011). Girdin is an intrinsic regulator of neuroblast chain migration in the rostral migratory stream of the postnatal brain. *J. Neurosci.* **31**: 8109–22.

Wei, J., Davis, K.M., Wu, H., Wu, J.-Y. (2004). Protein phosphorylation of human brain glutamic acid decarboxylase (GAD)65 and GAD67 and its physiological implications. *Biochemistry* **43**: 6182–9.

Wonders, C.P., Anderson, S. A. (2006). The origin and specification of cortical interneurons. *Nat. Rev. Neurosci.* **7**: 687–96.

Wood, J.N., Grafman, J. (2003). Human prefrontal cortex: processing and representational perspectives. *Nat. Rev. Neurosci.* **4**: 139–47.

Wu, K.Y., Zippin, J.H., Huron, D.R., Kamenetsky, M., Hengst, U., Buck, J., Levin, L.R., Jaffrey, S.R. (2006). Soluble adenylyl cyclase is required for netrin-1 signaling in nerve growth cones. *Nat. Neurosci.* **9**: 1257–64.

Xu, Q., Cobos, I., De La Cruz, E., Rubenstein, J.L., Anderson, S. A. (2004). Origins of cortical interneuron subtypes. *J. Neurosci.* **24**: 2612–22.

Xu, Q., Wonders, C.P., Anderson, S. A. (2005). Sonic hedgehog maintains the identity of cortical interneuron progenitors in the ventral telencephalon. *Development* **132**: 4987–98.

Xue, M., Atallah, B.V., Scanziani, M. (2014) Equalizing excitation–inhibition ratios across visual cortical neurons. *Nature* **511**: 596-600.

Ye, Q., Miao, Q.-L. (2013). Experience-dependent development of perineuronal nets and chondroitin sulfate proteoglycan receptors in mouse visual cortex. *Matrix Biol*. **32**: 352–63.

Yingling, J., Youn, Y.H., Darling, D., Toyo-Oka, K., Pramparo, T., Hirotsune, S., Wynshaw-Boris, A. (2008). Neuroepithelial stem cell proliferation requires LIS1 for precise spindle orientation and symmetric division. *Cell* **132**: 474–86.

Yizhar, O., Fenno, L.E., Prigge, M., Schneider, F., Davidson, T.J., O'Shea, D.J., Sohal, V.S., Goshen, I., Finkelstein, J., Paz, J.T., Stehfest, K., Fudim, R., Ramakrishnan, C., Huguenard, J.R., Hegemann, P., Deisseroth, K. (2011). Neocortical excitation/inhibition balance in information processing and social dysfunction. *Nature* **477**: 171–8.

Yokota, Y., Gashghaei, H.T., Han, C., Watson, H., Campbell, K.J., Anton, E.S. (2007). Radial glial dependent and independent dynamics of interneuronal migration in the developing cerebral cortex. *PLoS One* **8**: e794.

Youn, Y.H., Pramparo, T., Hirotsune, S., Wynshaw-Boris, A. (2009). Distinct dose-dependent cortical neuronal migration and neurite extension defects in Lis1 and Ndel1 mutant mice. *J. Neurosci.* **29**: 15520–30.

Young-Pearse, T.L., Suth, S., Luth, E.S., Sawa, A., Selkoe, D.J. (2010). Biochemical and functional interaction of disrupted-in-schizophrenia 1 and amyloid precursor protein regulates neuronal migration during mammalian cortical development. *J. Neurosci.* **30**: 10431–40.

Zechner, D., Fujita, Y., Hülsken, J., Müller, T., Walther, I., Taketo, M.M., Bryan Crenshaw, E., Birchmeier, W., Birchmeier, C. (2003). β-Catenin signals regulate cell growth and the balance between progenitor cell expansion and differentiation in the nervous system. *Dev. Biol.* **258**: 406–418.

Zhou, M., Li, W., Huang, S., Song, J., Kim, J.Y., Tian, X., Kang, E., Sano, Y., Liu, C., Balaji, J., Wu, S., Zhou, Yu, Zhou, Ying, Parivash, S.N., Ehninger, D., He, L., Song, H., Ming, G.-L., Silva, A.J. (2013). mTOR Inhibition ameliorates cognitive and affective deficits caused by Disc1 knockdown in adult-born dentate granule neurons. *Neuron* **77**: 647–54.

Žiburkus, J., Cressman, J.R., Schiff, S.J. (2013). Seizures as imbalanced up states: excitatory and inhibitory conductances during seizure-like events. *J. Neurophysiol.* **109**: 1296–306.

Appendix

Tables to chapter 3

Table 3.01 A-F corresponding to data in the Fig 4.02 B-G.

A. Cell density in the L100P mice (n = 3 per genotype).

Cortical region	Genotype	Mean [cells/mm^2]	SEM
fSSp	WT	2639.446	128.4256
	L100P/+	2397.991	85.30422
	L100P/L100P	2434.735	118.2784
SSp	WT	3258.901	34.31385
	L100P/+	3405.165	187.6367
	L100P/L100P	2826.345	112.0134
vAud	WT	2507.307	220.7116
	L100P/+	2227.83	118.3408
	L100P/L100P	2385.189	61.86141
Vis	WT	2663.102	155.8036
	L100P/+	2637.623	188.4037
	L100P/L100P	2082.321	94.29892

B. Cortical thickness in the L100P mice (n = 3 per genotype).

Cortical region	Genotype	N	Mean [µm]	SEM
fSSp	WT	5	1483.125	23.56424
	L100P/+	4	1500	90.05749
	L100P/L100P	3	1582.292	47.05982
SSp	WT	5	1395.625	56.53228
	L100P/+	4	1181.25	52.44665
	L100P/L100P	3	1419.792	48.75846
vAud	WT	5	1263.75	56.18573
	L100P/+	4	1312.5	38.35823
	L100P/L100P	3	1383.333	57.40519
Vis	WT	3	935.4167	40.55817
	L100P/+	4	917.1875	30.25768
	L100P/L100P	3	1062.5	73.995

C. Relative distribution of cells - fSSp

Layer	Genotype	Mean [cells/mm^2]	SEM
I	WT	1231.03	8.836195
	L100P/+	937.2923	255.2432
	L100P/L100P	1102.954	317.1768
II/III	WT	2923.845	431.2627
	L100P/+	2360.113	55.95454
	L100P/L100P	2218.649	344.3896
IV	WT	3029.394	331.9986
	L100P/+	3373.23	259.286
	L100P/L100P	3101.703	580.9633
V	WT	2320.796	182.1779
	L100P/+	2706.585	543.209
	L100P/L100P	2320.812	252.9868
VI	WT	2817.132	209.9318
	L100P/+	2141.923	193.1354
	L100P/L100P	2838.44	410.6356

D. Relative distribution of cells - SSp

Layer	Genotype	Mean [cells/mm^2]	SEM
I	WT	1588.108	128.4917
	L100P/+	1275.994	170.2065
	L100P/L100P	1432.015	162.1726
II/III	WT	2822.844	111.1604
	L100P/+	3471.538	207.6504
	L100P/L100P	2936.82	194.8343
IV	WT	3762.375	158.0436
	L100P/+	3952.314	536.866
	L100P/L100P	3469.458	176.669
V	WT	3053.246	218.2489
	L100P/+	2913.448	316.4652
	L100P/L100P	2871.328	123.9179
VI	WT	4242.708	178.7967
	L100P/+	4232.116	278.1516
	L100P/L100P	2680.335	297.5722

E. Relative distribution of cells - vAud

Layer	Genotype	Mean [cells/mm^2]	SEM
I	WT	1305.429	378.2906
	L100P/+	1647.48	328.595
	L100P/L100P	872.6349	401.4164
II/III	WT	2547.574	343.7222
	L100P/+	3194.872	380.811
	L100P/L100P	2279.58	221.9137
IV	WT	2283.327	118.236
	L100P/+	1619.05	167.9776
	L100P/L100P	2443.864	551.6526
V	WT	2127.799	77.37581
	L100P/+	2355.63	196.824
	L100P/L100P	2121.235	159.3775
VI	WT	3443.386	615.0143
	L100P/+	2138.664	283.2628
	L100P/L100P	3065.978	344.4541

F. Relative distribution of cells - Vis

Layer	Genotype	Mean [cells/mm^2]	SEM
I	WT	1089.603	245.3081
	L100P/+	1104.272	61.41515
	L100P/L100P	1040.598	82.48541
II/III	WT	2432.931	136.4105
	L100P/+	2705.371	261.9491
	L100P/L100P	2625.946	534.0329
IV	WT	2982.049	470.8669
	L100P/+	2583.462	405.9563
	L100P/L100P	2335.373	234.6387
V	WT	2934.461	188.2174
	L100P/+	2997.595	437.7618
	L100P/L100P	2390.505	234.8639
VI	WT	3349.99	363.2241
	L100P/+	3346.708	330.3069
	L100P/L100P	2013.659	620.2719

Table 3.02 A-E corresponding to Fig 3.02 A-E

A. Interneurons density across cortex.

Cortical region	Genotype	N	Mean [% cells/mm^2]	SEM
fSSp	WT	5	10.71237	0.577904
	L100P/+	4	10.31614	0.249413
	L100P/L100P	3	7.104016	0.920229
SSp	WT	5	9.415409	0.667642
	L100P/+	4	10.52361	0.647327
	L100P/L100P	3	8.357699	0.454264
vAud	WT	5	12.78401	0.667407
	L100P/+	4	13.18681	0.437101
	L100P/L100P	3	8.567984	0.628729
Vis	WT	4	16.40204	2.167471
	L100P/+	4	16.91509	1.832931
	L100P/L100P	3	11.90735	1.000549

B. Parvalbumin cells density across cortex.

Cortical region	Genotype	N	Mean [% cells/mm^2]	SEM
fSSp	WT	8	4.688393	0.329356
	L100P/+	4	4.474025	0.687285
	L100P/L100P	4	3.290497	0.136334
SSp	WT	8	4.09221	0.245774
	L100P/+	4	4.040802	0.241495
	L100P/L100P	4	2.471072	0.41131
vAud	WT	8	3.379666	0.283331
	L100P/+	4	1.736865	0.319537
	L100P/L100P	4	2.09412	0.167358
Vis	WT	3	7.61549	0.291656
	L100P/+	4	5.839182	0.537789
	L100P/L100P	3	4.676303	1.604469

C. Parvalbumin mRNA cells density across cortex (n = 4).

Cortical region	Genotype	Mean [% cells/mm^2]	SEM
fSSp	WT	5.812915	0.288454
	L100P/+	5.0379	0.618786
	L100P/L100P	3.677130065	0.209136
SSp	WT	5.1984372	0.591167
	L100P/+	4.664991	0.556513
	L100P/L100P	3.262518014	0.415054
vAud	WT	3.3734187	0.191939
	L100P/+	2.338087	0.323147
	L100P/L100P	1.173145565	0.15749
Vis	WT	8.9230548	0.709623
	L100P/+	7.85509	1.607309
	L100P/L100P	5.429864253	0.85657

D. CLR cells density across cortex.

Cortical region	Genotype	N	Mean [% cells/mm^2]	SEM
fSSp	WT	5	1.300986	0.07549
	L100P/+	3	1.688129	0.049453
	L100P/L100P	3	1.032417	0.021937
SSp	WT	5	1.543728	0.268561
	L100P/+	3	2.204738	0.415806
	L100P/L100P	3	1.071275	0.310218
vAud	WT	5	2.148993	0.167999
	L100P/+	3	2.351448	0.222497
	L100P/L100P	3	1.11913	0.32161
Vis	WT	4	5.108126	0.611014
	L100P/+	3	5.005013	0.516051
	L100P/L100P	3	3.636989	0.379518

E. STT cells density across cortex.

Cortical region	Genotype	N	Mean [% cells/mm^2]	SEM
fSSp	WT	5	4.3250855	0.311982
	L100P/+	3	3.664495	0.272446
	L100P/L100P	3	4.003437655	0.389491
SSp	WT	5	3.7861258	0.249725
	L100P/+	3	3.883842	0.632407
	L100P/L100P	3	3.634790959	0.23538
vAud	WT	5	5.9821958	0.242477
	L100P/+	3	4.346616	0.690163
	L100P/L100P	3	4.502539988	0.10233
Vis	WT	4	5.402687	0.44353
	L100P/+	3	7.044093	0.374584
	L100P/L100P	3	6.084828424	0.552027

Table 3.03 A-D for Fig 3.04 A-D

A. Relative distribution of interneurons - fSSp.

Layer	Genotype	Mean [%]	SEM
I	WT	8.604509	0.420922
	L100P/+	7.269856	1.018428
	L100P/L100P	5.831851	0.196875
II/III	WT	25.19578	1.667062
	L100P/+	20.32992	4.312162
	L100P/L100P	27.94436	3.142836
IV	WT	19.13748	0.987347
	L100P/+	21.87503	3.486095
	L100P/L100P	20.49739	1.484782
V	WT	26.69407	2.748376
	L100P/+	29.70745	1.636859
	L100P/L100P	25.72079	0.971092
VI	WT	20.36816	2.721267
	L100P/+	20.81775	2.25835
	L100P/L100P	20.00561	3.606365

B. Relative distribution of interneurons - SSp.

Layer	Genotype	Mean [%]	SEM
I	WT	9.220441	1.369443
	L100P/+	9.627285	0.592128
	L100P/L100P	6.807107	0.47171
II/III	WT	29.26482	1.14774
	L100P/+	30.17932	1.976741
	L100P/L100P	24.45822	1.427546
IV	WT	15.90581	2.225962
	L100P/+	18.62441	2.493462
	L100P/L100P	23.53556	2.941727
V	WT	26.16517	0.911849
	L100P/+	25.68909	2.363704
	L100P/L100P	27.14557	1.052398
VI	WT	19.44375	2.572924
	L100P/+	15.8799	2.492843
	L100P/L100P	18.05354	1.970482

C. Relative distribution of interneurons - vAud.

Layer	Genotype	Mean [%]	SEM
I	WT	12.49911	1.660399
	L100P/+	8.701751	1.20861
	L100P/L100P	9.763496	0.504536
II/III	WT	27.98711	2.89898
	L100P/+	22.84942	0.784601
	L100P/L100P	21.73621	1.510598
IV	WT	18.04777	1.256315
	L100P/+	16.5514	4.101264
	L100P/L100P	17.35015	1.70968
V	WT	18.84361	1.829721
	L100P/+	24.9762	4.033267
	L100P/L100P	27.72078	1.880979
VI	WT	22.6224	1.579523
	L100P/+	26.92123	1.78694
	L100P/L100P	26.29729	1.307056

D. Relative distribution of interneurons - Vis.

Layer	Genotype	Mean [%]	SEM
I	WT	13.41335	2.715679
	L100P/+	17.39799	2.984572
	L100P/L100P	14.35952	1.33114
II/III	WT	27.75069	2.48187
	L100P/+	23.74404	2.663561
	L100P/L100P	28.94634	0.765921
IV	WT	20.77394	4.494874
	L100P/+	14.77853	3.832415
	L100P/L100P	16.57997	2.037686
V	WT	26.62416	0.817704
	L100P/+	32.31727	3.277735
	L100P/L100P	27.41153	1.030047
VI	WT	11.43786	3.910978
	L100P/+	11.76217	3.749005
	L100P/L100P	12.70264	1.231188

Table 3.04 A-D for Fig 3.05 A-D

A. Relative distribution of PV interneurons - fSSp.

Layer	Genotype	N	Mean [%]	SEM
I	WT	5	0.461255	0.350548
	L100P/+	4	0	0
	L100P/L100P	3	0.25	0.229358
II/III	WT	5	13.09963	1.607462
	L100P/+	4	12.1562	2.032745
	L100P/L100P	3	9.75	2.197565
IV	WT	5	32.84133	2.738997
	L100P/+	4	32.0066	2.827046
	L100P/L100P	3	30.5	3.334289
V	WT	4	33.30258	2.524147
	L100P/+	4	40.45598	1.037391
	L100P/L100P	3	36.5	3.522468
VI	WT	5	20.2952	1.526321
	L100P/+	4	15.38123	1.893223
	L100P/L100P	3	23	1.614047

B. Relative distribution of PV interneurons - SSp.

Layer	Genotype	N	Mean [%]	SEM
I	WT	5	0	0
	L100P/+	4	0	0
	L100P/L100P	3	0	0
II/III	WT	5	10.38791	2.103491
	L100P/+	4	17.78455	1.052715
	L100P/L100P	3	9.608541	3.242864
IV	WT	5	31.50391	2.790568
	L100P/+	4	28.55691	2.093144
	L100P/L100P	3	30.24911	4.584728
V	WT	4	42.38745	2.853428
	L100P/+	4	31.30081	1.606358
	L100P/L100P	3	33.80783	7.032591
VI	WT	5	15.72073	4.008078
	L100P/+	4	22.35772	1.944049
	L100P/L100P	3	26.33452	3.544104

C. Relative distribution of PV interneurons - vAud.

Layer	Genotype	N	Mean [%]	SEM
I	WT	5	0	0
	L100P/+	4	0	0
	L100P/L100P	3	0	0
II/III	WT	5	16.01046	2.456739
	L100P/+	4	12.38447	2.151754
	L100P/L100P	3	14.13613	4.138779
IV	WT	5	23.72991	5.351697
	L100P/+	4	35.12015	3.233117
	L100P/L100P	3	29.84293	2.096317
V	WT	4	31.06983	6.180775
	L100P/+	4	31.60813	1.963414
	L100P/L100P	3	22.51309	1.39975
VI	WT	5	29.18981	6.224251
	L100P/+	4	20.88725	2.420965
	L100P/L100P	3	33.50785	5.566222

D. Relative distribution of PV interneurons - Vis.

Layer	Genotype	N	Mean [%]	SEM
I	WT	5	0	0
	L100P/+	4	0	0
	L100P/L100P	3	0	0
II/III	WT	5	14.00721	2.498137
	L100P/+	4	8.400847	3.694452
	L100P/L100P	3	20.71746	3.476085
IV	WT	5	30.69832	1.792752
	L100P/+	4	25.3365	2.452966
	L100P/L100P	3	24.11012	1.696329
V	WT	4	40.79207	2.573137
	L100P/+	4	46.74205	1.298803
	L100P/L100P	3	41.76863	3.058954
VI	WT	5	14.5024	0.73093
	L100P/+	4	19.5206	3.639357
	L100P/L100P	3	13.40378	2.113459

Table 3.05 A-D for Fig 3.06 B-E

A. Cell density in the MPFC L100P mice.

Cortical region	Genotype	N	Mean [cells/mm^2]	SEM
ILA	WT	3	3892.61	423.053
	L100P/+	3	4090.704	560.7175
	L100P/L100P	5	4818.623	714.4062
PLA	WT	3	3363.412	449.8605
	L100P/+	3	2173.464	257.0619
	L100P/L100P	5	2292.289	284.389
ACA	WT	3	2397.9	577.0784
	L100P/+	3	2250.126	456.206
	L100P/L100P	5	2607.566	471.6966
MPFC	WT	3	3347.983	413.7233
	L100P/+	3	2924.846	263.6694
	L100P/L100P	5	3471.088	481.0921
LA	WT	3	3677.394	390.4432
	L100P/+	3	3174.002	248.8085
	L100P/L100P	5	3736.671	521.8973

B. Parvalbumin cells density across cortex.

Cortical region	Genotype	N	Mean [% cells/mm^2]	SEM
ILA	WT	3	1.229836	0.096229
	L100P/+	4	1.515692	0.086111
	L100P/L100P	5	1.312885	0.276321
PLA	WT	3	2.437943	0.373861
	L100P/+	4	3.423454	0.812876
	L100P/L100P	5	2.688468	0.630123
ACA	WT	3	4.59647	1.270478
	L100P/+	4	4.850055	1.047217
	L100P/L100P	5	5.362482	1.314861
MPFC	WT	3	0.697731	0.089255
	L100P/+	4	0.86769	0.129085
	L100P/L100P	5	0.735282	0.09335
LA	WT	3	0.821532	0.083632
	L100P/+	4	1.055779	0.144369
	L100P/L100P	5	0.850971	0.130623

C. Relative cell distribution - MPFC.

Layer	Genotype	Mean [cells/mm^2]	SEM
I	WT	1203.185	195.0959
	L100P/+	1389.348	169.0206
	L100P/L100P	2187.958	293.927
II/III	WT	3411.987	491.1667
	L100P/+	3256.925	369.2204
	L100P/L100P	3201.139	424.9925
IV/VI	WT	4970.256	578.6703
	L100P/+	3185.186	284.7993
	L100P/L100P	4449.55	666.4761

D. Relative cell distribution - LA.

Layer	Genotype	Mean [cells/mm^2]	SEM
I	WT	1242.289	195.867
	L100P/+	1656.175	237.3875
	L100P/L100P	2791.83	399.2614
II/III	WT	3967.697	189.115
	L100P/+	3333.241	244.1464
	L100P/L100P	3432.407	458.2828
IV/VI	WT	5319.575	290.3121
	L100P/+	3627.411	374.7913
	L100P/L100P	4536.54	698.9704

Table 3.06 A-F corresponding to data in the Fig 4.07 A-F.

A. Cell density in the Q31L mice.

Cortical region	Genotype	N	Mean [cells/mm^2]	SEM
fSSp	WT	3	2363.658	39.10458
	Q31L/+	3	2679.866	80.79864
	Q31L / Q31L	5	2455.354	42.33016
SSp	WT	3	2664.903	58.26887
	Q31L/+	3	3194.631	61.43605
	Q31L / Q31L	5	2676.242	106.6735
vAud	WT	3	2434.055	119.2372
	Q31L/+	3	2432.749	94.55651
	Q31L / Q31L	5	2648.109	83.08527
Vis	WT	5	2442.184	122.7283
	Q31L/+	3	2599.658	6.837607
	Q31L / Q31L	5	2138.614	81.32746

B. Cortical thickness in the Q31L mice.

Cortical region	Genotype	N	Mean [µm]	SEM
fSSp	WT	3	1597.917	11.45833
	Q31L/+	3	1557.292	28.66003
	Q31L / Q31L	5	1580.208	21.84025
SSp	WT	3	1415.625	59.64849
	Q31L/+	3	1241.667	70.25654
	Q31L / Q31L	5	1397.396	42.8586
vAud	WT	3	1210.417	22.26829
	Q31L/+	3	1246.875	66.82923
	Q31L / Q31L	5	1260.417	37.74802
Vis	WT	5	1021.25	27.94037
	Q31L/+	3	1028.125	67.33873
	Q31L / Q31L	5	989.5833	37.00718

C. Relative distribution of cells - fSSp

Layer	Genotype	Mean [cells/mm^2]	SEM
I	WT	803.4043	55.03254
	Q31L/+	1052.71	83.09499
	Q31L / Q31L	986.8093	91.16923
II/III	WT	2292.356	123.4311
	Q31L/+	2795.38	38.85711
	Q31L / Q31L	2408.949	115.273
IV	WT	3604.84	125.4431
	Q31L/+	3449.027	71.70082
	Q31L / Q31L	3646.578	232.2982
V	WT	2091.464	104.421
	Q31L/+	2423.79	335.4088
	Q31L / Q31L	2256.616	106.4405
VI	WT	2473.846	165.6508
	Q31L/+	2737.081	152.1743
	Q31L / Q31L	2422.251	88.1702

D. Relative distribution of cells - SSp

Layer	Genotype	Mean [cells/mm^2]	SEM
I	WT	1166.046	102.364
	Q31L/+	1142.366	209.2994
	Q31L / Q31L	1120.298	100.7142
II/III	WT	2395.525	60.82171
	Q31L/+	3204.169	117.4663
	Q31L / Q31L	2849.373	80.37081
IV	WT	4057.358	223.9319
	Q31L/+	4296.268	232.7877
	Q31L / Q31L	3248.356	211.3324
V	WT	2486.574	237.3776
	Q31L/+	3209.884	221.0306
	Q31L / Q31L	2553.214	229.1238
VI	WT	2796.028	102.9709
	Q31L/+	3051.852	62.24573
	Q31L / Q31L	2733.934	164.4209

E. Relative distribution of cells - vAud

Layer	Genotype	Mean [cells/mm^2]	SEM
I	WT	1286.368	200.167
	Q31L/+	1054.426	80.75963
	Q31L / Q31L	1176.812	81.65463
II/III	WT	2639.503	60.19878
	Q31L/+	3498.667	270.518
	Q31L / Q31L	2829.694	199.2667
IV	WT	3210.561	496.0594
	Q31L/+	1525.738	79.69677
	Q31L / Q31L	2918.31	626.9425
V	WT	2377.625	10.31785
	Q31L/+	3046.107	90.38168
	Q31L / Q31L	2344.745	72.02612
VI	WT	2348.944	160.3247
	Q31L/+	2428.852	113.2839
	Q31L / Q31L	3048.613	70.80603

F. Relative distribution of cells - Vis

Layer	Genotype	Mean [cells/mm^2]	SEM
I	WT	1076.513	45.94872
	Q31L/+	1294.222	67.83568
	Q31L / Q31L	1821.138	160.4999
II/III	WT	2684.952	327.6297
	Q31L/+	3158.131	166.7273
	Q31L / Q31L	2166.486	115.5346
IV	WT	2238.155	92.10374
	Q31L/+	3094.634	90.76842
	Q31L / Q31L	2163.128	223.2281
V	WT	3027.302	11.73029
	Q31L/+	2386.939	167.8062
	Q31L / Q31L	2328.144	129.1326
VI	WT	2505.861	158.9424
	Q31L/+	2447.059	121.1936
	Q31L / Q31L	2038.051	177.6209

Table 3.07 A-D corresponding to Fig 3.08 A-B, D-E.

A. Interneurons density across cortex.

Cortical region	Genotype	N	Mean [% cells/mm^2]	SEM
fSSp	WT	4	10.53444	0.666240218
	Q31L/+	3	8.7704489	0.604864
	Q31L / Q31L	4	9.7139388	0.3755323
SSp	WT	4	11.630634	0.643007868
	Q31L/+	3	11.654165	0.722224
	Q31L / Q31L	4	11.480169	0.149136
vAud	WT	4	13.110584	0.279234422
	Q31L/+	3	12.620562	1.450521
	Q31L / Q31L	4	13.017412	0.2359116
Vis	WT	4	18.042128	1.395438883
	Q31L/+	3	16.401624	1.490306
	Q31L / Q31L	5	19.72864	1.9818526

B. Parvalbumin cells density across cortex.

Cortical region	Genotype	N	Mean [% cells/mm^2]	SEM
fSSp	WT	7	4.174283	0.344366
	Q31L/+	3	3.7543676	0.308248
	Q31L / Q31L	9	3.896942	0.226547
SSp	WT	7	3.283002	0.329055
	Q31L/+	3	4.331397	0.358885
	Q31L / Q31L	9	3.177427	0.264071
vAud	WT	7	2.241511	0.302
	Q31L/+	3	1.8155278	0.442772
	Q31L / Q31L	9	2.458435	0.361872
Vis	WT	4	6.755593	0.549041
	Q31L/+	3	5.9617745	0.257338
	Q31L / Q31L	5	6.398973	0.271026

C. CLR cells density across cortex.

Cortical region	Genotype	N	Mean [% cells/mm^2]	SEM
fSSp	WT	4	1.256593187	0.2464309
	Q31L/+	3	1.4566126	0.165084
	Q31L / Q31L	4	1.0473031	0.1454572
SSp	WT	4	1.541409319	0.0854496
	Q31L/+	3	2.1927697	0.293757
	Q31L / Q31L	4	1.5030688	0.0847301
vAud	WT	4	2.382545877	0.229886
	Q31L/+	3	2.696852	0.169984
	Q31L / Q31L	4	2.0650852	0.2235239
Vis	WT	5	4.83300444	0.1557565
	Q31L/+	3	5.4222474	0.203667
	Q31L / Q31L	5	5.4638797	0.6029734

D. STT cells density across cortex.

Cortical region	Genotype	N	Mean [% cells/mm^2]	SEM
fSSp	WT	7	3.3565	0.146689
	Q31L/+	3	3.1286397	0.151107
	Q31L / Q31L	8	3.450417	0.254505
SSp	WT	7	3.369303	0.167311
	Q31L/+	3	3.5598669	0.452381
	Q31L / Q31L	8	3.2518315	0.157048
vAud	WT	7	4.536929	0.293577
	Q31L/+	3	4.4242474	0.32929
	Q31L / Q31L	8	3.9212035	0.157896
Vis	WT	6	4.775857	0.294163
	Q31L/+	3	5.5301528	0.448976
	Q31L / Q31L	5	5.4455446	0.186983

Table 3.08 A-D for Fig 3.09 A-D

A. Relative distribution of interneurons - fSSp.

Layer	Genotype	N	Mean [%]	SEM
I	WT	3	22.881356	3.821398096
	Q31L/+	3	18.181818	5.0501105
	Q31L / Q31L	3	15.317919	1.2597974
II/III	WT	3	10.424564	0.595763216
	Q31L/+	3	8.4203201	0.2509082
	Q31L / Q31L	3	9.8811293	0.9309037
IV	WT	3	5.8203125	0.140841847
	Q31L/+	3	6.2815884	0.6498195
	Q31L / Q31L	3	5.7332293	0.4429726
V	WT	3	11.058151	1.180116149
	Q31L/+	3	9.9307159	0.3527772
	Q31L / Q31L	3	11.084719	0.3451226
VI	WT	3	4.8645661	0.552791598
	Q31L/+	3	3.8716251	0.0509424
	Q31L / Q31L	3	4.7484454	0.0979113

B. Relative distribution of interneurons - SSp.

Layer	Genotype	N	Mean [%]	SEM
I	WT	4	23.863636	3.806394142
	Q31L/+	3	17.771084	2.1084337
	Q31L / Q31L	4	20.146277	3.2957537
II/III	WT	4	10.147415	0.70714565
	Q31L/+	3	6.47365	0.1811244
	Q31L / Q31L	4	10.702372	0.3157288
IV	WT	4	6.2797619	0.936594108
	Q31L/+	3	6.1653599	1.2132605
	Q31L / Q31L	4	8.5212347	0.649243
V	WT	4	10.40004	0.763559514
	Q31L/+	3	9.6997691	0.4000117
	Q31L / Q31L	4	12.100291	0.1255543
VI	WT	4	4.549144	0.672753406
	Q31L/+	3	5.8576052	1.3642226
	Q31L / Q31L	4	5.1296134	0.4514218

C. Relative distribution of interneurons - vAud.

Layer	Genotype	N	Mean [%]	SEM
I	WT	4	16.243812	1.931496168
	Q31L/+	3	14.925373	1.4925373
	Q31L / Q31L	4	19.211823	2.0680857
II/III	WT	4	9.6950301	0.617420136
	Q31L/+	3	6.271777	0.9177399
	Q31L / Q31L	4	8.5802469	0.2783488
IV	WT	4	6.7845395	1.554798367
	Q31L/+	3	10.973451	1.448735
	Q31L / Q31L	4	8.542471	0.3728002
V	WT	4	9.2684659	0.617462185
	Q31L/+	3	8.0994387	1.0048087
	Q31L / Q31L	4	10.546875	0.2575047
VI	WT	4	6.3146412	0.454952918
	Q31L/+	3	6.7674586	1.333352
	Q31L / Q31L	4	6.1536815	0.2373026

D. Relative distribution of interneurons - Vis.

Layer	Genotype	N	Mean [%]	SEM
I	WT	4	13.490854	0.68597561
	Q31L/+	3	12.087912	1.0989011
	Q31L / Q31L	5	11.714286	3.3624578
II/III	WT	4	10.002838	0.441668059
	Q31L/+	3	8.0018939	0.8214655
	Q31L / Q31L	5	10.219561	1.1385997
IV	WT	4	11.081794	0.484727522
	Q31L/+	3	7.1878941	1.4322594
	Q31L / Q31L	5	10.330579	1.2618538
V	WT	4	10.10906	0.594691564
	Q31L/+	3	11.833105	0.9202205
	Q31L / Q31L	5	11.604938	1.4100281
VI	WT	4	5.8641975	0.886506581
	Q31L/+	3	5.2403846	0.7179416
	Q31L / Q31L	5	9.0346084	1.2267729

Table 4.01 A-E corresponding to data in the Fig 4.02 B-F.

A. Proportion of GFP positive cells per mm^2.

Cortical region	Construct	N	Mean [per 1000 cells/mm^2]	SEM
fSSp	IRES GFP	4	15.00238	2.987411
	Disc1-WT	7	25.74905	3.376118
	Disc1-100P	10	19.65209	2.034598
SSp	IRES GFP	5	29.30144	6.203179
	Disc1-WT	7	13.67422	1.939276
	Disc1-100P	9	18.37147	2.871091
vAud	IRES GFP	3	13.63809	1.550913
	Disc1-WT	3	10.01086	3.262659
	Disc1-100P	6	12.6806	2.85617
Vis	IRES GFP	3	39.98357	3.347235
	Disc1-WT	3	15.74422	3.057273
	Disc1-100P	6	16.53989	3.303519

B. Relative distribution of GFP positive cells - fSSp

Layer	Construct	Mean [%]	SEM
I	IRES GFP	1.473871	1.473871
	Disc1-WT	2.746377	1.012957
	Disc1-100P	2.288784	1.002817
II/III	IRES GFP	64.36464	64.36464
	Disc1-WT	57.19043	4.853829
	Disc1-100P	67.28783	4.941897
IV	IRES GFP	34.16149	34.16149
	Disc1-WT	38.31643	5.595936
	Disc1-100P	29.98266	4.787586
V	IRES GFP	0	0
	Disc1-WT	1.57842	1.000483
	Disc1-100P	0.30431	0.14703
VI	IRES GFP	0.16835	0.101466
	Disc1-WT	0	0
	Disc1-100P	0.136417	0.129417

C. Relative distribution of GFP positive cells - SSp

Layer	Construct	Mean [%]	SEM
I	IRES GFP	0	0
	Disc1-WT	0.415855	0.267697
	Disc1-100P	4.339374	1.44725
II/III	IRES GFP	47.28868	0.147677
	Disc1-WT	36.92891	4.111551
	Disc1-100P	54.54067	5.281663
IV	IRES GFP	50.71511	0.502156
	Disc1-WT	59.71243	3.857249
	Disc1-100P	39.12904	4.867211
V	IRES GFP	1.709364	0.426727
	Disc1-WT	2.822426	1.007274
	Disc1-100P	1.534098	0.916339
VI	IRES GFP	0	0.129439
	Disc1-WT	0.120377	0.111448
	Disc1-100P	0.456817	0.227522

D. Relative distribution of GFP positive cells - vAud

Layer	Construct	Mean [%]	SEM
I	IRES GFP	1.898339	1.549987
	Disc1-WT	2.400747	1.960202
	Disc1-100P	7.575213	3.837722
II/III	IRES GFP	87.6367	8.609702
	Disc1-WT	96.1911	1.706041
	Disc1-100P	80.63667	3.54103
IV	IRES GFP	10.11131	6.783291
	Disc1-WT	1.025984	0.837713
	Disc1-100P	8.668284	0.847923
V	IRES GFP	0.353653	0.288757
	Disc1-WT	0.382172	0.312042
	Disc1-100P	1.970317	0
VI	IRES GFP	0	0
	Disc1-WT	0	0
	Disc1-100P	1.14952	0

E. Relative distribution of GFP positive cells - Vis

Layer	Construct	Mean [%]	SEM
I	IRES GFP	0.359319	0.293383
	Disc1-WT	1.693661	0.808317
	Disc1-100P	2.104548	1.454974
II/III	IRES GFP	44.92975	0.997336
	Disc1-WT	52.94261	2.854143
	Disc1-100P	60.08545	4.434903
IV	IRES GFP	52.93812	0.699666
	Disc1-WT	43.13299	2.235983
	Disc1-100P	36.43494	5.689158
V	IRES GFP	1.772811	0.55632
	Disc1-WT	2.230735	1.051263
	Disc1-100P	1.375063	0.446487
VI	IRES GFP	0	0
	Disc1-WT	0	0
	Disc1-100P	0	0

Table 4.02 A-D corresponding to data in the Fig 4.03 A-D.

A. Cortical thickness - ipsilateral side

Cortical region	Construct	Mean [µm]	SEM
fSSp	IRES GFP	1496.81	87.47305
	Disc1-WT	1410.986	14.6794
	Disc1-100P	1469.029	35.63789
SSp	IRES GFP	1276.238	60.71332
	Disc1-WT	1103.893	30.86521
	Disc1-100P	1242.907	41.27806
vAud	IRES GFP	1287.965	6.390161
	Disc1-WT	1194.059	36.76109
	Disc1-100P	1404.582	35.40734
Vis	IRES GFP	1040.067	17.829
	Disc1-WT	932.1266	23.63152
	Disc1-100P	1017.902	27.72362

B. Cortical thickness - contralateral side

Cortical region	Construct	Mean [µm]	SEM
fSSp	IRES GFP	1503.183	20.17427
	Disc1-WT	1409.023	41.74225
	Disc1-100P	1479.856	11.98542
SSp	IRES GFP	1292.624	19.24958
	Disc1-WT	1110.681	21.19683
	Disc1-100P	1196.215	15.26681
vAud	IRES GFP	1257.308	18.27951
	Disc1-WT	1178.209	22.58606
	Disc1-100P	1325.645	24.84087
Vis	IRES GFP	1100.004	10.75615
	Disc1-WT	943.0264	37.59077
	Disc1-100P	1026.005	6.420474

C. Cell density - ipsilateral side

Cortical region	Construct	Mean [cells per mm^2]	SEM
fSSp	IRES GFP	2649.945	131.7069
	Disc1-WT	3659.956	187.185
	Disc1-100P	3061.452	111.9741
SSp	IRES GFP	3041.828	177.636
	Disc1-WT	4031.685	148.6182
	Disc1-100P	3334.69	104.6599
vAud	IRES GFP	3171.641	145.0747
	Disc1-WT	3204.911	76.93024
	Disc1-100P	2821.315	70.0778
Vis	IRES GFP	2981.195	209.7403
	Disc1-WT	3768.385	166.04
	Disc1-100P	3226.347	88.07493

D. Cell density - contralateral side

Cortical region	Construct	Mean [cells per mm^2]	SEM
fSSp	IRES GFP	2649.945	131.7069
	Disc1-WT	3659.956	187.185
	Disc1-100P	3061.452	111.9741
SSp	IRES GFP	3041.828	177.636
	Disc1-WT	4031.685	148.6182
	Disc1-100P	3334.69	104.6599
vAud	IRES GFP	3171.641	145.0747
	Disc1-WT	3204.911	76.93024
	Disc1-100P	2821.315	70.0778
Vis	IRES GFP	2981.195	209.7403
	Disc1-WT	3768.385	166.04
	Disc1-100P	3226.347	88.07493

Table 4.03 A-D corresponding to data in the Fig 4.04 A-D.

A. Distribution of cells - fSSp

Layer	Construct	Mean [cells/mm^2]	SEM
I	IRES GFP	1124.059	91.69814
	Disc1-WT	1464.102	151.7605
	Disc1-100P	1343.852	97.31076
II/III	IRES GFP	2569.553	154.3749
	Disc1-WT	3666.533	245.2323
	Disc1-100P	3003.084	128.137
IV	IRES GFP	3269.953	185.2515
	Disc1-WT	4509.666	457.3157
	Disc1-100P	3741.321	170.2836
V	IRES GFP	2339.489	129.2291
	Disc1-WT	3092.87	352.7461
	Disc1-100P	2928.132	114.3749
VI	IRES GFP	3059.131	126.7565
	Disc1-WT	4858.902	340.6888
	Disc1-100P	3372.049	267.865

B. Distribution of cells - SSp

Layer	Construct	Mean [cells/mm^2]	SEM
I	IRES GFP	1245.896	112.4495
	Disc1-WT	1640.474	63.57216
	Disc1-100P	1352.603	146.2055
II/III	IRES GFP	3073.61	231.7203
	Disc1-WT	4117.081	177.0948
	Disc1-100P	3259.042	160.9253
IV	IRES GFP	3583.174	247.173
	Disc1-WT	4582.084	704.7258
	Disc1-100P	4192.092	205.0723
V	IRES GFP	2839.935	265.3953
	Disc1-WT	3696.733	122.79
	Disc1-100P	2927.366	128.919
VI	IRES GFP	3567.007	301.7035
	Disc1-WT	4762.998	138.5494
	Disc1-100P	3970.299	198.772

C. Distribution of cells - vAud

Layer	Construct	Mean [cells/mm^2]	SEM
I	IRES GFP	1273.93	138.5563
	Disc1-WT	1380.099	51.21704
	Disc1-100P	1161.713	78.22321
II/III	IRES GFP	3384.115	119.5252
	Disc1-WT	3210.382	163.3253
	Disc1-100P	3061.268	150.9728
IV	IRES GFP	3383.623	210.8866
	Disc1-WT	3291.006	198.6853
	Disc1-100P	2794.633	61.95671
V	IRES GFP	2661.011	219.8836
	Disc1-WT	2910.665	125.4739
	Disc1-100P	2509.156	73.87375
VI	IRES GFP	4092.03	236.2096
	Disc1-WT	4217.104	30.14392
	Disc1-100P	3584.058	97.96475

D. Distribution of cells - Vis

Layer	Construct	Mean [cells/mm^2]	SEM
I	IRES GFP	1143.406	134.1355
	Disc1-WT	1321.954	124.7376
	Disc1-100P	1318.711	90.59546
II/III	IRES GFP	2873.979	305.098
	Disc1-WT	4060.993	198.4359
	Disc1-100P	3597.978	122.9243
IV	IRES GFP	3733.043	488.1453
	Disc1-WT	4400.483	50.2152
	Disc1-100P	3702.874	193.5049
V	IRES GFP	3107.062	284.7126
	Disc1-WT	3598.702	232.9601
	Disc1-100P	2927.894	59.14905
VI	IRES GFP	3293.875	177.8243
	Disc1-WT	4770.699	228.2595
	Disc1-100P	3806.339	98.05739

Table 4.04 A-B corresponding to data in the Fig 4.05 A-B.

A. PV cell density - ipsilateral side

Cortical region	Construct	Mean [cells/mm^2]	SEM
fSSp	IRES GFP	105.86	6.082974
	Disc1-WT	125.3257	5.751524
	Disc1-100P	96.66921	5.42702
SSp	IRES GFP	94.59378	3.318555
	Disc1-WT	135.3399	8.538726
	Disc1-100P	94.61261	4.000767
vAud	IRES GFP	81.69782	5.856786
	Disc1-WT	99.4196	14.04361
	Disc1-100P	61.44445	5.624328
Vis	IRES GFP	119.4626	4.685295
	Disc1-WT	127.2761	9.219432
	Disc1-100P	93.09763	4.503366

B. PV cell density - contralateral side

Cortical region	Construct	Mean [cells/mm^2]	SEM
fSSp	IRES GFP	116.5091	7.805359
	Disc1-WT	123.7878	8.120532
	Disc1-100P	113.7005	3.704814
SSp	IRES GFP	98.53447	3.380681
	Disc1-WT	131.8862	5.151762
	Disc1-100P	106.6702	4.917404
vAud	IRES GFP	64.80714	10.58772
	Disc1-WT	82.05065	7.286009
	Disc1-100P	63.28717	9.460444
Vis	IRES GFP	109.2813	11.22396
	Disc1-WT	132.7049	2.997432
	Disc1-100P	100.4146	4.143573

Table 4.05 A-B corresponding to data in the Fig 4.07 A-B.

A. Distribution of PV cells - fSSp, ipsilateral

Layer	Construct	Mean [cells per mm^2]	SEM
I	IRES GFP	2.368419	2.051111
	Disc1-WT	1.353386	1.252992
	Disc1-100P	0.870969	0.826274
II/III	IRES GFP	60.01279	7.765507
	Disc1-WT	92.78105	12.6494
	Disc1-100P	70.10911	6.512669
IV	IRES GFP	146.7521	11.39085
	Disc1-WT	214.7626	24.86998
	Disc1-100P	163.4433	13.79985
V	IRES GFP	199.1158	5.935351
	Disc1-WT	195.3946	17.53945
	Disc1-100P	130.5795	9.554512
VI	IRES GFP	64.40445	6.694402
	Disc1-WT	90.0621	9.129134
	Disc1-100P	76.70039	4.856057

B. Distribution of PV cells - fSSp, contralateral

Layer	Construct	Mean [cells per mm^2]	SEM
I	IRES GFP	0	0
	Disc1-WT	2.349527	2.17524
	Disc1-100P	0.972946	0.923017
II/III	IRES GFP	63.69565	2.669602
	Disc1-WT	95.43863	5.735892
	Disc1-100P	78.88976	6.891255
IV	IRES GFP	182.9014	24.5297
	Disc1-WT	215.3722	29.35814
	Disc1-100P	210.2779	10.26844
V	IRES GFP	202.3052	20.00604
	Disc1-WT	164.3821	13.91733
	Disc1-100P	159.3174	13.59792
VI	IRES GFP	85.6578	7.599974
	Disc1-WT	96.9696	8.55755
	Disc1-100P	80.24701	4.90963

C. Distribution of PV cells - SSp, ipsilateral

Layer	Construct	Mean [cells per mm^2]	SEM
I	IRES GFP	0	0
	Disc1-WT	4.262366	2.711474
	Disc1-100P	0.952381	0.897913
II/III	IRES GFP	65.69126	7.328324
	Disc1-WT	93.40831	10.62394
	Disc1-100P	61.69398	5.678571
IV	IRES GFP	147.4829	8.275003
	Disc1-WT	208.9765	10.7872
	Disc1-100P	135.7835	12.33802
V	IRES GFP	156.4253	4.296825
	Disc1-WT	231.1017	17.11335
	Disc1-100P	155.26	11.16588
VI	IRES GFP	71.80973	10.63763
	Disc1-WT	93.95435	11.99409
	Disc1-100P	80.24506	7.389221

D. Distribution of PV cells - SSp, contralateral

Layer	Construct	Mean [cells per mm^2]	SEM
I	IRES GFP	0	0
	Disc1-WT	2.242479	1.460952
	Disc1-100P	0	0
II/III	IRES GFP	61.91846	7.952707
	Disc1-WT	93.34292	9.816061
	Disc1-100P	53.42061	6.787913
IV	IRES GFP	151.3247	11.66181
	Disc1-WT	195.3205	8.204851
	Disc1-100P	166.7131	9.61437
V	IRES GFP	165.1618	10.68115
	Disc1-WT	219.0366	10.90482
	Disc1-100P	190.3139	10.55617
VI	IRES GFP	83.52871	9.416065
	Disc1-WT	119.5487	14.51002
	Disc1-100P	77.78637	7.215374

Table 4.06 A-B corresponding to data in the Fig 4.08 A-B.

A. Distribution of PV cells - vAud, ipsilateral

Layer	Construct	Mean [cells per mm^2]	SEM
I	IRES GFP	0	0
	Disc1-WT	0	0
	Disc1-100P	0	0
II/III	IRES GFP	42.83444	4.745502
	Disc1-WT	66.14964	24.22793
	Disc1-100P	50.88229	7.315639
IV	IRES GFP	193.0952	18.65477
	Disc1-WT	184.0596	19.5905
	Disc1-100P	111.5633	15.56476
V	IRES GFP	91.12648	15.27376
	Disc1-WT	135.3425	12.33962
	Disc1-100P	76.69002	7.585252
VI	IRES GFP	79.57191	3.958634
	Disc1-WT	96.19553	15.5638
	Disc1-100P	52.6537	9.162642

B. Distribution of PV cells - vAud, contralateral

Layer	Construct	Mean [cells per mm^2]	SEM
I	IRES GFP	0	0
	Disc1-WT	0	0
	Disc1-100P	1.313871	1.706768
II/III	IRES GFP	51.44561	6.874484
	Disc1-WT	51.50951	10.01514
	Disc1-100P	41.76321	12.9285
IV	IRES GFP	100.6409	19.39515
	Disc1-WT	147.9191	10.29188
	Disc1-100P	116.5199	15.53756
V	IRES GFP	87.4751	20.5201
	Disc1-WT	118.2536	14.16786
	Disc1-100P	85.5131	12.12899
VI	IRES GFP	55.83645	12.95446
	Disc1-WT	77.5453	10.99702
	Disc1-100P	60.98543	13.34189

C. Distribution of PV cells - Vis, ipsilateral

Layer	Construct	Mean [cells per mm^2]	SEM
I	IRES GFP	0	0
	Disc1-WT	0	0
	Disc1-100P	0	0
II/III	IRES GFP	84.83016	12.60833
	Disc1-WT	97.88376	19.45264
	Disc1-100P	88.4241	4.5519
IV	IRES GFP	182.9621	11.40026
	Disc1-WT	204.2826	11.8928
	Disc1-100P	164.9409	18.77692
V	IRES GFP	214.6632	14.44613
	Disc1-WT	171.2435	7.379304
	Disc1-100P	122.4976	7.352662
VI	IRES GFP	88.32357	15.35468
	Disc1-WT	114.2143	12.45609
	Disc1-100P	59.14396	9.022443

D. Distribution of PV cells - Vis, contralateral

Layer	Construct	Mean [cells per mm^2]	SEM
I	IRES GFP	0	0
	Disc1-WT	0	0
	Disc1-100P	0	0
II/III	IRES GFP	114.2586	19.68785
	Disc1-WT	105.6301	20.13669
	Disc1-100P	80.01262	3.040227
IV	IRES GFP	155.669	17.70388
	Disc1-WT	191.6488	18.09343
	Disc1-100P	167.6384	13.80336
V	IRES GFP	147.3692	4.84488
	Disc1-WT	202.9024	13.1886
	Disc1-100P	140.368	6.579398
VI	IRES GFP	88.60097	15.35895
	Disc1-WT	99.87413	14.73232
	Disc1-100P	72.34727	5.407209